(5) 229 100

Glass Laser Research

(1)

ANNUAL REPORT for
Office of Naval Research
Contract No. Nonr-38 33(00)

JUNE 1963

CORNING
CORNING GLASS WORKS

(5) 229 100

(9)

Annual Technical Rep~~or~~t,

May ~~1~~962 ~~to~~ June ~~19~~63,

Contract No. Nonr-3833(00)

June 28, 1963

(6)

Glass Laser Research,

Corning Glass Works

Corning, New York

ARPA Order No. 306-62

Project Code No. 7300

Authors:

(10) by T. C. MacAvoy,
M. L. Charters,
R. D. Maurer,
W. H. Dumbaugh and
N. F. Borrelli.
~~P. E. Gordon~~

NJB

Abstract

A study of the spectral properties of neodymium-doped glasses has been undertaken, ~~with the objects of (1) determining how the properties of glass influence the performance of a Nd-doped glass laser and (2) developing the best possible glasses for high power applications~~. The work consists of an extensive study of a wide variety of different glass compositions in parallel with a detailed study of the spectral properties of one glass. Emphasis has been on silicate glasses, especially on those which could be manufactured on a moderately large scale. As a result of this study, the main features of the influence of glass properties on spectral properties are now known. The silicates show the longest lifetimes and most intense fluorescence, while the borates show the shortest lifetimes and weakest fluorescence. Since oscillator strengths are about equal for all glasses studied, the borates are apparently quenched.

In addition to gross compositional effects, certain impurities such as iron, copper, and nickel, quench the neodymium fluorescence.

One of the more promising glasses has been prepared in the best optical quality available and is currently undergoing intensive study.

Table of Contents

Page

1. INTRODUCTION 1

2. INTENSIVE FLUORESCENCE STUDY OF A SINGLE GLASS COMPOSITION 3

2.1 The Glass Composition 3

2.2 Fluorescence Spectrum and Level Scheme 3

2.3 Quantum Efficiency of Fluorescence 9

2.3.1 Rate of Photon Absorption 9

2.3.2 Photon Emission Rate 14

2.4 Fluorescence Decay 17

2.5 Application of Fluorescence Data to Some Stimulated Emission Processes 20

2.5.1 9100 Å Stimulated Emission 20

2.5.2 Maximum Gain Cross Section 23

2.5.3 The Wavelength Spread of Stimulated Emission 24

3. STUDY OF THE SPECTRAL PROPERTIES OF Nd^{+3} AS A FUNCTION OF GLASS COMPOSITION 26

3.1 Composition Selection 26

3.2 Measurements of the Spectral Properties 36

3.2.1 Fluorescence Intensity and Line Width Measurements 38

3.2.2 Spectral Absorption Measurements 41

3.2.3 Experimental Lifetime Measurements 43

3.3 The Effect of Impurities on the Fluorescence Properties of Nd Doped Glasses 46

3.3.1 Pure Glasses 47

3.3.2 Effect of Added Impurities on Fluorescent Properties 53

Table of Contents (continued)

Page

3.3.2.1 Iron 53

3.3.2.2 Copper and Nickel 56

3.3.2.3 Co^{+2}, Mn^{+4}, Y^{+3} 60

3.3.2.4 Other Rare Earth Ions 61

3.3.3 Effect of Temperature on Lifetime 64

3.3.4 Possible Impurity Quenching Mechanism 66

3.3.4.1 Estimation of β_{aq} for Cu and Fe 72

3.4 Effects of Base Glass Composition on Neodymium Fluorescence 73

3.4.1 Expected Effects 75

3.4.2 Observed Effects 77

4. NEODYMIUM GLASS LASER PERFORMANCE 84

4.1 Theoretical Analysis of Pulsed Laser Threshold 85

4.2 Experimental Verification of Predicted Pulse Thresholds 89

5. LARGE SCALE LASER GLASS MELT 89

6. SUMMARY 91

Appendix A EXPERIMENTAL DATA TAKEN ON NEODYMIUM LASER GLASSES 94

Appendix B DERIVATION OF CALCULATED PULSE THRESHOLD EQUATION 118

Appendix C RELATION BETWEEN LIFETIME AND REFRACTIVE INDEX 125

Figures

Page

2-1 Optical Absorption vs. Wavelength 4

2-2 Relative Fluorescence in Vicinity of 9000 Å 5

2-3 Level Scheme for Nd^{+3} Obtained from Glass Data 6

2-4 Relative Fluorescence in Vicinity of 1 Micron 8

2-5 Schematic Diagram of Apparatus Used to Measure the Nd^{+3} Fluorescence 16

2-6 Typical Fluorescence Decay for a Soda Lime Glass 18

2-7 Approximate Distribution of Transition Probabilities 21

2-8 Lifetime vs. Nd Concentration in a Soda Lime Glass 22

2-9 Stimulated Emission Spectrum of Nd Glass 25

2-10 Wavelength Spread of Stimulated Emission vs. Input Energy 27

3-1 Fluorescence Intensity Measuring Equipment Diagram 39

3-2 Typical Fluorescence Spectra of Neodymium in Glasses 42

3-3 Typical Absorbance Spectra of Neodymium in Glasses 44

3-4 Fluorescence Lifetime Measuring Equipment Diagram 45

3-5 Lifetime vs. Weight % Nd_2O_3 in $22Na_2O \cdot 5CaO \cdot 73SiO_2$ 49

3-6 Lifetime vs. Weight % Nd_2O_3 in $25Na_2O \cdot 75SiO_2$ 51

3-7 Lifetime vs. Weight % Nd_2O_3 in $Na_2O \cdot 2B_2O_3$ 52

3-8 Effect of Ferrous Iron Concentration on Lifetime 55

3-9 Lifetime vs. Product of Nd and Fe^{+2} Concentrations 58

3-10 Lifetime vs. (Nd_2O_3 Concentration) x (Impurity Concentration) 59

3-11 ($1 - \tau/\tau_0$) vs. Cation Fraction Nd^{+3} in a Soda Lime Silicate Glass 70

3-12 ($1 - \tau/\tau_0$) vs. Cation Fraction Nd^{+3} in a Soda Silica Glass 71

3-13 ($1 - \tau/\tau_0$) vs. (Cation Fraction Nd) x (Fe^{+2} Concentration) 74

Figures (continued)

		Page
3-14	Level Diagram	65
3-15	Lifetime x Index^3 vs. Oxygen ions/cm^3 in Various Glasses	82
4-1	Measured Lifetime vs. $f(t)_{max}$	86
4-2	Neodymium Concentration vs. Calculated Threshold	88
4-3	Interferometer Photograph of Continuous Tank Melt Laser Glass	90

1. INTRODUCTION

Shortly after the development of the ruby laser by T. H. Maiman(1-1) in 1960, a number of research groups began to study the possible use of glass as a laser host material. Attention was concentrated on rare earth ions dissolved in glass, primarily because the fluorescent transitions occur in the shielded 4f levels and the fluorescent spectra should therefore be relatively undisturbed by the random structure of glass. It has been known for some time that trivalent lanthanide absorption spectra in glass are much sharper than transition metal ion spectra, although not as sharp as in crystals. Subsequent study has revealed that rare earth fluorescence spectra are also relatively sharp in glass. Further, the energy levels for rare earths in glass are approximately the same as in crystals, although the glasses generally have longer lifetimes at room temperature.

At the present time four rare earth ions are known to exhibit stimulated emission in glass, the most important being trivalent neodymium. Properties of the others (Y^{+3}, Gd^{+3}, Ho^{+3}) as well as the properties of Nd^{+3} doped glasses have been reviewed and compared with crystals by Yariv and Gordon. Neodymium is the ion which most readily exhibits stimulated emission in glass. Threshold energies are low as a result of the many absorption bands effective in pumping as well as the fairly high oscillator strength of the pertinent transition. Furthermore, cooling is unneccessary since the terminal level is several thousand wave numbers above the ground state and is normally empty at room temperature (see Figure 2-3).

Beyond its spectral properties, glass has a number of distinct advantages for use as a laser material. The major advantage is that it may be formed in very high optical quality in a variety of shapes from thin fibers to massive pieces. Since the solubility of rare earth ions in glass is fairly high, the concentration of the active element can be adjusted over wide limits. Furthermore, the other physical properties of glass can be varied widely through wide changes in the base glass composition. It should thus be possible to adjust a number of the glass properties for optimum performance in a particular application. There are, unfortunately, some properties of glass which are not advantageous in a laser material, primarily its low thermal conductivity. The mechanical strength of glass is not as high as that of ruby but is equal to or better than the strength of most ionic crystals (such as CaF_2 or $CaWO_4$).

The objectives of Corning's glass laser research program on behalf of the Office of Naval Research have been to determine how the properties of glass influence the performance of a Nd-doped glass laser, and to develop the best possible Nd-doped glass for a high power laser device. Since it was not known initially how much of an effect the glass composition would have, a large part of our work has been devoted to a survey of the spectral properties of neodymium in a wide variety of base glass compositions. Such information, coupled with already existing information on the effect of composition on the physical properties of glass, will allow a sensible choice of the best glass for a particular application.

The number of glasses involved in the exploratory phase of this program is so extensive as to prohibit detailed study of laser performance in all of them. To provide basic information on the detailed performance of a Nd-doped glass laser therefore, we have selected one particular base glass composition for more extensive study. The following section of the report deals with this work. Later sections deal with the exploratory composition studies.

2. INTENSIVE FLUORESCENCE STUDY OF A SINGLE GLASS COMPOSITION

2.1 The Glass Composition

Although the base glass composition definitely has an effect on Nd^{+3} fluorescence as is shown further on in this report, the general features revealed by this intensive study of fluorescence and stimulated emission in a soda lime silicate glass seem to be more or less common to all the glasses studied. It is helpful, therefore, to keep these features in mind when analyzing the extensive data on the large number of glasses given later.

The base glass used in this study had the approximate composition by weight of 71% SiO_2, 15% Na_2O, 12% CaO, 1% Al_2O_3, 1% Sb_2O_3, and had a density of 2.56 g cm $^{-3}$. Various percentages of Nd_2O_3 were added keeping the weight ratio of the base glass oxides unchanged. This glass was chosen because it was of a common type studied extensively in the literature and it can be made in small amounts with fair optical quality.

2.2 Fluorescence Spectrum and Level Scheme

Figure 2-1 shows the optical absorption near 80°K and near 300°K for the region around 9000 Å. This absorption corresponds to transitions from the $^4I_{9/2}$ to $^4F_{3/2}$ state.(2-1) Figure 2-2 shows the relative fluorescence intensity in the same wavelength region after correcting for self-absorption and the apparatus response. At room temperature there appear to be weak fluorescence bands near 8970 Å and 8680 Å which are not present at low temperatures. The main feature, however, is two prominent bands at 8860 Å and 9170 Å.

Figure 2-3 shows the proposed level scheme which accounts for the predominant features of these broad peak spectra characteristic of glasses.

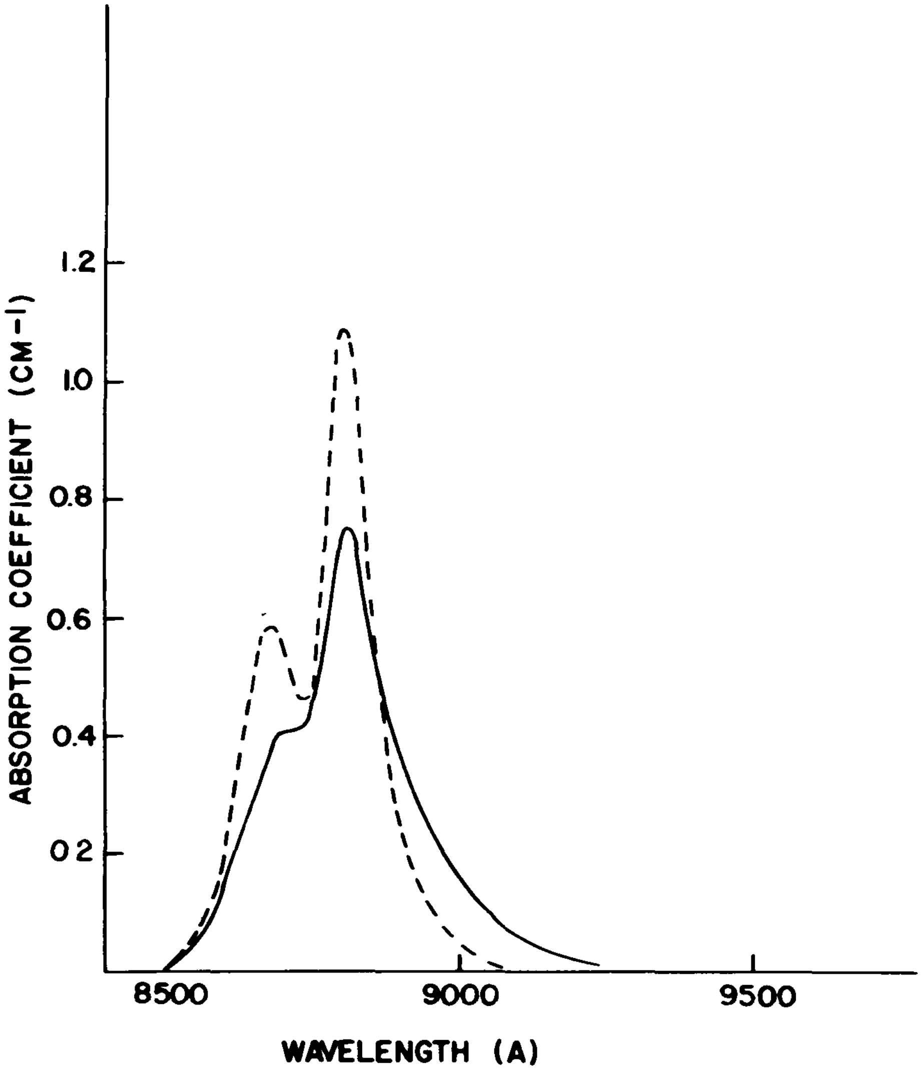

Fig. 2-1 Optical absorption versus wavelength for a glass with about 2.1% neodymium oxide by weight. Solid line, 300°K; dashed line, 80°K.

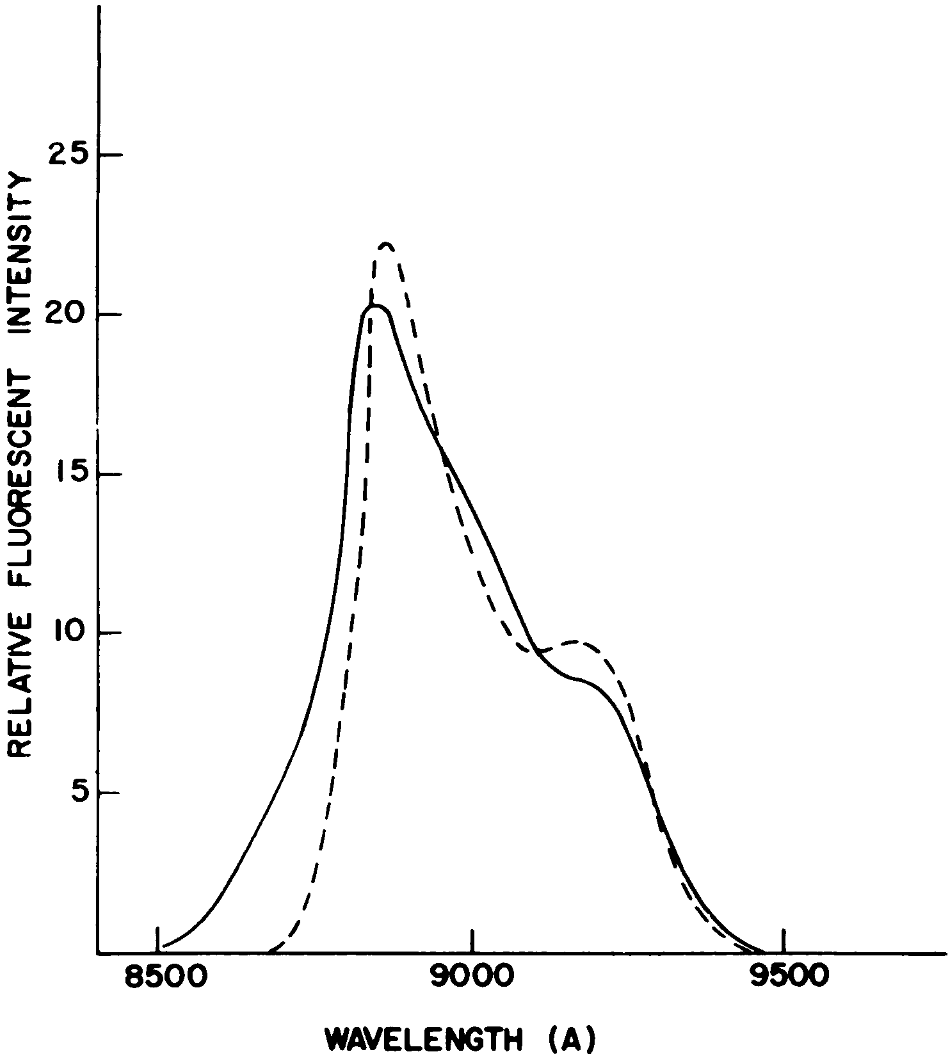

Fig. 2-2 Relative fluorescence around 0.9 for a glass with about 6% neodymium oxide by weight. Solid line, 300°K; dashed line, 80°K. Resolution is about 20 A.

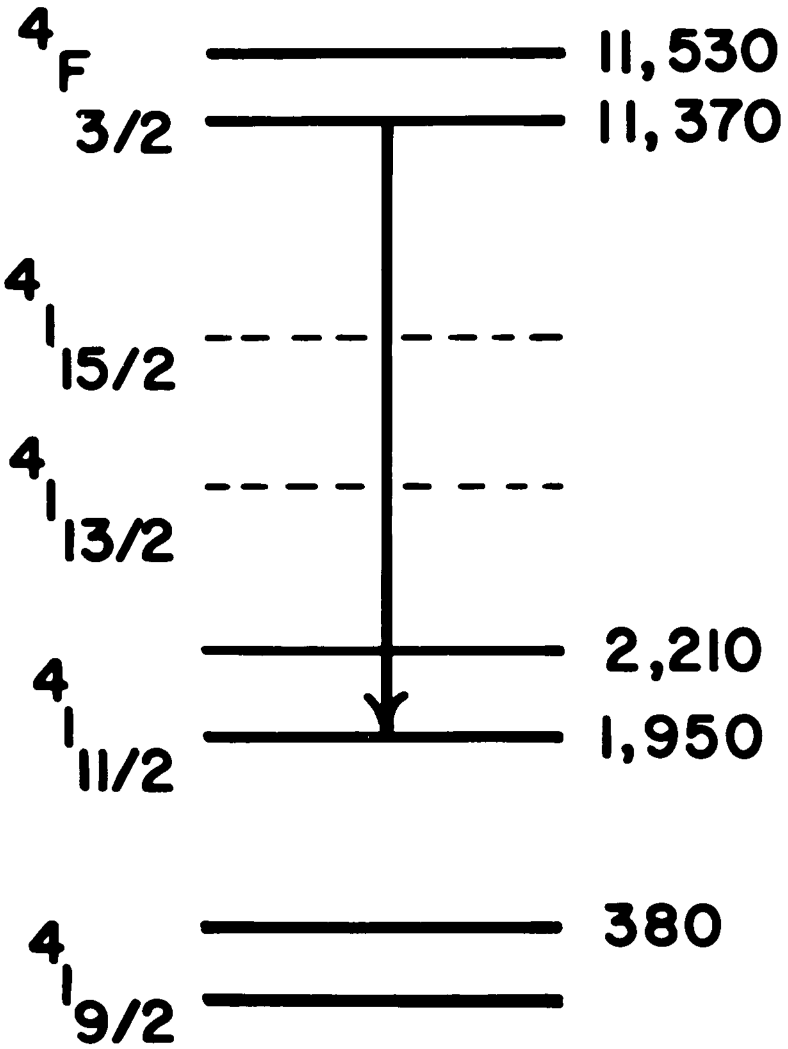

Fig. 2-3 Level scheme of trivalent neodymium in soda lime glass as far as derivable from present measurements. Arrow shows the strongest transition.

Presumably each "peak" contains several unresolved crystal field levels.(2-2) First, consider the optical absorption. At room temperature the prominent absorption occurs from the lower $^4I_{9/2}$ level to the two $^4F_{3/2}$ levels giving two peaks. In addition, there is some absorption from the upper $^4I_{9/2}$ level but it is weak since only about 14% of the atoms are in this state. At 80°K, the main peaks have about the same peak height ratio as at 300°K; this is to be expected from the level scheme. However, the absorption at long wavelengths has disappeared since only about 10^{-3} of the ions are now in the upper $^4I_{9/2}$ level. The energies of the two $^4F_{3/2}$ levels were determined from the two main absorption peaks. Next, consider the fluorescence. The two main peaks arise from transitions from the lower $^4F_{3/2}$ level to the two $^4I_{9/2}$ levels. The lifetime is long enough for thermal equilibrium to be achieved in the excited states so about 30% of the excited ions occupy the upper $^4F_{3/2}$ state at 300°K. The 8970 Å and 8680 Å bands are therefore weakened by the occupation of the upper $^4F_{3/2}$ level. At low temperatures, the two weak peaks disappear since the upper $^4F_{3/2}$ level is practically empty. There is an unexplained small wavelength difference between the fluorescence and absorption peaks, so the energy of the upper $^4I_{9/2}$ level was obtained from the separation of the two main fluorescence peaks.

The steady state fluorescence around one micron at 300°K and 80°K is given in Fig. 2-4. The 80°K curve with the two peaks shows that the $^4I_{11/2}$ state is split into two groups. It was shown above that the fluorescing $^4F_{3/2}$ state is also split into two groups of levels spaced to have the upper partially occupied at 300°K but empty at 80°K. Transitions down from this upper $^4F_{3/2}$ group give a contribution on the low wavelength side of the two main peaks which appears to broaden the main peak at 300°K. Thus, the line

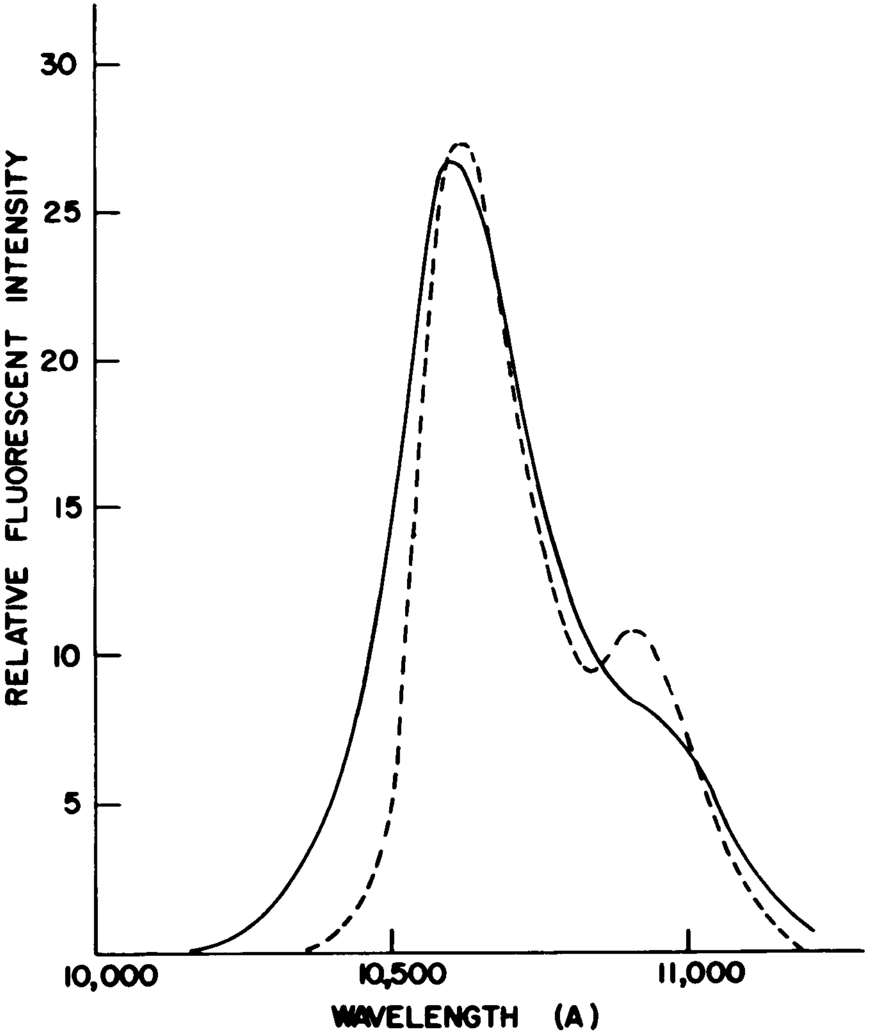

Fig. 2-4 Wavelength dependence of fluorescence around I for neodymium in a soda lime glass. Solid line, 300°K; dashed line, 80°K. These data have been corrected for the apparatus response and are on the same scale as those of Fig. 2-2.

narrowing at 80°K can be explained by static crystal field effects in the $^4F_{3/2}$ group and there is, as yet, no definite evidence of vibrational broadening in the spectra.

2.3 Quantum Efficiency of Fluorescence

The glass used contained 0.8% Nd_2O_3. A polished rectangular parallelepiped of this glass was exposed to the light of a sodium arc after that light passed through Corning Glass Works 3482 and 4600 filters. The rate of photon absorption was calculated from the optical absorption spectra of the sample and the measured intensity and spectral distribution of the sodium arc light. The rate of photon emission in the 1.06 micron fluorescence band was computed from the measured intensity and spectral distribution of photon emission. The ratio of these two rates is the quantum yield of photons in the 1.06 micron Nd^{3+} emission band. While this experiment is straightforward, there are several distinctly different measurements that must be made. For this reason, this report is organized as a series of small, independent experiments. The experimental details, as well as the necessary mathematics, for each of these small experiments are discussed below.

When the Nd^{3+}-containing glass is exposed to a constant light intensity, the quantum yield of photons in the 1.06 micron emission band is given by

$$\eta = \frac{E}{A} \tag{1}$$

where η is the quantum yield, A is the rate of photon absorption and E is the rate of photon emission in the 1.06 micron band.

2.3.1 Rate of Photon Absorption

The absorption spectrum of the Nd^{3+} and of the various filters was measured with a Cary Model 14 spectrophotometer. The relative spectral distribution of the photon flux from the sodium arc was determined with a calibrated monochromator. The absolute intensity of this sodium arc light was determined with a calibrated thermopile.

The spectral distribution of the sodium arc emission was measured by comparison with the intensity of light emitted by a General Electric 200 watt projection lamp operated at 96.7 volts. The filament of this lamp is at a color temperature of 2850°K and the relative spectral output of the lamp was available. The comparison of the two light sources was made with a Bausch and Lomb 500 mm focal length grating monochromator containing a 300 lines/mm grating. The grating was used in orders 1 to 4. The monochromator output was measured with an RCA 931 A photomultiplier at wavelengths less than 7000 A and an RCA 7102 photomultiplier, cooled to dry ice temperatures, at wavelengths greater than 7000 A. Table 2-1 gives the relative intensities of the sodium arc lines important here.

The absolute intensities of these lines at the sample were measured by replacing the sample with a calibrated, windowless Eppley thermopile connected to a galvanometer. The thermopile was calibrated against an Electronic Communications Inc. thermal radiation standard (TRS) operated at 1158°K. On the basis of this calibration, the intensity of the light at the thermopile is

2) $$I = 50.5\ D\ \mu\text{watts cm}^{-2}$$

I = incident light intensity

D = galvanometer deflection in mm

The standard deviation of I/D is 6-1/2%.

Table 2-1

Quantities Used to Calculate the Rate of Photon Absorption

i	Wavelength (A)	c_i	$P_i/\Delta D$	$A_i/\Delta D$
1	5670	0.024	3.7×10^{12}	0.4×10^{12}
2	5890	1.00	166	101
3	6160	0.014	2.5	.05
4	7700	0.27	58	3.5
5	8190	0.22	50	9

i = line number

c_i = intensity of line in watts/cm^2 divided by intensity of 5890 A line in watts/cm^2

P_i = photon flux at the sample in photons/cm^2-sec.

A_i = rate of photon absorption in photons/sec.

ΔD = total intensity of sodium arc light passed by C.G.W. 3484 filter but not by C.G.W. 2403 filter. The units are mm of galvanometer deflection.

The total intensity of the sodium arc light passed by a C.G.W. 3484 filter but not by a C.G.W. 2403 filter was measured with the thermopile. The absolute intensities of the sodium arc lines incident on the sample were computed from:

3) $$I_i = c_i \quad I_2$$

4) $$\Delta I = \sum_i \quad I_i \, \Delta T_i = I_2 \sum_i c_i \, \Delta T_i$$

I_i = intensity of the i'th sodium arc line

i = sodium arc line number (see Table 2-1)

I_2 = intensity in watts/cm^2 of the 5890 A sodium arc line

ΔI = total intensity in watts/cm^2 of the sodium arc light transmitted by the 3484 filter but not by the 2403 filter

ΔT_i = difference in per cent transmission of the 3484 filter and the 2403 filter

c_i = relative sodium arc line intensities

The values of c_i are listed in Table 2-1. The values of ΔT_i are determined from the transmission spectra of the filters. The value of ΔI is computed from Equation 2 and the difference in galvanometer deflections ΔD for sodium arc light transmitted by the 3484 filter but not the 2403 filter. The absolute intensities of the sodium arc lines at the sample are listed in column 4 of Table 2-1.

The photon absorption rate is calculated from the absorption spectra of the sample and its geometry by assuming that the sodium arc light incident on the sample is parallel. The surface of the sample normal to the incident sodium arc light had an area of 2.74 cm^2. The sample thickness was 0.745 cm.

The rate of photon absorption was computed from

5) $$A = 2.74 \sum_i A_i = 2.74 \sum_i a_i \text{ photons/sec.}$$

A_i = photon absorption rate due to arc line i

P_i = photon flux at the sample due to arc line i

a_i = fraction of incident photons absorbed

Multiple internal reflections were taken into account in computing the a_i's. The values of A_i are tabulated in Table 2-1. Most of the excitation comes from the 5890 A line. The 5670 A and 6160 A lines make a negligible contribution while the 7700 A and 8190 A lines contribute about 11% of the photons absorbed.

The contribution of the 7700 A and 8190 A lines was checked by measuring the intensity of the Nd^{3+} emission spectra at 1.06 microns when no filter, a 3484 filter, or a 2403 filter was interposed between the arc and the sample. Since the fluorescence intensity is directly proportional to the rate of photon absorption, these data could be used to compute the per cent of the total photon absorption rate due to photons transmitted by both the 3484 filter and the 2403 filter. The result was that these lines contributed 5% of the total photon absorption rate. The cause of the discrepancy between this number and the 11% contribution computed above is now known. Therefore, it is assumed that these infrared lines contribute 1/2 (5 + 11) = 8.0% of the total photon absorption rate. The value of this rate used in Equation 1 is

6) $$A = 302 \times 10^{12} \Delta D \text{ photons/sec.}$$

2.3.2 Photon Emission Rate

A point source of light radiates isotropically at a rate where r is

$$R_\lambda = 4\pi r^2 \quad I_\lambda \quad \text{watts/micron}$$

the distance in cm from the source to a detector at which the intensity is I_λ watts/cm^2-micron band width. The value of I_λ is measured by comparing the detector readings for the point source and for a source of known spectral distribution. If the TRS is used as the known source, then

$$R_\lambda = \pi \left(\frac{rD_s}{a}\right)^2 \frac{I_F}{I_B} W_\lambda$$

D_s = diameter in cm of TRS limiting aperature

a = distance in cm from TRS limiting aperature to detector

I_F = detector reading for Nd^{3+} fluorescence intensity

I_B = detector reading for TRS intensity

W_λ = black body emission rate in watts/cm^2-micron band width (see p. 23 of TRS manual)

The rate of photon emission in a band width d microns is

$$\frac{dE}{d\lambda}\, d\lambda = 1.58 \times 10^{19} \left(\frac{rD_s}{a}\right)^2 \left[\lambda \; W_\lambda \; \frac{I_F}{I_B}\right] d\lambda$$

integration yields

7) $$E = k\, c \quad \text{photons/sec.}$$

8) $$k = 1.58 \times 10^{19} \left(\frac{D_s r}{a}\right)^2$$

9) $$c = \int_{\lambda_1}^{\lambda_2} \lambda \; W_\lambda \; \frac{I_F}{I_B} \; d\lambda$$

In practice, it is convenient to define

$$f(\lambda) = \frac{1}{c} \lambda W_\lambda \frac{I_F}{I_B} \tag{10}$$

Equation 10 can be used to compute $f(\lambda)$ from the Nd^{3+} emission spectra without knowing the absolute intensity of the fluorescence. A measurement of the absolute intensity at one wavelength is then sufficient to determine c and E.

The experimental apparatus used to determine the photon emission rate is shown schematically in Fig. 2-5. Light from the sodium arc, after passing through the C.G.W. 3482 and 4600 filters, is absorbed by the Nd^{3+} in the glass. The fluorescence emitted at right angles to the incident sodium arc light is analyzed by the previously described monochromator. The monochromator receives light from all parts of the sample. The monochromator output strikes a fused silica plate having finely ground surfaces. All slits are removed from the photomultiplier housing so that the whole cathode of the RCA 7102 photomultiplier, cooled to dry ice temperature, receives light from the diffuse source on the fused silica plate. This arrangement for detection of the monochromator output eliminates the need to precisely align the optical components. C.G.W. filters, No. 2030 and 5030, were placed in the condenser lens system for the monochromator to limit detection to wavelengths in the near infrared.

After measuring the Nd^{3+} emission spectra, the sample was replaced by the previously described, calibrated thermopile in order to measure the total light transmitted by the C.G.W. 3484 filter but not by the C.G.W. 2403 filter. After this measurement, the thermopile was removed and the TRS was used to calibrate the detector system.

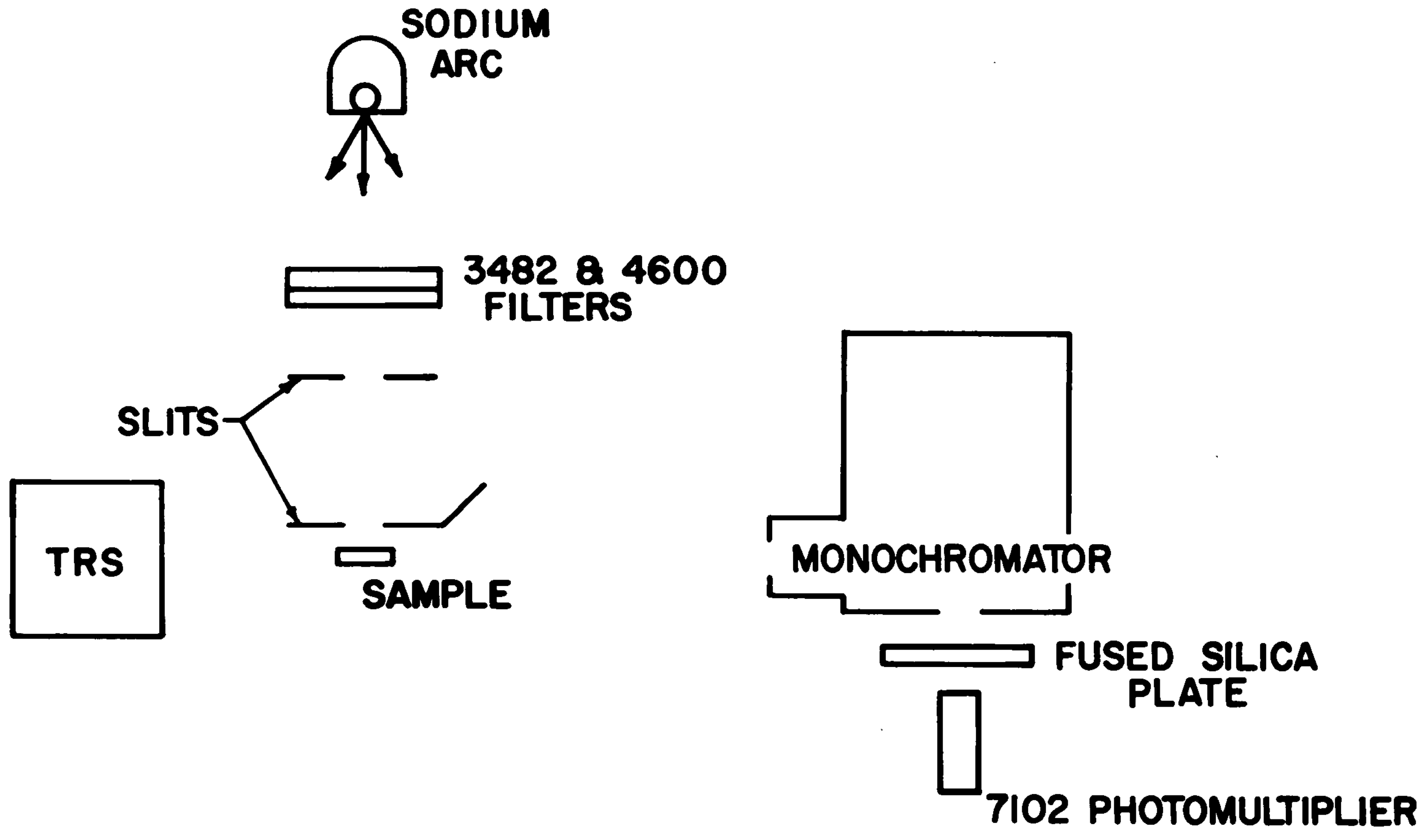

SCHEMATIC DIAGRAM OF APPARATUS USED TO MEASURE
THE Nd^{3+} FLUORESCENCE

Fig. 2-5 Schematic of apparatus used for quantum efficiency measurements.

Figure 2-4 shows the Nd^{3+} emission spectra in the 1 micron region. The ordinate is proportional to photons/cm^2-sec-micron band width. For this 1.06 micron band,

$$\frac{1}{f\ (10600\ A)} = 4.17 \times 10^{-2} \text{ microns}$$

with a standard deviation of 0.4%.

The absolute intensity of the Nd^{3+} emission at 1.06 microns was measured with $r = 53.5$ cm, $a > 41.0$ cm, and $D_s = 0.0996$ cm. From these data and from Equations 7, 8 and 10, the computed photon emission rate is $E = 2.6 \times 10^{14}$ photons/sec. when $\Delta D = 3$ mm. From this result and from Equations 1 and 6, the computed quantum yield of the 1.06 micron band is 0.29.

The accuracy of this quantum yield should not be over estimated. It is notoriously difficult to make quantum yield measurements accurate to two significant figures. The least accurate measurement made in obtaining this quantum yield was the measurement of the sodium arc intensity with the thermopile. The galvanometer deflection was only 3 mm. Deflections less than 1 mm are uncertain. Other errors arising from excitation with non-parallel light, from anisotropic emission by the sample, and from self absorption of the fluorescence emission band near 9000 A are probably small compared to the possible error in measuring the sodium arc intensity. Accordingly, a realistic value of the quantum yield is $= 0.3 \pm 0.1$.

2.4 Fluorescence Decay

The decay curve for this glass with 0.8% Nd_2O_3 added to the base composition is shown in Fig. 2-6. It is not a pure exponential -- the slope changes by a factor of three over the range examined. These measurements at

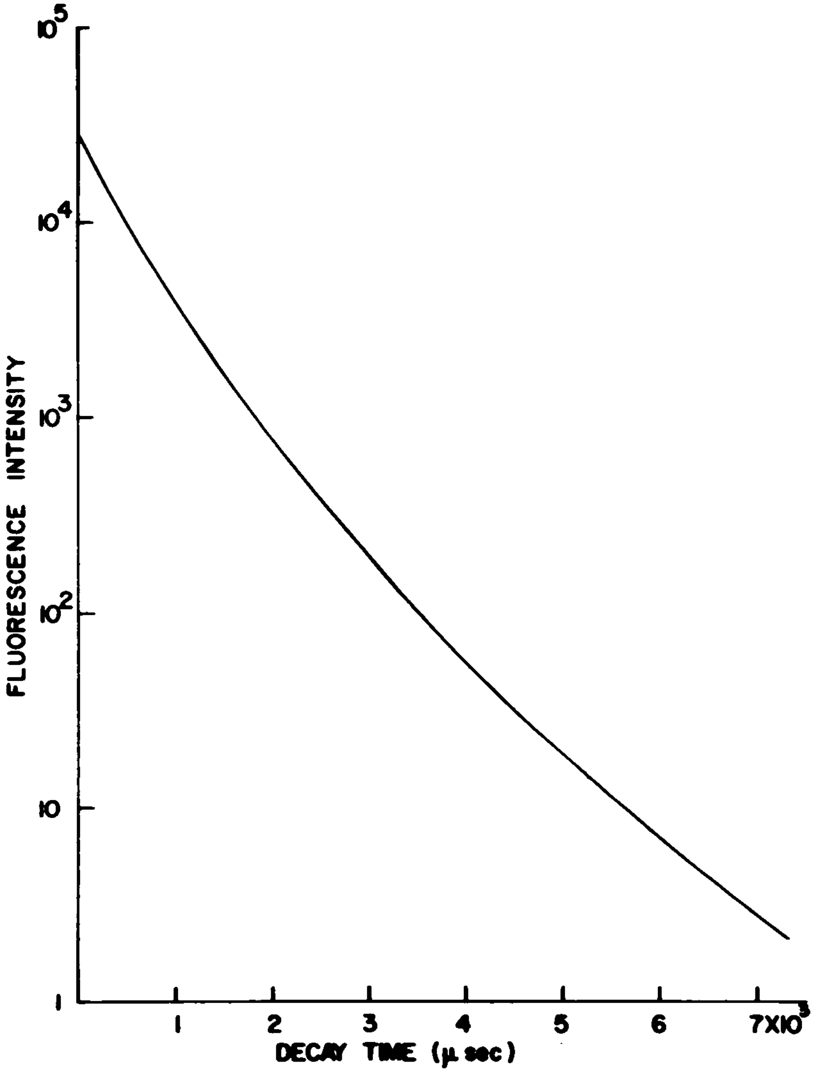

Fig. 2-6 Typical fluorescence decay of a soda lime glass containing 0.8 percent Nd_2O_3 by weight. Excitation was by xenon flash tube with 70 sec pulse.

long times were made with a mechanical shutter that shielded the phototube from the intense initial fluorescence. Where this was not done, hysteresis in the phototube gave spurious results. Variation of excitation by a factor of a hundred did not change the initial slope. In constrast to the glass, $CaWO_4:Nd^{3+}$ (2.5×10^{-4} atom fraction Nd) gave an exponential over a span ten times its lifetime of 160μsec.

The curvature of plots like Fig. 2-6 increases with neodymium concentration. On the other hand, the variation in lifetime indicated by this curve does not appear due to quenching of a portion of the ions and not of the others. For such an explanation, the longest lifetime would be representative of unquenched ions. The initial slope represents the major portion of the energy out so the quantum efficiency would be the ratio of initial to final slopes — or about one-third. Energy measurements, described above, yield a value of 0.3 ± 0.1 quanta in the 1.06 micron line for each quantum absorbed. Adding the quanta in the $^4F_{3/2} - {}^4I_{9/2}$, $^4I_{13/2}$, $^4I_{15/2}$ transitions from relative fluorescence intensity gives 0.7 ± 0.2 or greater. Absorption and re-emission of fluorescence can lengthen radiation decay times. But different geometrical shapes of the 0.8% Nd_2O_3 glass gave the same decay curve — a 5 cm x 5 cm x 0.5 cm slab irradiated on the large face and observed through the other large face, irradiated on edge and observed through the opposite edge, and a 0.5 cm cube were all equivalent. The decay may be tentatively assigned to a distribution of transition probabilities due to a distribution of crystal fields. The fluorescence is given by $F = \int_0^\infty Pe^{-Pt} \rho(P)dP$ where $\rho(P)$ is the number having a transition probability between P and P + dP. This may be inverted by well known transform methods but an approximation will suffice for the present.

Letting $\rho(P) = \sum_i N_i \delta(P-P_i)$, the curve may be fit by a series of equally spaced exponentials as shown in Fig. 2-7. The envelope gives an estimate of the distribution but the precision of the data must be greatly increased before the true shape can be ascertained. It is safe to say that Fig. 2-6 would require a distribution of transition probabilities about as wide as the mean value. In all that follows, "lifetime" will refer to the value obtained from the initial part of the curve.

Figure 2-8 shows the lifetime versus concentration of neodymium. Fluorescence quenching as shown here illustrates why values should be taken for low concentration in order to be more nearly characteristic of the glass matrix.

2.5 Application of Fluorescence Data to Some Stimulated Emission Processes

2.5.1 9100Å Stimulated Emission

The level scheme suggests the possibility of inducing optical maser action at low temperatures with the $^4F_{3/2}$ - $^4I_{9/2}$ transition. Such oscillations were obtained using 5-cm long cylindrical samples with dielectric end coatings that suppressed the 1.06 micron oscillation. Transmissions of the ends at 0.92 microns and 1.06 microns were respecitvely $< 1\%$ and $> 60\%$ for one end and $< 2\%$ and $> 80\%$ for the other. Threshold at 80°K, deduced from the typical output "spikes" on the oscilloscope trace, was 700 J using an EG and G Model 513 Laser Stimulator with the sample in a clear dewar cooled by the flow of nitrogen gas. Under comparable experimental conditions, threshold for the 1.06μ oscillation would be of the order of 100 J. No oscillations were detected at room temperature with an input of 1100 J. At energies 50% above threshold, the stimulated emission spread over a range of about 80 Å centered near 9180 Å.

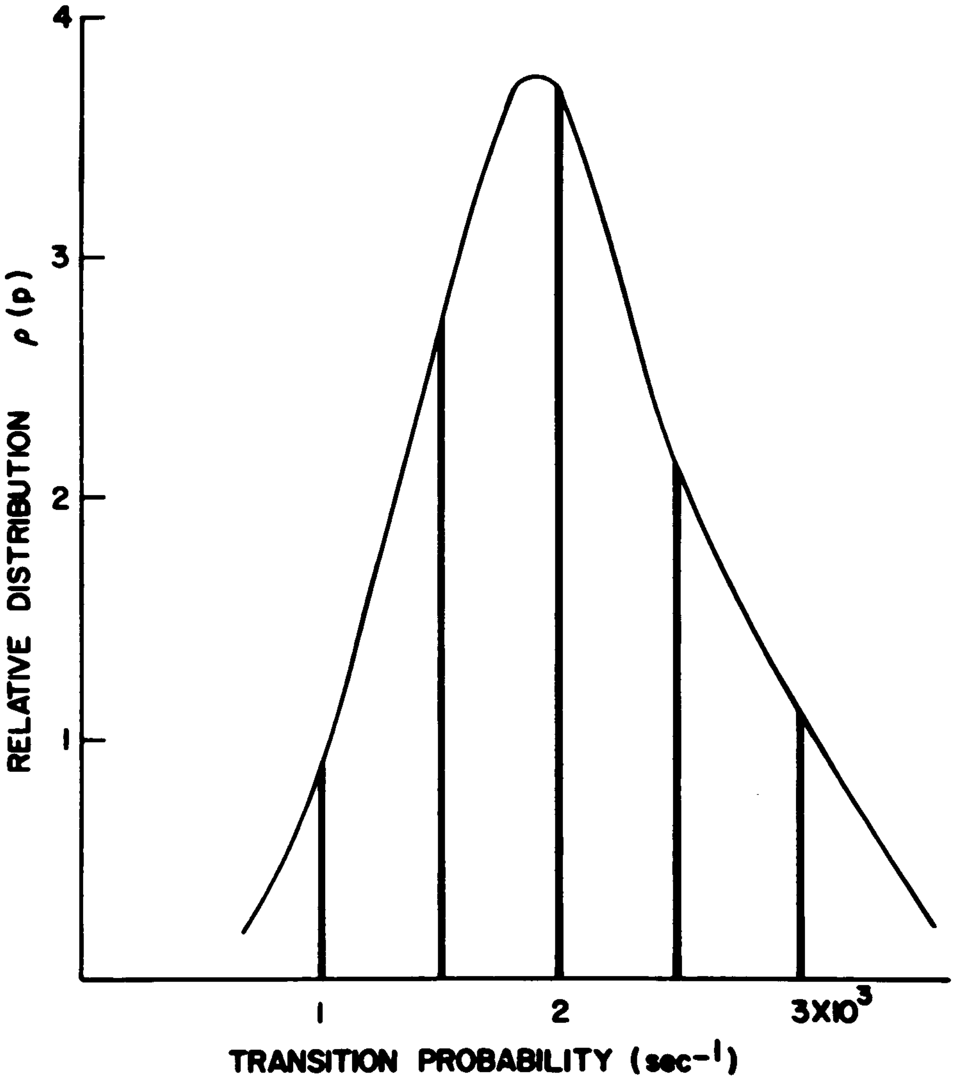

Fig. 2-7 Approximate distribution of transition probabilities which would be required to explain the curvature of Fig. 2-6.

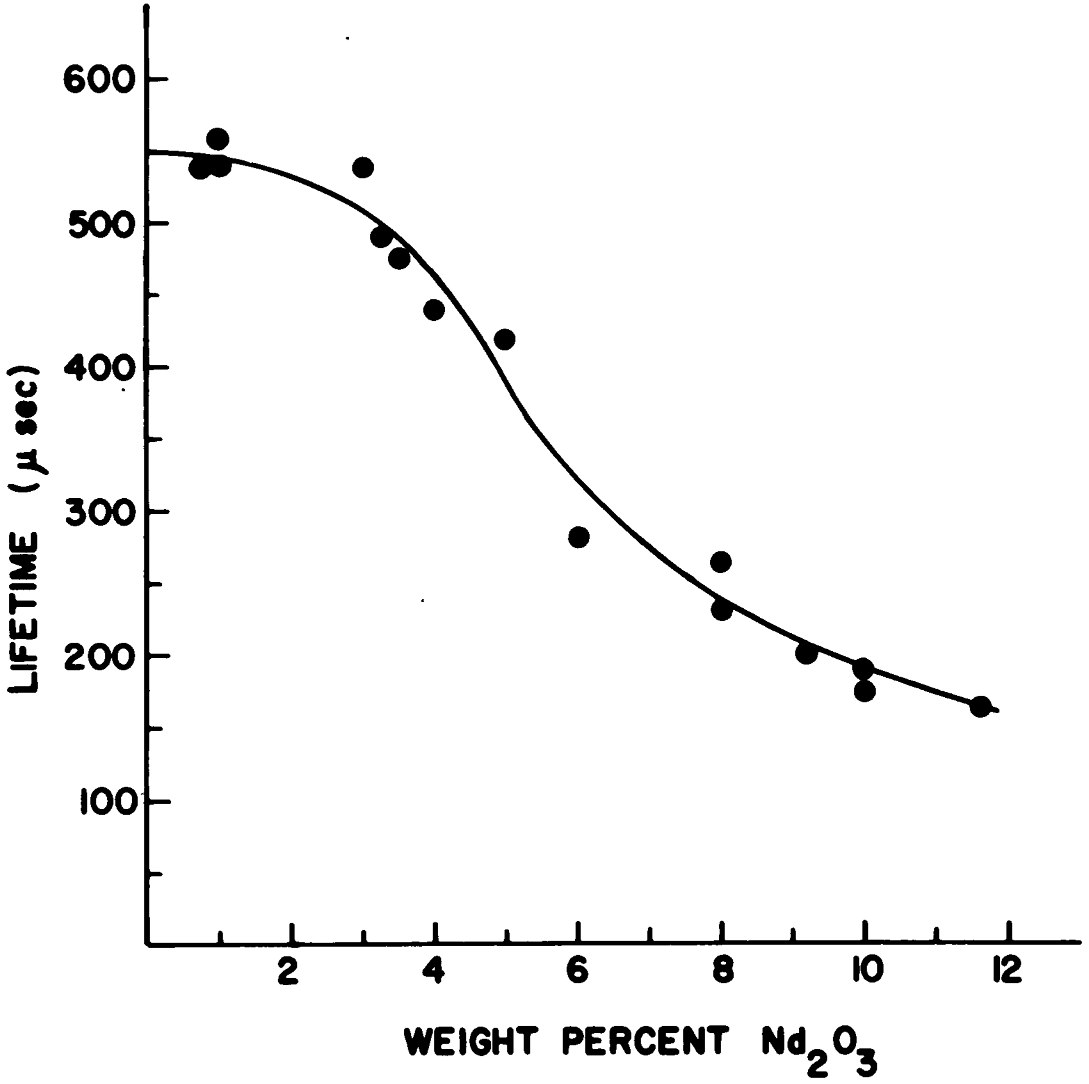

Fig. 2-8 Fluorescence lifetime versus concentration of neodymium oxide in a soda lime glass.

2.5.2 Maximum Gain Cross Section

First, the fluorescence peak and the stimulated emission process will be considered to arise from a two state transition; the accuracy of this approximation has been examined by Fowler and Dexter.

Then

$$\int \sigma \, d\nu = P\lambda_0^2 / 8\pi\eta^2 \qquad (1)$$

with σ the cross section for absorption of stimulated emission, P the transition probability, λ_0 the free space wavelength, and η the index of refraction. The number of ions (cm^{-3}) in the excited state, n, can be related to the losses and gain cross section at threshold by setting

$$R_1 R_2 \exp\left[(n\sigma_m - \alpha_i)2l\right]$$

equal unity, where α_i is the absorption due to internal losses and $R_1 R_2$ is the product of the end reflectances. Taking the reflectances as near unity and expanding the exponetial, all the losses may be expressed by $\alpha_t = \alpha_i + \alpha_e$ where $\alpha_e = (1 - R_1 R_2)/2l$.

A special case of interest is that of very short pumping pulses so that the spontaneous emission losses may be neglected. Consider a first experiment in which threshold is measured and a second one where the output energy is measured with input electrical energy, E, considerably above threshold. The resonator dissipates power via internal loss and output power.(2-4) Therefore, the total available energy, ϵ, for stimulated emission may be written $\epsilon_{total} + \epsilon_{out} (\alpha_e + \alpha_i)/\alpha_e$. Also, $\epsilon_{total} = (N_2 - N_1)h\nu$ with N_1 the total number of ions pumped to the excited state. Since $N_2 = (N_1 E_2)/E_1$ and $N_1 \sigma_m = \alpha_e + \alpha_i$, we have

$$\sigma_m = \left(\frac{E_2}{E_1} - 1\right) h\nu \alpha_e / \epsilon_{out} \qquad (2)$$

The internal losses need not be known.

Calculated and measured values of σ_m may be compared. Equation (1) provides the calculated values of the gain cross section. A more clear identification of the groups of states is obtained with the data at 80°K and this will be used for computation. The optical absorption at 0.88 microns gives a maximum absorption cross section of 6.12×10^{-21} cm^2 per ion. This, together with the ratio (1.33) of peak fluorescence intensity at 1.06 microns to that at 0.88 microns, gives $\sigma_m = 1.43 \times 10^{-20}$ cm^2. Another estimate can be made from the quantum efficiency measurement above if it is assumed that all quanta absorbed yield an excited ion in the $^4F_{3/2}$ state — e.i., there are no transitions from states above the $^4F_{3/2}$ to states below it. Experimentally, no such fluorescing transitions have been found. Then, $P = q/\gamma$ where q is the quantum efficiency for the 1.06 micron line and γ the measured lifetime. Substituting in (1) yields 1.21×10^{-20} cm^2. A measured value of 1.9×10^{-20} cm^2 was obtained from Eq. 7 using 30 microsec. pumping pulses with a laser having a spontaneous emission of 515 microsec. Independent estimates with longer pulses but subject to the same assumptions (which sets an upper limit on σ_m) have been obtained by measuring the ratio of input to output energy and the energy required for oscillation threshold for two different values of end plate reflectance.(2-5) High reflectance gave 1.1×10^{-20} and low reflectance 1.7×10^{-20} cm^2.

2.5.3 The Wavelength Spread of Stimulated Emission

It has not yet proved possible to predict the wavelength spread of stimulated emission from the fluorescence line shape. Figure 2-9 shows the output spectrum for increasing levels of excitation.(2-6) Multimode

Fig. 2-9 Stimulated emission spectrum of neodymium in soda lime glass for various excitations above threshold.

phenomena are easily apparent because of the wide wavelength range over which stimulated emission occurs. The third line, for example, shows a large number of frequencies from only 6 or 7 "spikes". For short lasers, series of individual lines have been found with a spacing of 0.2 A — equal to the calculated difference between adjacent axial modes. Figure 2-10 shows the wavelength spread of stimulated emission for various levels above threshold.(2-6) Some inference that the 1.06 micron fluorescence is an inhomogeneous line has been given above. If the individual components were very narrow compared to the line width, the frequency spread versus input energy should follow the line shape. That is, at double threshold the frequency spread of stimulated emission should be equal to the width of the fluorescence line at half maximum. Cross relaxation will feed energy into the central part of the line but the line narrowing occurs at concentrations lower than where appreciable interaction effects appear in the lifetime (Figure 2-8). Figure 2-10 for glasses with 1.5% Nd_2O_3 and 4.5% Nd_2O_3 did not show a narrower spread of stimulated emission at higher concentration when operated at the same fractional increase over threshold. Another possibility is that the main fluorescence peak at 1.06 microns has several crystal field components for a single ion. Stimulated emission will occur at the strongest transition and eliminate the ion's contribution in other crystal field transitions near the edge of the line. The strongest transition would have to be ≈ 70 Å wide.

3. STUDY OF THE SPECTRAL PROPERTIES OF Nd^{3+} AS A FUNCTION OF GLASS COMPOSITION

3.1 Composition Selection

A systematic study of glass composition to find the best glass host for neodymium must necessarily include as many devices as possible to change the

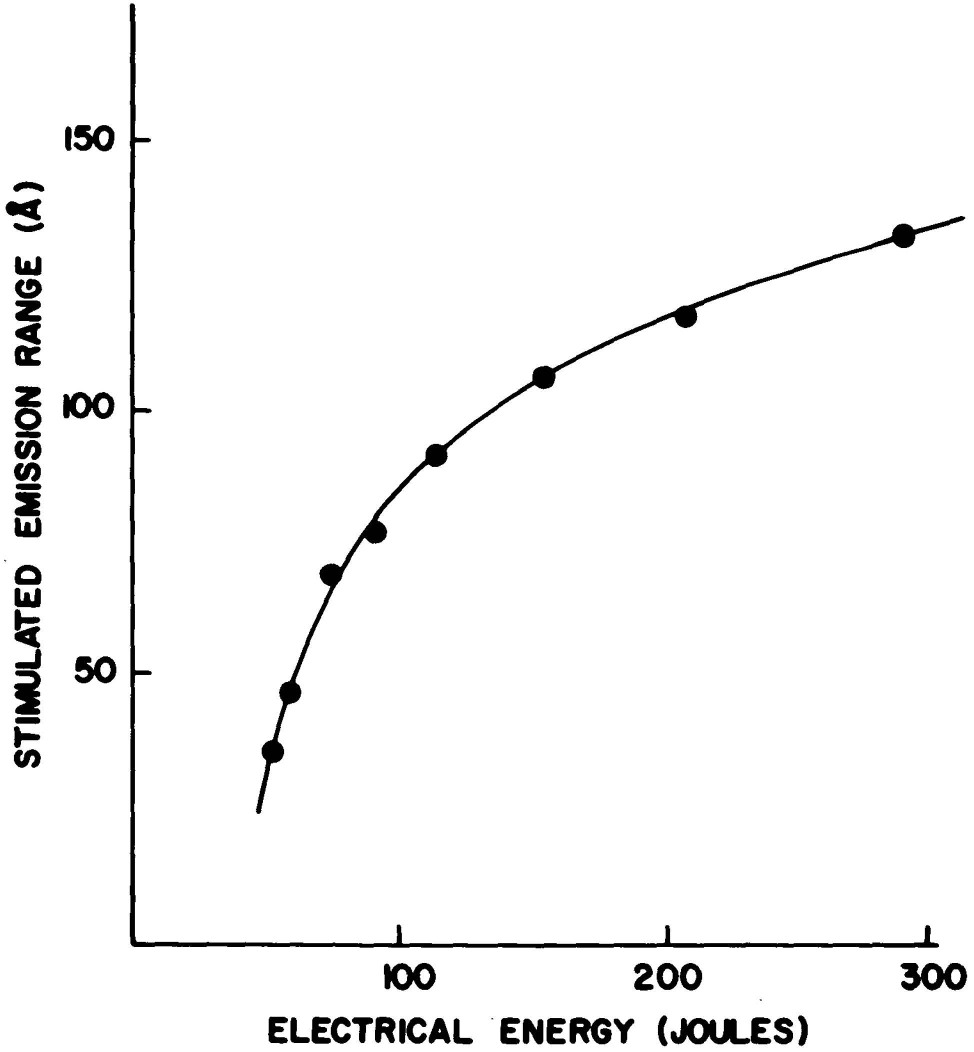

Fig. 2-10 Wavelength spread of stimulated emission, illustrated in Fig. 2-9, versus input electrical energy.

neodymium environment. Perhaps the best way to approach an understanding as to the reason for the various compositions melted is to review breifly the fundamental nature of glass. A simple definition is proposed by A.S.T.M.(3-1): "Glass is an inorganic product of fusion which has cooled to a rigid state without crystallizing."

The properties of glass are determined primarily by the nature of the anions and cations and their arrangement. By far the most important anion is oxygen although glasses of minor technical importance can be made using other anions such as fluorine or sulfur. Cations are classified as network formers, modifiers, and intermediates. A network forming cation is one which can form a vitreous oxide in a three-dimensional random network; the most important are Si^{+4}, B^{+3}, P^{+5} and Ge^{+4}. Modifying cations are those which break network bonding and fit into holes in the network thus modifying glass properties. Intermediate cations are those which can either fit into the network itself or assume a modifying position depending on the type and concentration of other cations present. Aluminum is an example of an intermediate cation. A more complete discussion of the structure of glass may be found in the original paper of Zachariasen(3-2) who first proposed the random network theory of glass structure and in monographs by Stanworth(3-3), Stevels(3-4), and Jones.(3-5)

The properties of glass can be roughly divided into two categories: those related to size and volume or packing effects, and those related to orientation and bonding characteristics. Properties of the first type, such as density and refractive index, usually show an additive relationship or linear correlation with properties of the individual constituents. For example, density, in general, increases with increasing atomic weight of components as does refractive index. A glass containing a given amount of calcium oxide would have a lower density and lower refractive index than the analogous glass containing barium oxide in place of calcium oxide. The second category includes properties which have a relaxational character such as viscosity and dielectric and mechanical losses, and properties which depend directly on the entropy changes of the systems such as thermal expansion. These will be covered in more detail in the discussion of specific types of glasses.

The subject of glass properties and their correlation with composition is very extensive; therefore, this discussion will only outline very briefly the general characteristics of the glasses studied. Probably the best single sources of detailed information on glass properties are monographs by Morey(3-6) and Volf.(3-7)

One of the chief advantages of glass over crystal for laser applications is that physical properties can be tailored to specific applications. The most pronounced differences in properties are between glasses with different network formers. A few very general statements can be made regarding a comparison of characteristics of glass forming systems. Of course, specific properties are very dependent on type and amount of modifying ions.

(1) Silicates - high melting, high viscosity, low thermal expansion, good chemical durability (except in hydrofluoric acid) the widest range of stable glass compositions.

(2) Borates - low melting, low density, poor infrared transmittance, good ultraviolet transmittance, poor chemical durability, higher thermal expansion than silicates.

(3) Phosphates - low melting and very fluid, relatively high thermal expansion, poor chemical durability except resistant to hydrofluoric acid, good ultraviolet transmittance, high refractive index for a given chromatic dispersion compared to silicates.

(4) Germanates - lower melting and lower viscosity than silicates, higher thermal expansion, high density, high refractive index and dispersion, poor ultraviolet transmittance but best system in infrared, poor chemical durability.

Since silica, by far, is the best glass former due to the wide variety of compositions which produce stable glasses of good quality, the major portion of the composition work emphasizes silicates. The following summary lists some of the major glass types and the effect of composition changes on their properties.

(1) Soda Lime Glass: Network Former - SiO_2
Network Modifiers - Na_2O
CaO

This system provides an easy starting point since melting to good quality glass is readily accomplished and many modifications can be made without moving out of good glass areas. At a given silica level substitution of heavier alkaline oxides for soda or heavier alkaline earth oxides for calcia results in increasing thermal expansion, density, and refractive index. At most silica levels, substitution of lithia for soda results in opal glasses.

(2) Aluminosilicate and Borosilicate Glasses:

Network Formers - SiO_2, B_2O_3
Intermediate - Al_2O_3
Network Modifiers - Na_2O, MgO, CaO, BaO

The prediction of properties of glasses containing alumina and/or boric oxide is slightly more complicated than for the soda lime system due to the dual nature of both alumina and boric oxide in glass. Boric oxide is a network former and the boron may assume either a planar three coordination or a tetrahedral four coordination depending on the amount of basic oxides (modifiers) present. This effect, called the boric oxide anomaly, has been shown in alkali-boric oxide glasses(3-8, 3-9) and is evidenced by an anomalous change in properties as alkali is added to boric oxide changing the boron coordination from three to four. For example, as sodium oxide is added to boric oxide there is an initial decrease in thermal exapnsion (in silicate glasses expansion would increase) up to about 16 weight percent sodium oxide. At this point the expansion increases with increasing sodium oxide additions. The same type of effect holds true in borosilicate glasses.

Another characteristic of borosilicate glasses is the large area of liquid immiscibility; i.e., a phase separation occurs at certain temperatures creating two immiscible liquids. This is the basis of formation of Corning's reconstituted high silica glasses. An easily melted borosilicate glass which can be readily formed into various shapes is heat treated to cause phase separation. One of the phases is leached out with acid leaving a glass containing about 96% silica which is then fired to consolidate the structure. Products made from these glasses are sold under the VYCOR trade mark.

Borosilicates are characterized by a flat slope of the viscosity-temperature curve; i.e., fairly viscous at high temperatures but relatively low annealing points. They also have low thermal expansion. Boric oxide is considered a good flux to facilitate melting of silicate glasses.

Aluminum also undergoes a change in coordination with increasing basic oxide content of a given glass. However, in a pure aluminosilicate glass aluminum assumes a six-fold coordination and acts as a network modifier. As basic modifying oxides are added the aluminum is converted to four-fold tetrahedral coordination and assumes a position in the silica network since silicon is also four-fold tetrahedral coordination. Once again such a phenomenon is evidenced by anomalous property changes.

Aluminosilicate glasses are characterized by high viscosity both at low and high temperatures and low thermal expansion. Alumina is noted for improving the chemical durability of glasses; even one or two percent has a marked effect on the durability of some glasses. If boric oxide is substituted for part of the alumina, meltability of the glass is improved.

At a given level of silica, alumina, and boric oxide, the effect of substituting heavier alkali oxides and heavier alkaline earth oxides for lighter ones results in predictable changes, as for the soda lime glass, with increasing expansion, density, etc.

(3) Lead Glasses: Network Former - SiO_2
Network Modifiers - Na_2O, K_2O, Cs_2O
PbO

Lead is rather unusual in its role in that it does not fit into the glass structure only as the usual modifying ions. Lead, in high concentration ranges, takes a position in the network coordinating to the oxygens of two silica tetrahedra. For this reason it is possible to introduce as much as 91.8 weight percent PbO in a lead silicate glass. One difficulty with lead glasses, particularly over 30 mole percent is the tendency of Pb^{+2} to reduce to Pb.

Lead glasses are relatively low melting and have low viscosities for silicates. They have high thermal expansion and high refractive index.

(4) Invert Glasses: Network Former - SiO_2
Network Modifiers - MgO, CaO, SrO, BaO, ZnO
(Possibly MgO and ZnO may act as intermediates)

Invert glasses were first proposed by Trap and Stevels and details of their nature may be found in the original papers.(3-10) Basically, they are glasses with a low amount of network former and a high amount of modifiers.

The Y factor is defined as the number of bridging oxygens per silica tetrahedron. The Y factor for fused silica is 4 and most commercial glasses have Y's between 3 and 3.4. Below Y = 2 it should be impossible to form glasses; however, this is the area where the invert glasses are formed. The method used to form glasses is based on adding a number of different modifying oxides so that, as the melt cools, the rate of structural rearrangement to form crystals is retarded and a vitreous state results.

The properties depend, of course, on the type of modifiers. With the system listed above, the glasses have relatively high annealing points but low viscosities at high temperature. Infrared transmittance is very good for silicate glasses. Density and refractive index are relatively high. Thermal expansion is moderately high.

(5) High Temperature Invert Glasses:

Network Former - SiO_2
Network Modifiers - ThO_2, La_2O_3, Ta_2O_5, BaO

These glasses have low silica content and require high melting temperatures. Annealing point, density, and refractive index are very high. The modifiers were selected not only because of their high molecular weights but also for their relatively low vapor pressures at high temperatures to minimize volatilization of batch constituents during melting. Some compositions in this field have a tendency to form opal glasses.

(6) Zirconia Containing Glasses:

Network Former - SiO_2
Network Modifier - Na_2O, ZrO_2

In general as zirconia content increases, the melting temperature increases. High zirconia glasses are difficult to obtain free of undissolved zirconia. Most glasses containing zirconia have good chemical durability.

The desirability of a complete composition search is often hindered by glass forming limits and other factors which do not permit proper evaluation of samples. The heating of a given combination of batch materials at a designated melting temperature may result in one of the following:

(1) the batch does not melt;
(2) the batch melts but devitrifies as it cools;
(3) the batch melts but opalizes as it cools either due to partial devitrification or formation of two immiscible liquids;

(4) the batch partially melts and on cooling forms a glassy material which contains one or more of the batch constituents undissolved resulting in crystalline inclusions called stones;

(5) the batch melts and on cooling forms a glass which contains many small gaseous inclusions called seeds (High viscosity at the melting temperature is an important factor which may cause seedy glasses.);

(6) the batch melts and on cooling forms a clear glass.

A glass may also contain more than one of the inhomogeneities described above. Another type of inhomogeneity affecting optical quality is cord or stria. Cord is defined by Shand(3-11) as "An attenuated glassy inclusion possessing optical and other properties differing from those of the surrounding glass". Stria is "A cord of low intensity, generally of interest only in optical glass".

One method of classifying glasses, particularly those used for optical applications, is on the basis of refractive index and dispersion. The dispersions of glasses are commonly compared on the basis of reciprocal relative dispersions at ν values (Nu values). ν values of most glasses fall between 20 and 70. Glasses with ν value less than 50 are arbitrarily classified as flints and above 50 as crowns. The flints and crowns are further classified as dense for high index and light for low index. In addition, a designation is often made as to the typical chemical constituent of the glass. For example, a dense barium crown would have a ν value over 50, a high refractive index, and would contain barium as the distinguishing constituent. Flint glasses usually contain lead, ranging from extra dense with very high lead content to extra light with low lead. Crown glasses often contain barium, with a high amount of barium in the dense crowns and low barium in the light crowns. A standard soda lime glass has low index and low dispersion and is classified as a crown.

We are not primarily interested in the dispersion and refractive index, therefore, we have not classified laser glasses in this manner.

The melting temperatures of the glasses were selected on the basis of composition and were in the vicinity of 1300°C to 1550°C. The batches were mixed by ball milling for four hours then placed in 500 cc. platinum crucibles for melting. A typical melting schedule was melt for one hour, stir for one hour using a platinum stirrer, soak for two hours, stir for one hour, then soak for one hour. The glass was then poured into a mold of about 2-1/2 inches by 8 inches which gave a thickness of 1 inch. The melting furnace was heated electrically using Globar rods. The hot glass was placed in an annealing furnace set at the estimated annealing temperature, held for one hour, then cooled at about 30°C per hour. The slabs were examined for sections of best optical quality for evaluation.

3.2 Measurements of the Spectral Properties

The results of measurements of neodymium glass fluorescence at 1.06 microns and of absorption at four selected bands are tabulated in Appendix A. The glasses listed in Appendix A are classified into 22 series by base glass composition.

Compositional variations within a base glass system are given in a column following the glass code number. In some cases, the glasses within a series will be seen to vary only in neodymium concentration, reported in units of 10^{20} ions per cc.

The column labeled "Relative Intensity" lists the relative fluorescent intensities of the 1.06 micron fluorescence line for each glass. The details of the measurement techniques and estimated precision will be given in Section 3.2.1.

The column labeled "τ" lists the spontaneous fluorescence decay lifetimes in microseconds measured at 1.06 microns.

The column "Calc. Rel. Pulse Thresh." lists the relative pulse thresholds of each glass, calculated from the measured relative intensities and the fluorescent lifetimes, using the expression developed in Section 4.

The column labeled "Meas. Thresh." lists measured thresholds in joules. Laser thresholds were determined with the EG & G Model 513 apparatus using ten flash tubes — two groups in parallel with each group consisting of five in series. The samples were resting in a Corning Code 7740 glass tube of 12.7 mm I.D. and 16 mm O.D.

The "full bank" capacitance of 160 microfarads was used, with a 60 second time lapse between successive pulses allowed to improve the reproducibility of the measurements. The threshold of any given sample was reproducible to a standard deviation in the measurement of 2%.

The laser rods themselves were polished with ends flat to 1/10 wavelength of visible light and parallel to 5 sec. of arc. One end was completely reflecting Ag coated, the other specified as 2% transmitting.

The column labeled $\Delta\lambda$ lists the measured width of the 1.06 micron fluorescence line at half-maximum, in Angstrom units.

The last eight columns list the absorption cross sections and absorption line widths of the four indicated absorption lines of neodymium in each glass. The line widths at half-maximum are given in wave numbers (cm^{-1}). The cross sections were calculated using the peak absorbance of the line occurring at roughly the indicated wavelength. In the case of the visible 5800 Å absorption, the line was often split, exhibiting two distinct absorption peaks. In this case, the wavelength at each on-scale peak is listed under the "σ" column, with its corresponding cross section under it. If the peaks were sufficiently resolved to permit measurement of separate widths at half-maximum, they are both given. For details of absorbance measurements and typical spectra, see Section 3.2.2.

3.2.1 Fluorescence Intensity and Line Width Measurements

Figure 3-1 is a block diagram of the measurement apparatus. The xenon lamp is an Osram 900 watt D.C. lamp focused by means of a spherical and an elliptical mirror to a spot on the sample face of about 1/2 inch diameter.

Interposed between the lamp and the sample is a 150 cycles per second sector chopper.

The sample is wedged by a spring into the corner of a sample box which admits the exciting light through a 3/4 inch by 3/4 inch hole and permits the escape of fluorescence light at right angles through a 3/4 inch high slit adjusted to a width of 1 mm. By looking at only the first millimeter of fluorescence from the sample we are justified in assuming that the effects of absorption are negligible. The box design prevents reflection of the exciting light from the sample edge into the monochromator, while permitting the emission from the leading face (to a depth of 1 mm.) to be measured. The arrangement requires a sample which has flat polished faces with at least one square corner including a flat polished edge at least 1 mm. wide.

We tested this equipment with seedy and cordy samples containing no neodymium in order to determine the magnitude of scattered exciting light which may have invalidated our measurements. The results showed that a maximum error within ± 10% could be expected from this source. The error is

FLUORESCENCE INTENSITY MEASURING EQUIPMENT

FIG. 3-1

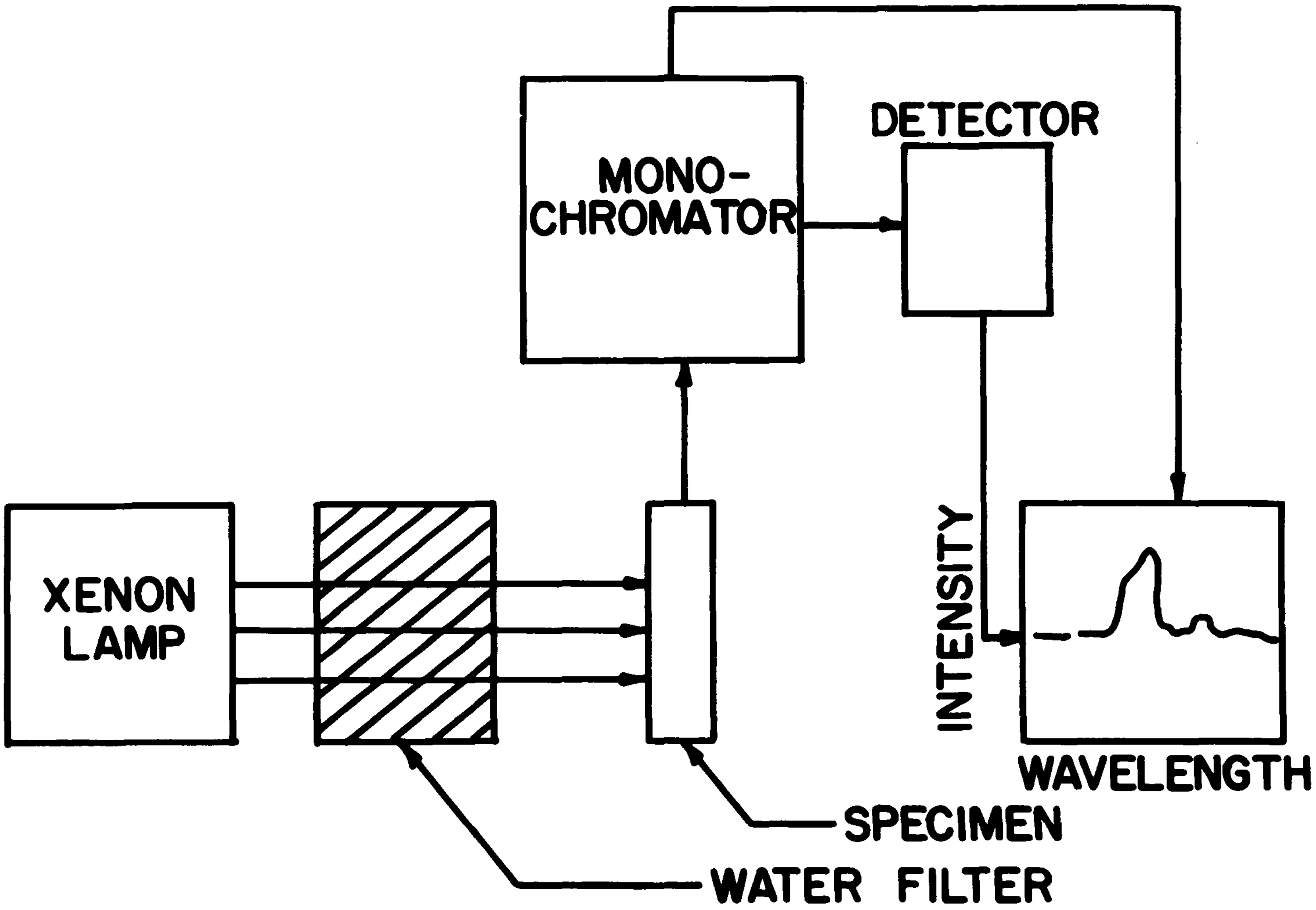

greater on samples having lowest fluorescence intensity, and compositions therefore, not of the greatest interest.

A mirror arrangement focuses the fluorescent radiation onto the entrance slit of a Leiss single pass vitreous silica prism monochromator. The entrance and exit slits are normally set at 0.05 and 0.04 mm., respectively. This provides a resolution of about 60 angstrom units in the vicinity of I micron for the examination of fluorescence lines which have invariably been greater than 200 Å wide.

A Kodak lead sulphide detector mounted at the exit slit provides a 150 cycle signal to a Princeton Applied Research model JB-4 lock-in amplifier. The 150 cycle reference signal to the amplifier is provided by a cadmium sulphide detector which monitors the exciting light reflected from the chopper wheel. The lock-in amplifier integrates the output signal over two seconds.

The D.C. output from the amplifier is fed to the Y axis of a Moseley X-Y recorder.

For relative intensity measurements, the X axis of the recorder is made inoperative, while the monochromator is slowly scanned through the 1.06 micron line. It takes thirty seconds to scan between the half-maximum points of a 300 Å wide line. The record then consists of a straight line of length proportional to the peak emission intensity of the sample. This length is compared to that obtained from a "standard" sample which is run periodically for comparison. The "standard" sample was chosen to be free of solarization and have a "normal" intensity (268 on our relative scale).

Short term instabilities in the excitation-detection-amplification system and orientation effects for inhomogeneous samples combine to give a reproducibility in intensity measurements estimated at ± 10%. Measurements on a given glass of reasonable quality reproduce to better than 5%.

Most samples become warm during a run, and some become quite hot. Measured intensity falls off slightly with increasing temperature, so an attempt is made to scan over a narrow wavelength range centered on 1.06 microns.

Linewidths are measured similarly to intensities except that the X axis of the recorder is driven by a 40-turn Helipot across a Zener diode controlled source. The Helipot is geared to the monochromator drum, so that drum position can be read directly from the record. Representative spectra obtained are shown in Figure 3-2. These spectra are direct records, uncorrected for instrument response.

3.2.2 Spectral Absorption Measurements

A Perkin-Elmer Corporation Model 350 spectrophotometer was used to measure spectral transmittances in three ranges from 200 to 2700 millimicrons wavelength. The quantity recorded was the common (base-10) logarithm of the reciprocal of spectral transmittance, plotted as a function of wavelength. This quantity does not have a standard designation; the term "spectral absorbance" applies to the common logarithm of the reciprocal of internal transmittance, i.e., the transmittance corrected for superficial losses. Such correction is not necessary for comparing the spectral absorption properties of various glasses whose refractive indices are similar. Except where great accuracy is required, even this qualification may be ignored. Although true absorbance was not measured or recorded, it is customary to say that the measurement was made on the absorbance scale of the spectrophotometer, and this term will be used to discuss the accuracy of the results.

Both wavelength accuracy and spectral resolution are functions of the

FIG. 3-2

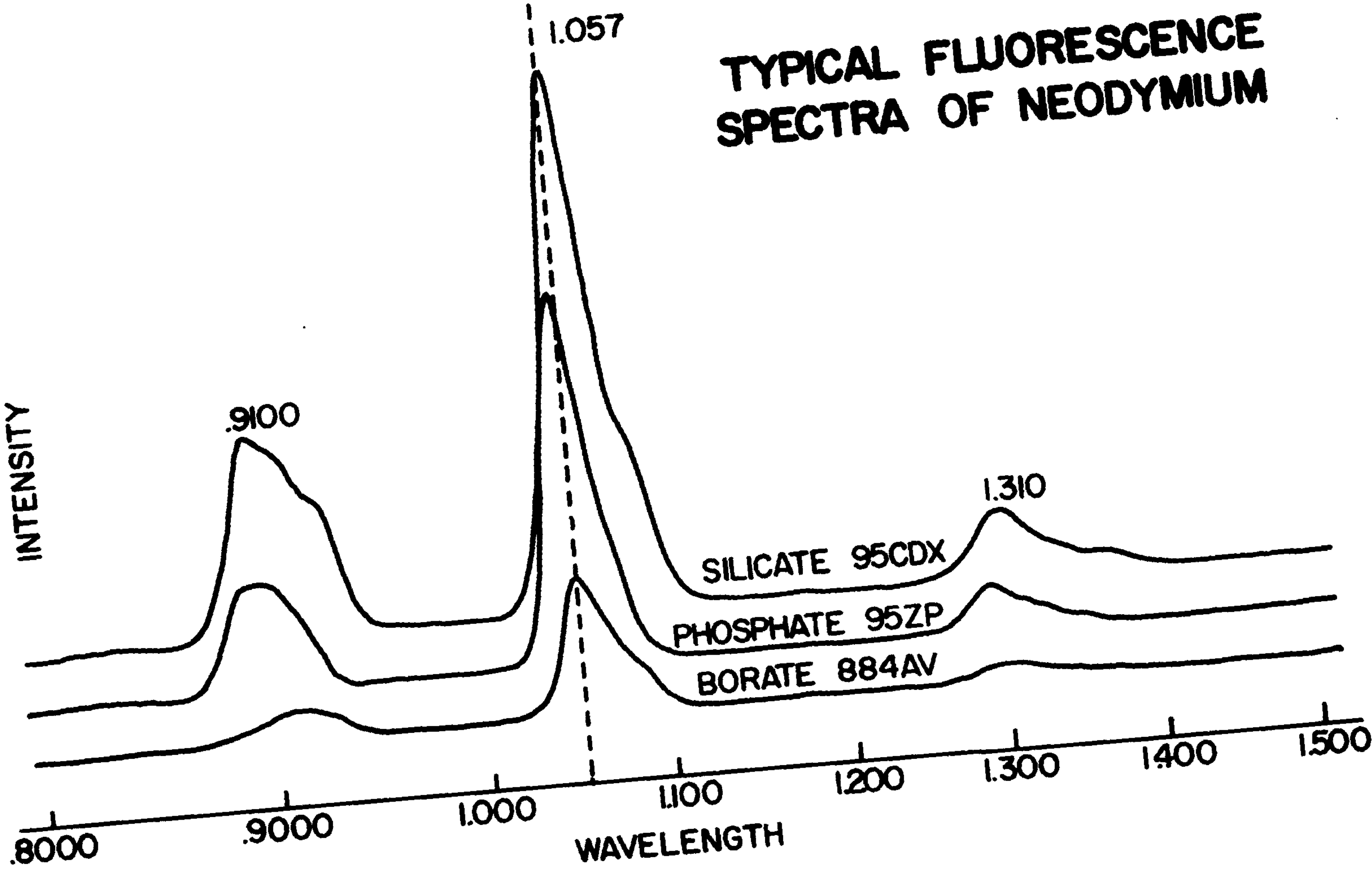

TYPICAL FLUORESCENCE SPECTRA OF NEODYMIUM wavelength of measurement, and photometric accuracy is a function of the reading of the absorbance scale. Wavelengths read from the chart record are accurate within 0.1%, throughout the ultraviolet, visible, and near infrared spectral regions. Resolutions are better than 3 millimicrons in the near infrared region, 1.5 millimicrons in the visible region, and 0.5 millimicrons in the ultraviolet region. Photometric accuracy is better than 3%, after compensation is made for the I_o (zero absorbance) reading.

Since the present measurements were of a survey nature, no attempt was made to achieve accuracy beyond about 2% in wavelength, line width, and absorbance.

A standard sample thickness of five millimeters was chosen to keep most absorption peaks within the 0-2 absorbance scale of the spectrophotometer. Those samples which gave off-scale readings were not repeated except in cases of special interest.

The reported cross sections were arrived at by recording the peak "absorbance" at roughly the indicated wavelength and substracting an amount corresponding to the base line in the vicinity of the peak. Multiplication by 2.3 and division by the sample thickness times the Nd concentration in ions per cc gave a cross section of the order of 10^{-20} cm^2. Since the peaks at 3500 Å and at 8800 Å were relatively weak, those cross sections were subject to greater error than those at 5800 Å and 8000 Å, which usually ran closer to mid-scale or full-scale.

Figure 3-3 shows a typical set of "absorbance" curves.

3.2.3 Experimental Lifetime Measurements

The experimental setup for the measurement of fluorescence lifetime is shown schematically in Figure 3-4. The flash tubes are two General Electric

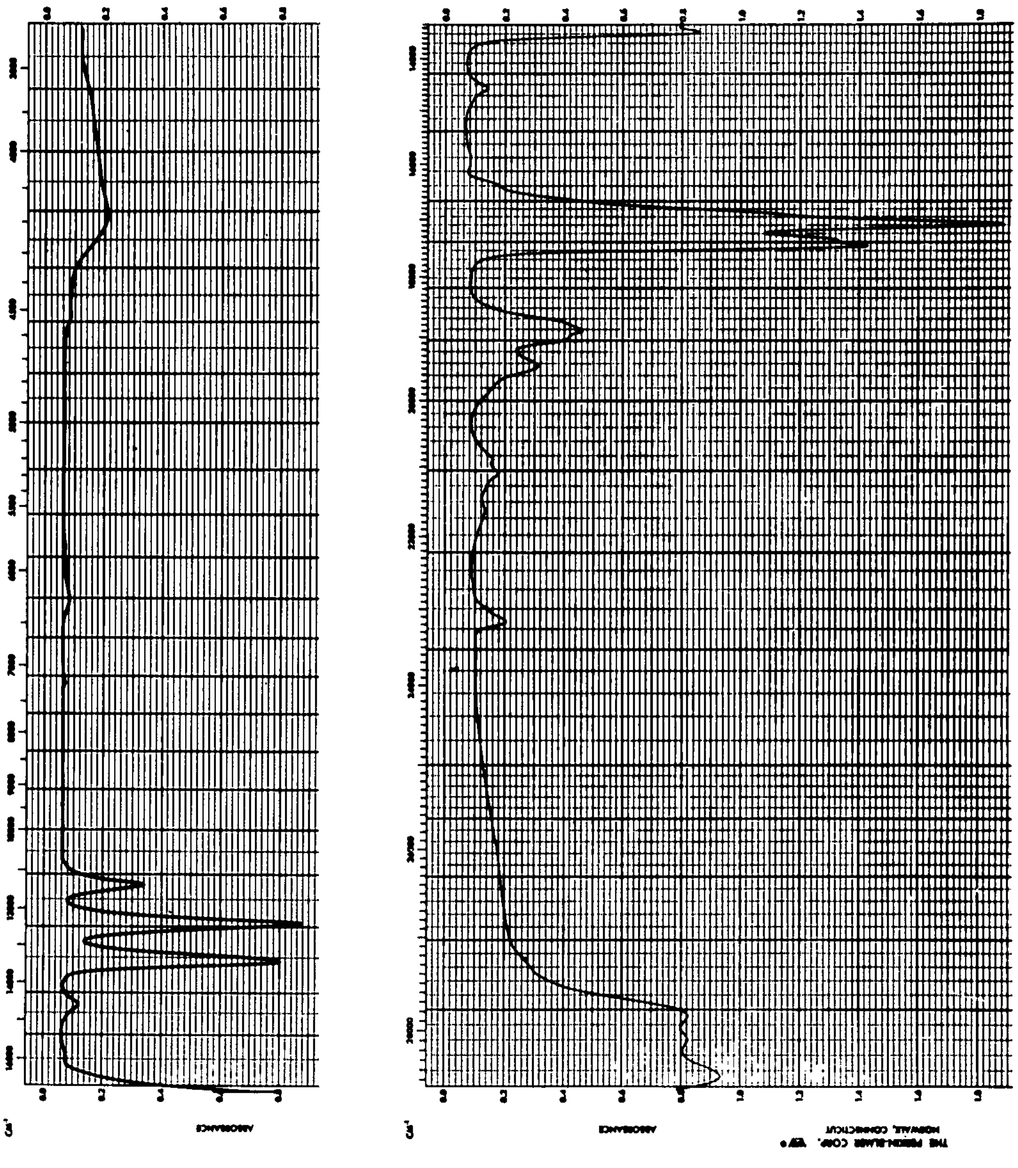

Fig. 3-3 Typical absorbance spectra of neodymium in glasses.

FLUORESCENCE LIFETIME MEASURING EQUIPMENT

FIG. 3-4

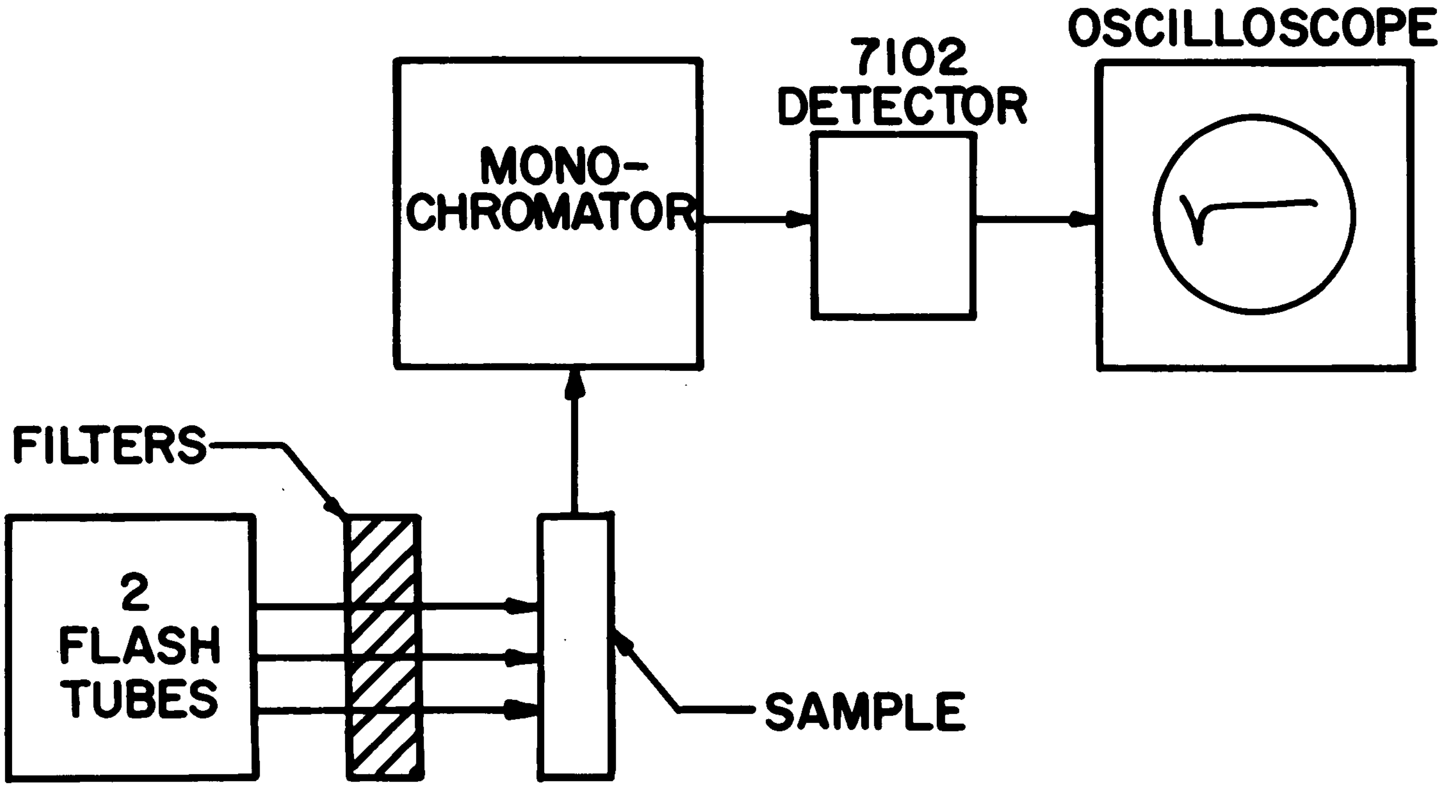

FL91 tubes connected in parallel, with an output of about 100J and a time constant of about 40μsec. The filter is a heat absorbing glass (CGW 4600) to filter out the energy above 1 micron. The monochromator is the same one that is described above. The detector is a RCA 7102 photomultiplier tube (S-1 surface), and was cooled by means of a jacket containing dry ice and acetone. The oscilloscope is a Tetronix model 555, equipped with a Polaroid camera. All fluorescence lifetimes were measured with a 200 sec delay from the onset of the flash unless otherwise noted.

The accuracy of the lifetime data reported here is estimated conservatively at about ± 10%.

The liquid N_2 lifetime measurements were made by inserting a small glass dewar on the sample position. The sample was placed in the dewar and immersed into liquid N_2.

3.3 The Effect of Impurities on the Fluorescence Properties of Nd Doped Glasses

The concentration quenching effect, that is the decrease in fluorescence lifetime with increasing Nd^{+3} concentration, has been observed in all glasses that have been investigated in this work. The degree of this quenching depends on the particular glass forming system, e.g., the borate glasses quench at a much slower rate than the silicate but they have a very short lifetime even at low Nd^{+3} concentration.

The problem in this part of the program was to determine what role impurities play in this concentration quenching process. The investigation was made up of three parts, viz. 1) determination of the effect of very pure starting materials on the fluorescence properties of Nd laser glasses; 2) determination of which impurities have an adverse effect on the fluorescence properties and to what extent they must be present to cause significant changes in the fluorescent properties; 3) identification of the mechanism of the quenching action of these impurities, if possible.

3.3.1 Pure Glasses

To determine the effect of using pure starting materials on the fluorescence lifetime, a number of melts were made in the laboratory in small 50g batches. The glasses were melted in pure fused silica crucibles for about one hour at 1400°C. The melts were not stirred. The glasses were poured onto a polished stainless steel mold into 1" x 1" slabs. The samples were annealed, and then ground and polished into 1" x 1" by 5 mm. samples. The base compositions of the glasses were $73SiO_2 \cdot 5CaO \cdot 22Na_2O$ by weight, $75SiO_2 \cdot 25Na_2O$ by weight and $Na_2O \cdot 2B_2O_3$ molar composition. A list of the raw materials used are given in Table 3-1.

Table 3-1

Supplier	Purity
Silica	
Light and Co.	99.999%*
Corning Fused Silica (Code 7940)	> 99.9
African Sand	99.9
52-S Quartz	99.6
Nd_2O_3	
Lindsay Code 629.9, Lot 0920	99.9
Lindsay Code 629.9, Lot 0701	99.9
Lindsay Code 629.9, Lot 1109	99.9
Michigan Chemical Co., Lot 71-11-00	99.99
Johnson, Matthey and Co., Lot 14062	99.98
Na_2O and CaO	
Baker Analyzed Reagents, of Na_2CO_3 and $CaCO_3$	purest available
B_2O_3	
Baker Reagent H_3BO_3	

* Our analysis of this material showed it to be less pure than the stated purity. The major impurities were 100 ppm Zr and 20 ppm Ca, atomic.

The purity of the Nd_2O_3 varied from supplier to supplier as well as from lot to lot as determined by our analysis of these samples. The purity of the Nd_2O_3 could play a large role in the concentration quenching effect since the Nd_2O_3 contains other rare earth oxides and other impurities that may well represent important quenching sites for the neodymium fluorescence.

Figure 3-5 shows the fluorescence lifetime vs. weight % Nd_2O_3 for the soda-lime-silicate glass using the various raw materials as listed. There are small differences in lifetime due to the purity of the listed starting materials but the overall quenching effect is still observed. It was found, however, that the homogeneity of the glasses had some effect on the lifetime measurement, i.e., the points on the curve corresponding to glasses that were made by a stirred melt method had a somewhat longer lifetime than those that were melted in the laboratory in small batches. The glasses made in the laboratory were usually of very poor quality and it is probable that a certain amount of compositional inhomogeneity existed. For the poorest quality glasses the lifetime varied by 5-10% depending on the orientation of the sample. For the stirred melt glasses this effect was not observed. A chemical analysis of a representative set of the glasses is presently in progress, but at the time of the writing of this report, the analyses are not yet completed. The purity of these glasses is expected to be quite good considering the purity of the raw materials and the method of melting. Therefore, if the quenching mechanism is an impurity sponsored effect, the level of the impurities does not have to be very high to cause quenching. Also in Figure 3-5 the relative fluorescence intensity at 1.06μ vs. wt. % Nd_2O_3 is plotted. The shape of this curve is what would be expected where two competing and opposing processes are occurring, viz., the increasing

FIG. 3-5

LIFETIME VS. WT. % Nd_2O_3
IN SODA-LIME-SILICATE
22 - 5 - 73

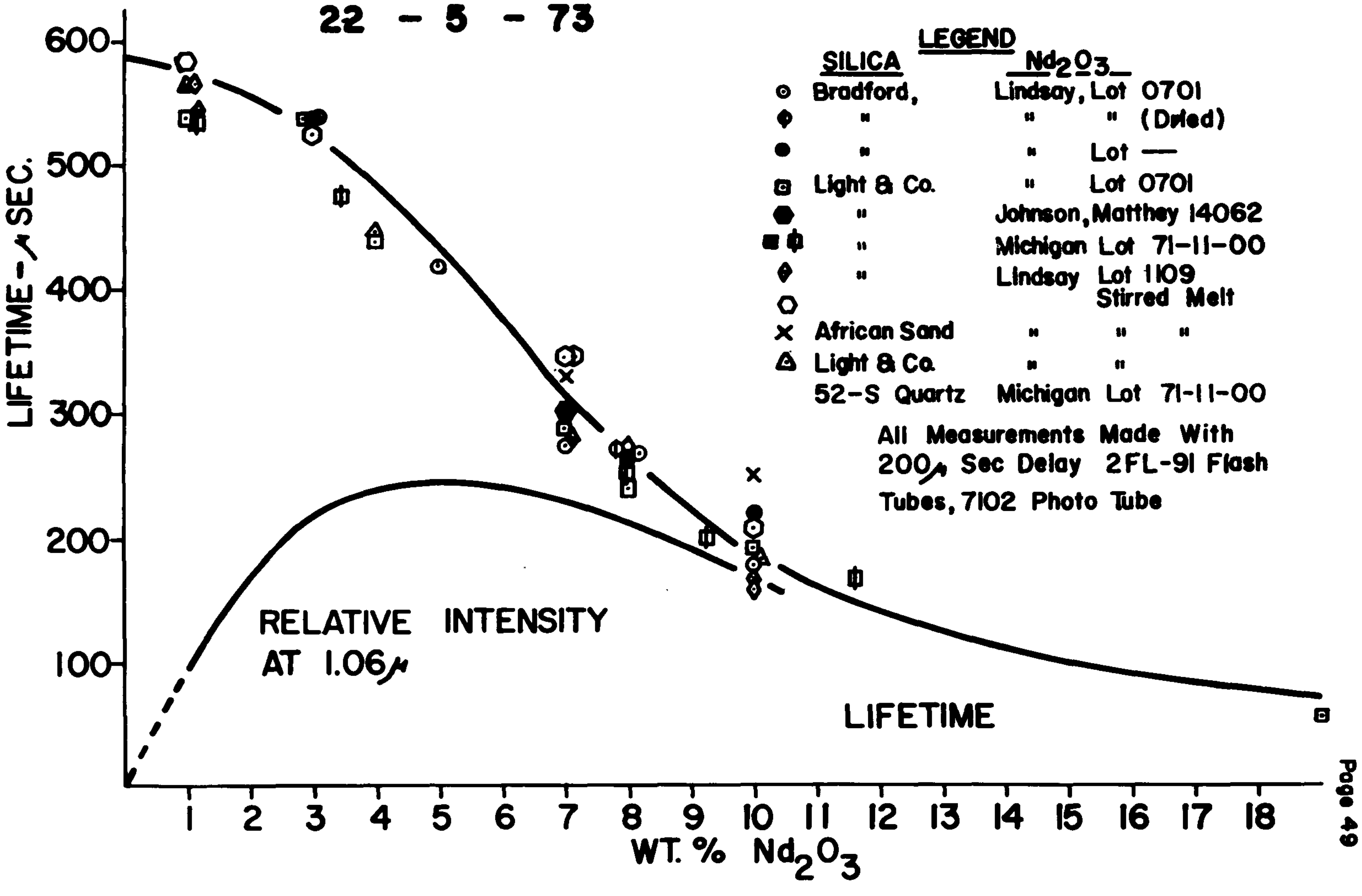

concentration of Nd^{+3} tends to both increase the intensity due to the increase in the number of fluorescing sites, and decrease the intensity due to its part in the quenching process.

Figure 3-6 shows a graph of the lifetime of a soda silicate glass vs. wt. % Nd_2O_3, for a number of different sources of Nd_2O_3 and silica. There is for the most part, a certain amount of scatter in the lifetime data but it is difficult to ascertain how much is due to the relative purity of the individual glasses. One exception to this, however, is a series of glasses made with Light and Co. silica and Lindsay Lot 0920 Nd_2O_3. These glasses show much less quenching than the other glasses melted to date, e.g., at 7% Nd_2O_3 the Lot 0920 glass had a lifetime of about 500 sec while ordinarily at this Nd_2O_3 level the lifetime would be about 400 sec. The 0920 Nd_2O_3 used in these glasses has been analyzed but no obvious conclusions can be drawn as to the cause of the longer lifetime from the standpoint of purity. However, analysis of all the sources of Nd_2O_3 used have not as yet been completed.

On Figure 3-7 is plotted the lifetime vs. wt. % Nd_2O_3 for a pure sodium borate glass. It is known that the borate glasses exhibit a very short lifetime and low fluorescence intensity, it was therefore of interest to see if these properties were due to impurities. The concentration quenching effect, as seen from Figure 3-7, is much less pronounced than that for the silicate glasses discussed before. The borate glasses present somewhat of an anomaly, since the absorption data show that the Nd absorption is quite strong yet the fluorescent intensity at all emissions is weak. This together with the short lifetime certainly suggest a quenching process. It has been suggested (3-12) that the borate network itself has something

FIG. 3-6

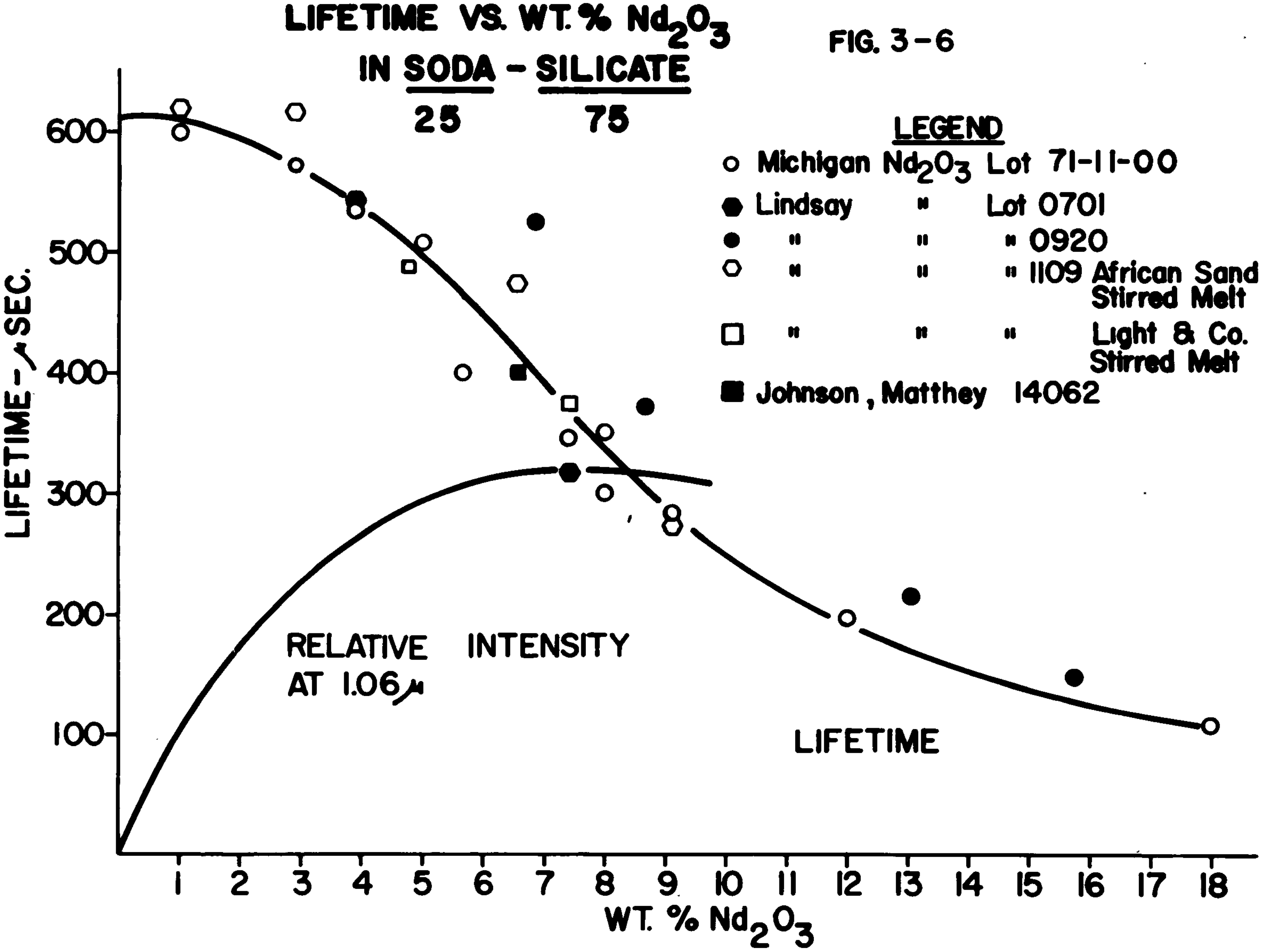

LIFETIME VS. WT. % Nd_2O_3 IN SODA - SILICATE 25 75

FIG. 3-7

LIFETIME VS. WT.% Nd_2O_3 IN $Na_2O \cdot 2B_2O_3$

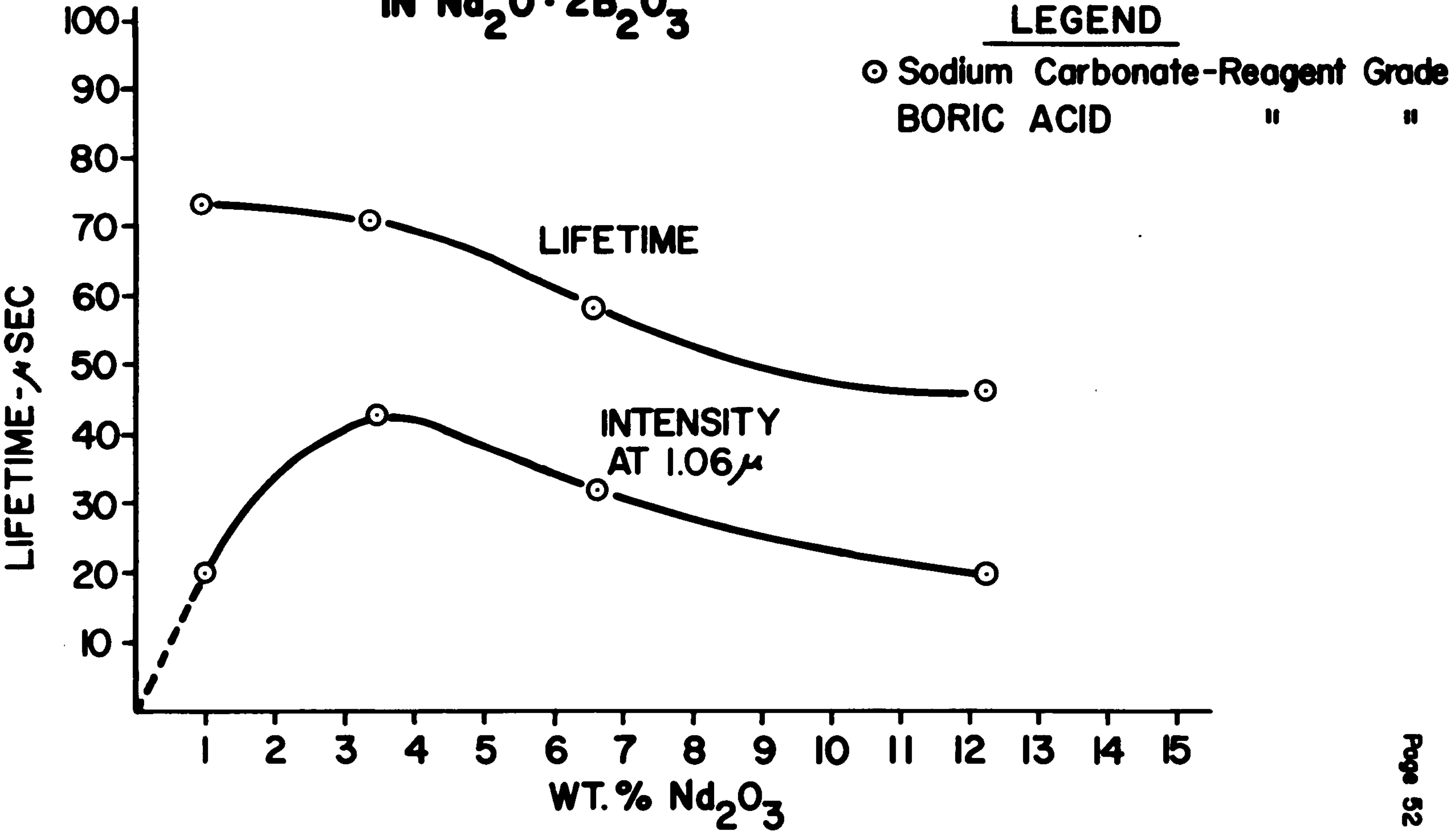

to do with the quenching process although it has not been stated clearly by what mechanism this quenching of excited Nd atoms occurs.

The conclusions that can be drawn from the present work so far are: 1) the use of very pure starting materials does not eliminate the concentration quenching effect in the silicate glasses or the borate glass, 2) if the presence of certain impurities cause the quenching effect, the level of the impurities need not be high.

3.3.2 Effect of Added Impurities on Fluorescent Properties

To determine which impurities have an adverse effect on the fluorescence lifetime and intensity and to what extent they can be tolerated in the glass, a number of impurities have been added to neodymium doped glasses made from pure starting materials. The fluorescence properties have been measured and the results are presented below.

3.3.2.1 Iron

To glasses of base composition $73SiO_2 \cdot 22Na_2O \cdot 5CaO$ at four levels of Nd_2O_3 concentration, 0.01 and 0.1 wt. % Fe_2O_3 were added. The lifetime and intensities are listed in Table 3-II, along with the absorption coefficient of the broad 1.1μ Fe^{+2} absorption. It is quite apparent from the data that the quenching of the lifetime is not dependent on the Fe_2O_3 content but rather on the Fe^{+2} content (which we have assumed to be proportional to the absorption coefficient at 1.1μ). This point can be shown by plotting the lifetime vs. the 1.1μ absorption coefficient (see Figure 3-8). It is interesting to note from this graph that quenching is more rapid for Fe^{+2} content at 3% Nd_2O_3 than at 10% Nd_2O_3. A further example of the quenching of the Fe^{+2} is from the following set of data (Table 3-III) which shows the effect of using a glass which contains a high proportion of modifier oxide

Table 3-11

Base Glass $73SiO_2 \cdot 22Na_2O \cdot 5CaO$ (by weight)

Sample #	% Nd_2O_3	% Fe_2O_3	OD/cm at 1.1μ	τ μsec	Rel. Intensity at 1.06μ
DO	1	0.01	0.02	518	64
CH	1	0.01	0	530	64
AD	3	0.01	0.04	410	114
CR	3	0.01	0.03	400	143
FJ	3	0.01	0	523	190
CI	7	0.01	0	285	173
DP	7	0.01	0.04	268	169
AE	10	0.01	0.06	127	97
CS	10	0.01	0.03	150	93
FK	10	0.01	0	173	151
AB	1	0.1	0.37	277	17
Z	3	0.1	0.34	245	46
CT	3	0.1	0.17	337	84
FH	3	0.1	0.10	391	115
AC	7.5	0.1	0.32	141	46
AA	10	0.1	-	100	-
CU	10	0.1	0.16	118	68
FI	10	0.1	0.10	154	104

EFFECT OF Fe^{+2} CONC. ON LIFETIME

FIG. 3-8

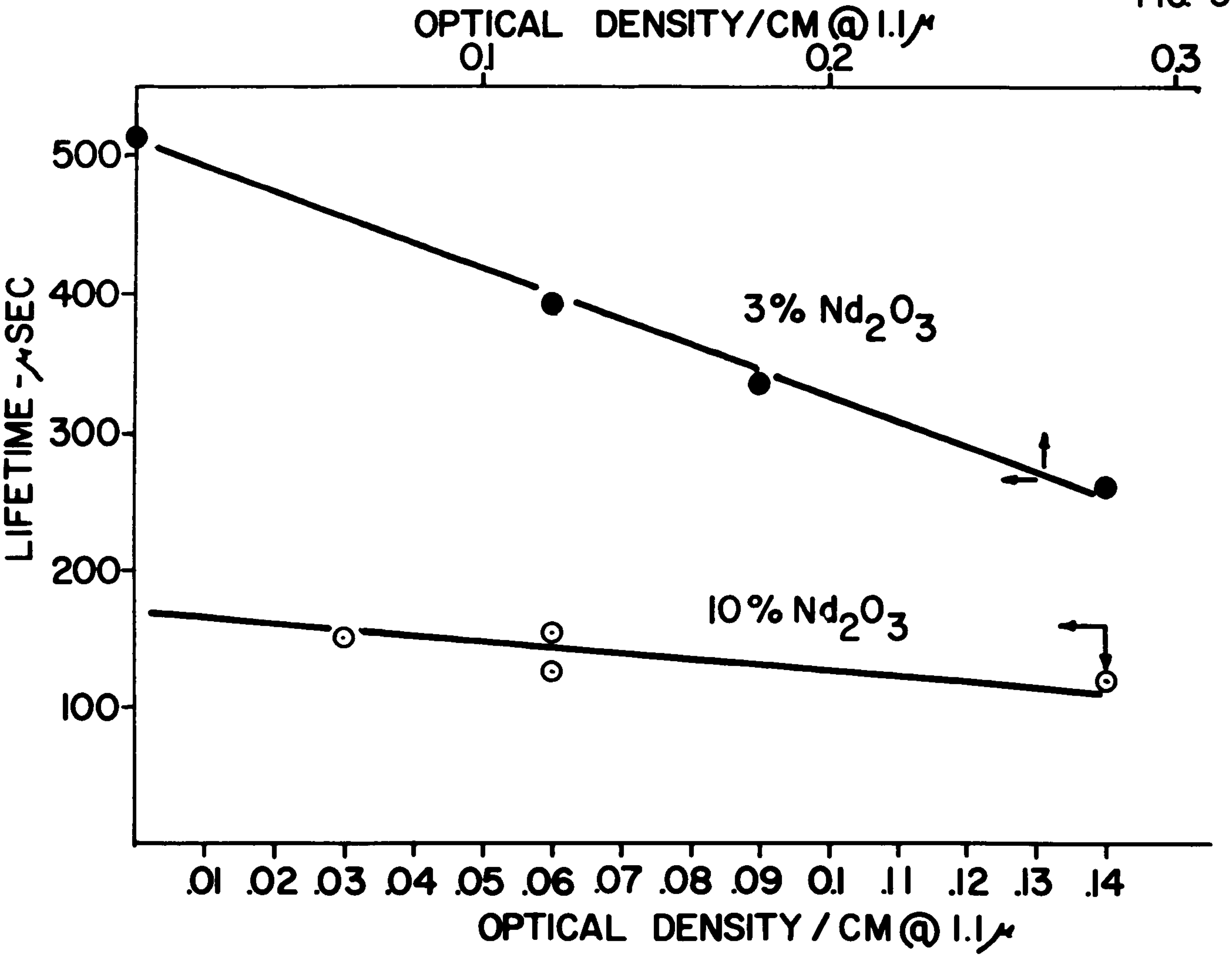

to network oxide (this tends to keep iron in the +3 state). The composition of the glass is $50SiO_2 \cdot 11Na_2O \cdot 17K_2O \cdot 10CaO \cdot 5Li_2O \cdot 7MgO$.

Table 3-III

$\%Fe_2O_3$ \ $\%Nd_2O_3$	1 μsec ± 30	2.5 μsec ± 30	5.0 μsec ± 15
0	450	350	210
0.01	470	360	214
0.1	420	340	191

It is observed from Table 3-III that the quenching due to the addition of Fe_2O_3 is practically absent in these glasses even at the 0.1 % Fe_2O_3 level, indicating that the iron is probably all in the oxidized Fe^{+3} state.

It is likely that the quenching action of impurities on the Nd^{+3} lifetime should be proportional to both the Nd^{+3} concentration and the impurity concentration, in this case Fe^{+2}. Figure 3-9 is a plot of the fluorescence lifetime vs. the product of the Nd^{+3} concentration, using the wt. % Nd_2O_3, and the Fe^{+2} concentration, where we have assumed that the absorption coefficient at 1.1μ is proportional to the Fe^{+2} content. The shape of this curve is interesting, insofar as it shows that at low impurity levels the quenching rate is higher than that at high impurity levels.

The addition of 0.1 Fe_2O_3 to a $Na_2O \cdot 2B_2O_3$ glass showed no decrease in lifetime.

3.3.2.2 Copper and Nickel

The presence of Cu^{+2} and Ni^{+2} ions in a Nd glass have been observed to quench the fluorescence lifetime as shown in Table 3-IV. Figure 3-10 shows a graph of the lifetime vs. the product of the Nd_2O_3 concentration and

Table 3-IV

Sample #	Copper % Nd_2O_3	% CuO	O.D./cm at .8μ	τ μ sec	Relative Intensity
CL	1	.01	0	545	102
CM	3	.01	0	518	239
CN	7	.01	0	290	245
CO	10	.01	0	173	187
FX	0.5	0.1	0.16	480	-
CJ	1	0.1	0.24	460	63
FN	1	0.1	0.32	418	37
BT	3	0.1	0.42	318	52
FO	3	0.1	0.36	370	72
CK	7	0.1	0.28	218	146
FP	7	0.1	0.46	227	88
BU	10	0.1	0.44	127	52
FQ	10	0.1	0.46	132	59
	Nickel		O.D./cm at .63μ		
DJ	3	0.01	.12	430	-
DL	10	0.01	.16	137	-
FR	1	0.1	.66	273	18
FS	3	0.1	.70	244	40
FT	7	0.1	.70	157	42
FU	10	0.1	.74	110	32

FIG. 3-9

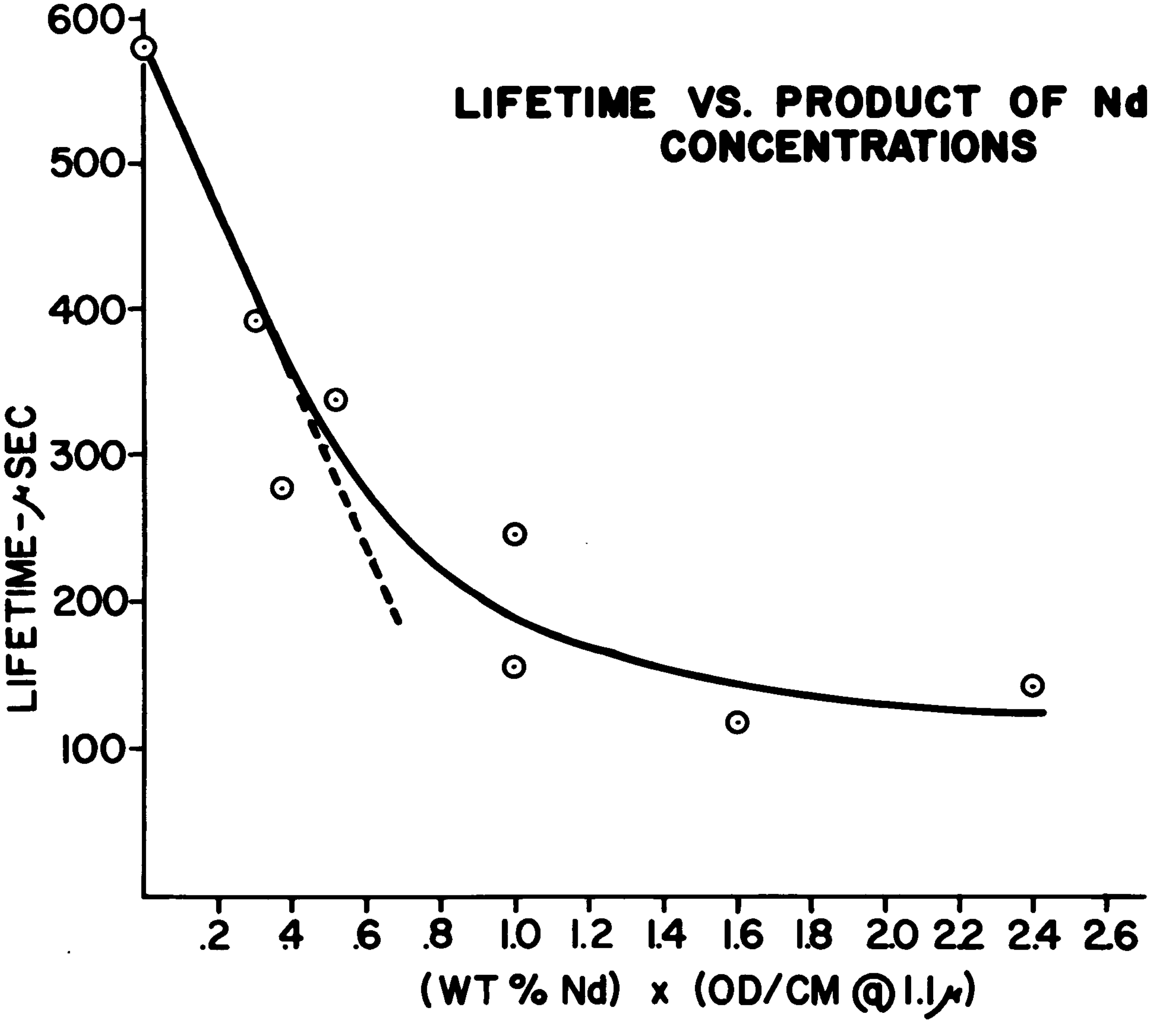

LIFETIME VS. PRODUCT OF Nd & Fe^{+2} CONCENTRATIONS

FIG 3-10

LIFETIME VS. (Nd_2O_3 CONC) x (IMPURITY CONC)

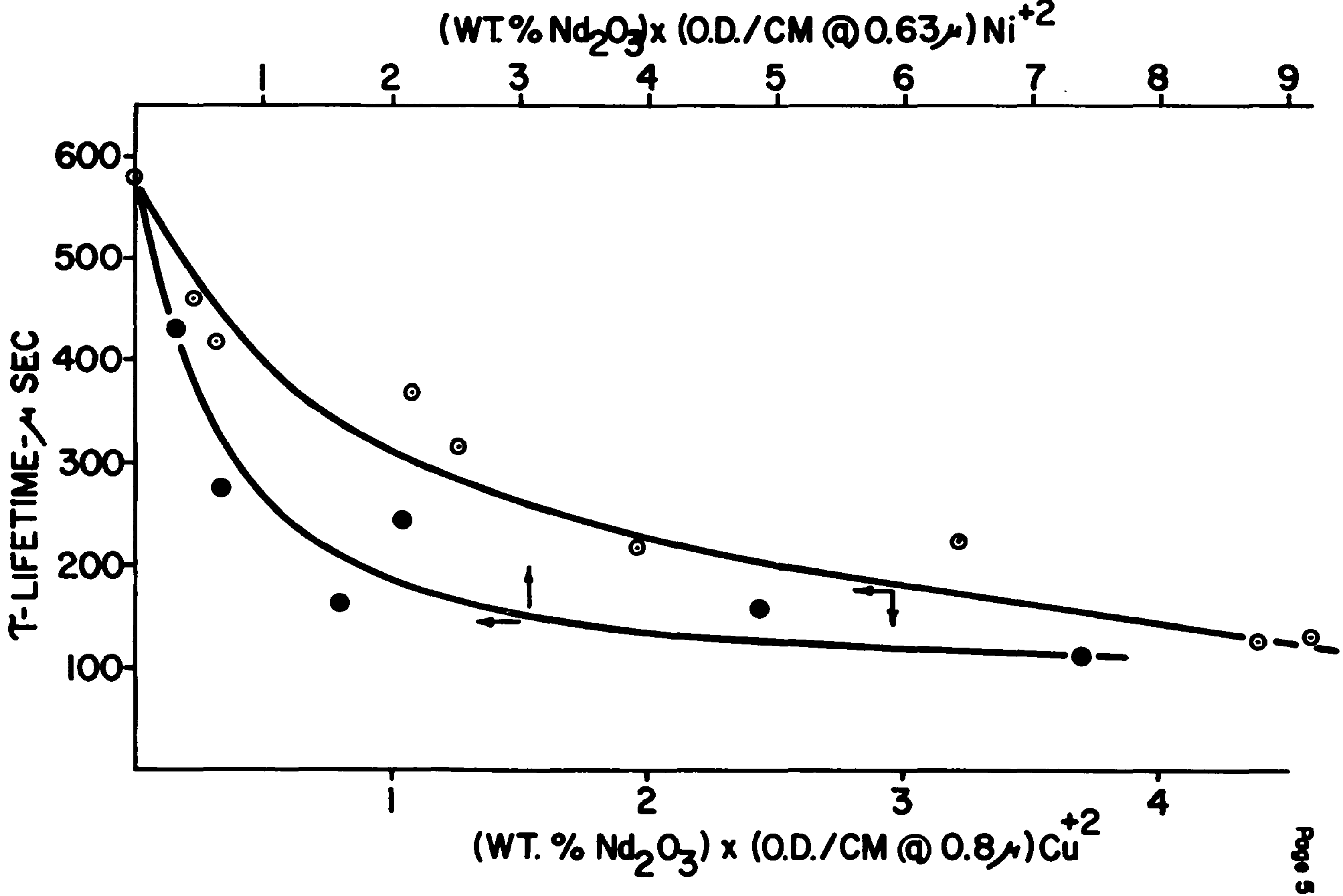

the Cu^{+2} and Ni^{+2} concentrations, respectively. The concentration of the Cu^{+2} was assumed to be proportional to the strength of the absorption at 0.8μ expressed in optical density per cm., likewise the concentration of Ni^{+2} was taken to be proportional to the absorption coefficient at 0.63μ . The shape of these curves is similar to that obtained for the Fe^{+2} quenching. It appears likely that the quenching mechanism by which these ions drain the $^4F_{3/2}$ state of Nd is the same in each case.

3.3.2.3 Co^{+2}, Mn^{+4}, Y^{+3}

To a few glasses of soda lime base composition, CoO, MnO_2 and Y_2O_3 were added at 3 and 10 wt. % Nd_2O_3. The lifetime data is given in Table 3-V below. Due to the small number of samples no graphs were made as was done for the Fe, Ni, and Cu data. It appears, however, that Co^{+2} has the same effect on the lifetime as dc the three previously discussed ions. Y_2O_3 and MnO_2 appear to have no effect on the lifetime.

Table 3-V

Sample #	% Nd_2O_3	% Impurity	Lifetime
884DI	3	0.01 CoO	465 ± 30
DK	10	0.01 CoO	177 ± 15
DM	3	0.01 MnO_2	565
DN	10	0.01 MnO_2	204
AF	3	0.01 Y_2O_3	490
AG	10	0.01 Y_2O_3	186
BX	3	0.1 Y_2O_3	490
BY	10	0.1 Y_2O_3	180

3.3.2.4 Other Rare Earth Ions

There has been some work reported in the literature on the effect of other rare earth ions in the fluorescence lifetime and intensity of Tb and Eu(3-13, 3-14). No such data pertaining to Nd has been reported. To investigate this effect, a number of trivalent rare earth ions were added to a Nd^{+3} doped soda lime silicate glass. Table 3-VI shows the data obtained.

Table 3-VI

Sample #	% Nd_2O_3 Wt.	Impurity Level	τ μsec	Rel. Intensity at 1.06μ
884V	3	0.1 Pr_2O_3	426	181
W	10	"	143	125
CV	1	0.01 Dy_2O_3	565	96
CW	3	"	510	230
CX	7	"	300	265
CY	10	"	200	244
CZ	1	0.1 Dy_2O_3	528	75
BR	3	"	465	162
DA	7	"	318	-
BS	10	"	177	142
CD	3	0.1 Sm_2O_3	445	172
CE	10	"	176	149
CF	3	0.1 Ho_2O_3	500	216
CG	10	"	182	182
BV	3	0.1 C_2O_3	500	196
BW	10	"	187	140
FL	3	0.1 Tb_2O_3	495	219
FM	3	1.0 "	391	193

From the above data it appears that at 0.1% impurity (about 125 ppm, atomic), Pr^{+3}, Dy^{+3} and Sm^{+3} quench the neodymium fluorescence lifetime to some extent while Ho^{+3}, Ce^{+3} and Tb^{+3} have little effect, if any.

Van Uitert and Ida^(3-13) correlated the quenching effect of other rare earth ions on the relative fluorescence intensity of Tb^{+3} and Eu^{+3}, respectively. They plotted the log of the intensity vs. the energy gap between the fluorescing levels and the closest lower-lying level of the second rare earth ion. They obtained a series of roughly parallel lines for each set of ions with the same total orbital angular momentum of the ground state of the second rare earth ion. If one attempts the same type of correlation for the effect of other rare earth ions on the fluorescence intensity of Nd^{+3}, using some of the data of Table 3-VII, one obtains the results shown in Table 3-VIII.

Table 3-VII

Impurity Ions Wt. %	Wt. % Nd	τ μsec	I	ΔE	Ground State
0.1 Pr_2O_3	3	426	181	1700 cm^{-1}	$^3H_4$
	10	143	125		
0.1 Sm_2O_3	3	445	172	1100	$^6H_{5/2}$
	10	176	149		
0.1 Dy_2O_3	3	465	162	500	$^6H_{5/2}$
	10	177	142		

Although the intensity appears to increase with increasing energy gap at 3% Nd_2O_3, at 10% Nd_2O_3 there is no such trend. In any event, the differences in intensity and lifetime between the glass at the same Nd_2O_3 level are not significant within the ± 10% accuracy of the data. It is definitely shown, however, that the intensity does not decrease exponentially with decreasing energy gap as was found to be the case for the crystal systems studied by Van Uitert and Ida.

Peterson and Bridenbaugh(3-14) proposed that the fluorescence lifetime quenching of Tb^{+3} by certain other rare earth ions was by a resonance exchange mechanism. The criterion here is that the second rare earth must have an absorption band overlapping one or more of the emission lines of the primary rare earth ion. From the absorption spectra of the rare earth ions one observes that only Dy and Sm have significant absorption bands which overlap the Nd emission lines at 0.88μ and 1.06μ. From Table 3-VI it is seen that the lifetime of the Nd glasses containing Sm, Dy and Pr are quenched at 3% Nd_2O_3, while at 10% Nd_2O_3 only Dy caused any lifetime reduction.

3.3.3 Effect of Temperature on Lifetime

The effect of temperature on the fluorescence lifetime of a few neodymium doped soda-lime-silicate glasses and borate glasses were measured. The purpose here was to see if the reduction of lattice vibration effects which accompany a decrease in temperature would affect the fluorescent lifetime. The results are shown below:

Table 3-VIII

Sample #	% Nd_2O_3	Room Temperature τ μ-sec	Liquid N_2 τ μ-sec
X	3	540 ± 20	485 ± 20
AI	5	418 ± 20	391 ± 20
AY	10	182 ± 10	195 ± 10
Borate			
F	2	60 ± 5	61 ± 5

The results seem to show no significant difference in lifetime at liquid nitrogen temperature from that at room temperature. The lifetime is slightly increased at the 10% Nd_2O_3 level and slightly decreased at the 3 and 5 wt. % Nd_2O_3 levels. Woodcock$^{(3-15)}$ has reported the same effect.

The decrease on the lifetime with decreasing temperature for Nd concentrations $\leq$ 5 wt. % (little or no concentration quenching) can be explained in terms of a coupled set of split $^4F_{3/2}$ states. From Maurer's (3-18) study of the energy level scheme of Nd^{+3} in glass it is shown that the excited $^4F_{3/2}$ state is split into two states (see Fig. 3-14). If one postulates that these two levels are thermally coupled so that

$$N_2/N_1 = \exp(-\Delta E/kT)$$

is true, then one can explain the observed temperature effect. Let P_1 and P_2 represent the total transition probabilities from the first and second levels respectively, — i.e., $P_1 = \sum^{N_1} P_{3/2} - 4_I$, $P_2 = \sum^{N_2} P_{3/2} - 4_I$

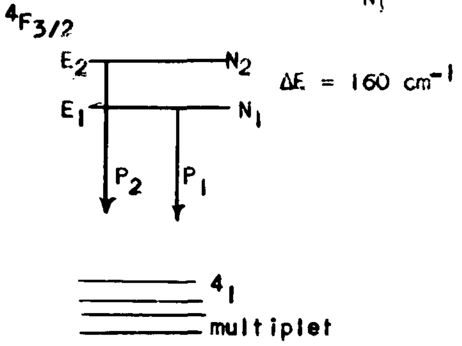

Figure 3-14

then

$$\frac{dN}{db} = \frac{dN_1}{dt} + \frac{dN_2}{dt} = -(P_1 N_1 + P_2 N_2)$$

Using the above expression for N_2/N_1 one obtains for the measured lifetime

$$\tau_m = \frac{1 + \exp(-\Delta E/kT)}{P_1 + P_2 \exp(-\Delta E/kT)}$$

Evaluating this expression at 300°K and 80°K gives the following ratio of lifetimes

$$\frac{\tau_{300°K}}{\tau_{80°K}} = 1.39 \frac{(\alpha + 0.057)}{(\alpha + 0.465)}$$

where we have used $P_1 = \alpha P_2$

It can be seen that for $\alpha > 1$ τ_{300}/τ_{80} will be less than 1. Maurer's (3-18) experimental data seems to indicate that $P_2 < P_1$, hence $\alpha > 1$, therefore accounting for the decrease in lifetime with decreasing temperature.

After 5% Nd where concentration quenching becomes a factor, the decreasing of the temperature merely reduces the lattice effects and, hence, since it is the dominant factor in the lifetime, the lifetime should increase.

3.3.4 <u>Possible Impurity Quenching Mechanism</u>

In order to explain the concentration quenching effect in Nd doped glasses by an impurity mechanism one must deal with a process whereby a relatively small impurity level is responsible for the observed quenching action.

Dexter(3-16, 3-17) has developed a theory by which it is found that energy transfer can occur with high probability between centers separated by several dozen Å if their absorption bands overlap their emission bands appreciably, and if the transition is an allowed one. The transfer probability per unit time by the dipole-dipole mechanism is given by

$$W_{tr}\ (dd) = 9/16\pi^2\ \beta^2/R^6\ \ W_r\ (d)$$

where $$\beta = \left[\frac{4\,\pi\hbar^4\,c^4}{3\,\eta^4}\quad A\int f_a\,(E)\,f_e\,(E)\,dE/_{E^4}\right]^{1/2}$$

where $A = \int\sigma(E)dE$, σ = absorption cross section of absorption f_a (E), f_e (E) are the normalized shape function of the absorption and emission lines respectively, η = index of refraction, and c = velocity of light.

Hence, we have then a radiationless transfer of energy from an excited molecule to another unexcited molecule of the same species separated from the first by comparatively large distances. In this way the primarily excited molecule returns to the ground state, and the second molecule is raised to the excited state. By repetition of a resonance process of this sort, the absorbed energy may traverse a considerable distance in the system, jumping from one molecule to the next, until the energy is finally dissipated by jumping to a "quencher" site. The observed lifetime should decrease with increasing concentration directly as the quantum yield decreases.

Dexter has shown that a considerable degree of quenching can occur at quite low impurity levels. For example, for a typical system on which transfer occurs, $\eta/\eta_0\ (\therefore\ \gamma/\gamma_0)$ = 0.4 at a 1% level of activator with an impurity level of 10 ppm. This high degree of quenching at low impurity levels seems to agree with the concentration quenching effect observed in the Nd glasses. The purity of the pure melts made in the lab should be good. (A chemical trace analysis of a series of glasses is presently underway.) In the pure glasses concentration quenching still occurs, indicating that if this is an impurity sponsored effect, then the level of impurity need not be appreciable. It seems worthwhile to pursue this proposed mechanism further to see if it can be established as being operative in the Nd system. As was stated above, the necessary conditions for this transfer process are that the emission and absorption bands of the fluorescing constituent overlap at some point, and that the quenching atom has an absorption band overlapping this same emission line. This condition is fulfilled in Nd, at 8800 Å, and the second is fulfilled for such ions as Fe^{+2}, Cu^{+2}, Ni^{+2}, and Sm^{+3} among others. Dexter derived an expression for the rate of quenching in terms of the quantum yield, viz.,

$$\eta/\eta_0 = 1 - \frac{\beta_{aq}}{\beta_{aa}} \left[C^+ \beta_{aa} \right]^2 \chi_a \chi_q$$

where χ_i = fraction of sites per total sites available

C^+ = conc. (per cm^3) of total lattice sites

β_{aa}, β_{aq} = effective volume of influence of activator and quencher respectively.

For our purposes we shall replace η/η_0 by γ/γ_0 hence

$$\gamma/\gamma_0 = 1 - \frac{\beta_{aq}}{\beta_{aa}} \left(C^+ \beta_{aa} \right)^2 \chi_{Nd} \chi_q$$

where γ_0 is the value of γ at $\chi_{Nd} \longrightarrow 0$

According to this relation a plot of $(1 - \gamma/\gamma_0)$ vs. χ_{Nd}, expressed in our case as the cation fraction of Nd^{+3}, should give a straight line. Figs.

3-11 and 3-12 show the lifetime data for a soda lime silicate and a soda silicate glass plotted in this way. The data seems to show a fair fit to a straight line. The shape of the lines, assuming a number of different impurity ions, each having an overlapping absorption with the 8800 Å emission line of Nd^{+3} and assuming the impurity level remains constant throughout the concentration range of Nd^{+3}, would be

$$\text{Slope} = \beta_{aa} \; C^{+2} \sum_{j} \beta^{j}_{aq} \; \chi^{j}_{q}$$

It seems worthwhile to try to get an order of magnitude estimate of the parameters β_{aa} and β_{aq} in order to get some idea of the impurity levels, χ^{j}_{q}, which would account for the observed quenching effect.

As written above, β_{aa}, is defined by the following expression:

$$\beta_{aa} = \left[\frac{4\pi \hbar^4 c^4}{3 \eta^4} A \int f_a(E)\, f_e(E)\, dE/E^4 \right]^{1/2}$$

For an order of magnitude estimate of this parameter one can remove E^{-4} from under the integral and use $\langle E^{-4} \rangle \approx \langle 1.09\,\text{ev}^{-4} \rangle = 1/1.43\ \text{ev}^{-4}$ (correspond to 8800 Å). Also $\eta^4 \approx 5$. A can be set approximately equal to $\sigma_{8800}\, \Delta E_{1/2}$. From the absorption data on a large number of Nd glasses a typical value of σ at 8800 Å was found to be equal to $0.4 \times 10^{20}\ \text{cm}^2$ and a value of $\Delta E_{1/2}$ to be 0.04 ev. Hence

$$A \approx 1.8 \times 10^{-22}\ \text{cm}^2\,\text{ev}$$

The next term to be evaluated is the overlap integral. Using the emission and absorption line at 8800 Å given by Maurer(3-18) one can fit the shapes fairly well with a Gaussian distribution

FIG. 3-11

(1-T/To) VS. CATION FRACTION OF Nd^{+3}

73% SiO_2-22% Na_2O-5% CaO

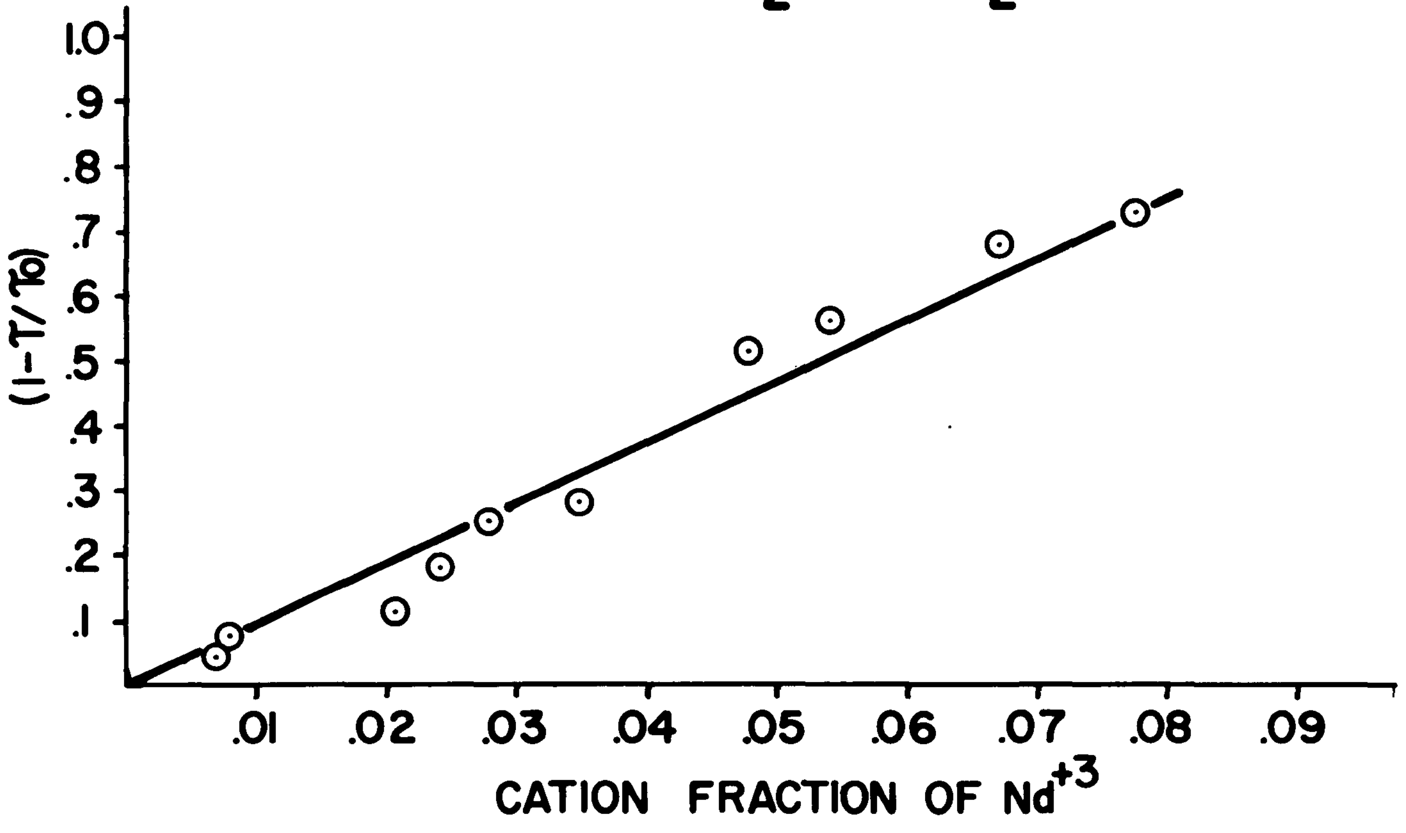

FIG. 3-12

(1-T/To) VS. CATION FRACTION OF Nd^{+3}

75% SiO_2 25% Na_2O

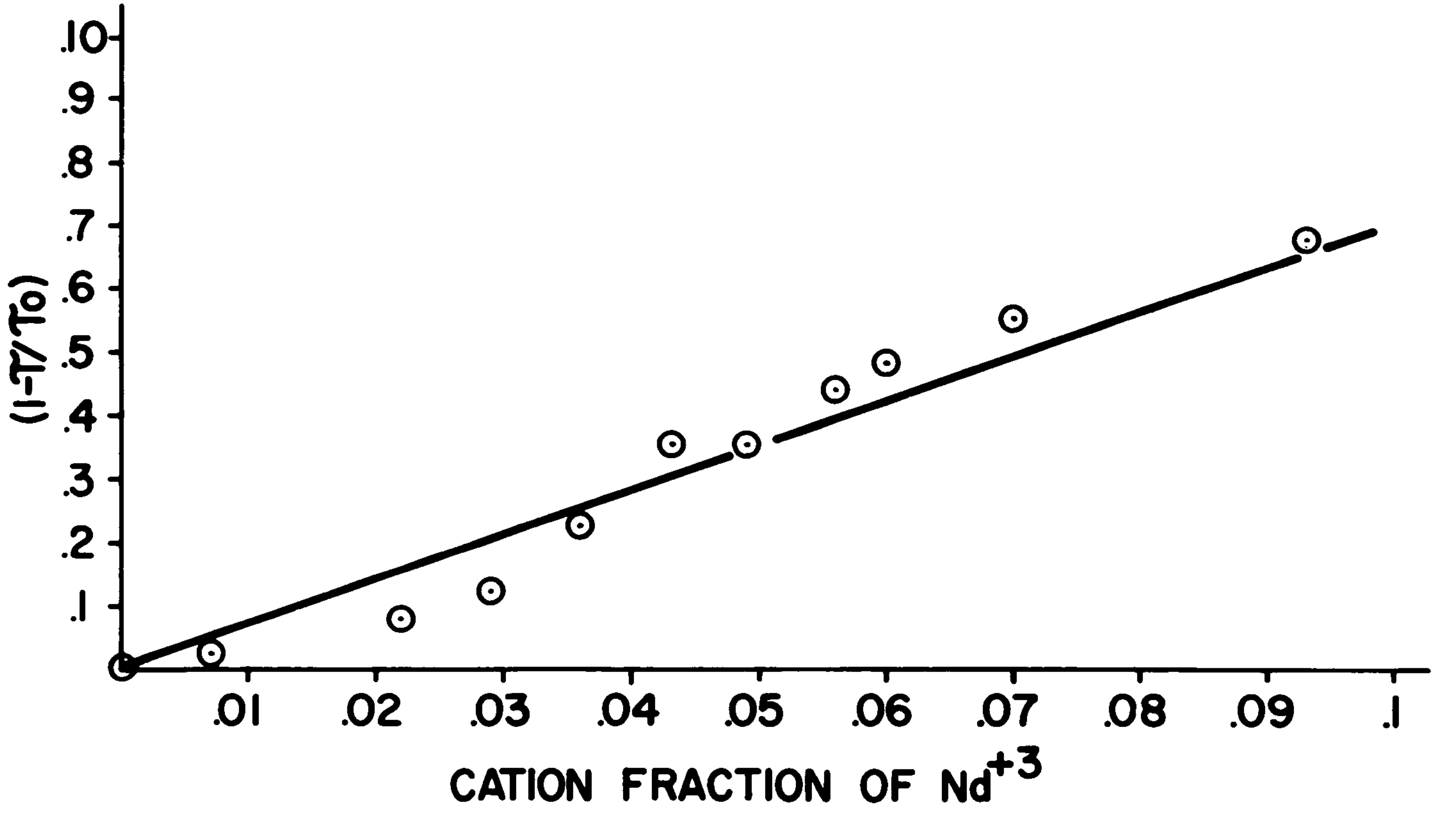

$$f_{aa} = 29 \exp - 2725\, E''^{2} \quad ev^{-1}$$

$$f_{ae} = 18.2 \exp - 1000\, E'^{2} \quad ev^{-1}$$

where

$$E'' = E - 1.404 \text{ ev}$$

$$E' = E - 1.395 \text{ ev}$$

Evaluating $\int f_{aa} f_{ae}\, dE$ one obtains as an approximation, a value of 15.7 ev^{-1}. Putting these values into the equation for β_{aa} one obtains a value of 4.73×10^{-21} cm^2. Using C^+ as 1.27×10^{22} cation/cc the equation for the quenching becomes

$$\eta/\eta_0 \approx 1 - 3.6 \times 10^3 \left(\frac{\beta_{aq}}{\beta_{aa}}\right) \chi_a \chi_q$$

3.3.4.1 Estimation of β_{aq} for Cu and Fe

Order of magnitude estimates of the β_{aq}'s for Fe^{+2} and Cu^{+2} were made. The Fe^{+2} absorption band centered at about 1.1μ and the Cu^{+2} absorption band centered at about 0.78μ both are broad enough to overlap the Nd^{+3} 8800 Å emission band.

$$\left(\frac{\beta_{aq}{}^{Fe}}{\beta_{aa}}\right) \approx 5.6$$

$$\left(\frac{\beta_{aq}{}^{Cu}}{\beta_{aa}}\right) \approx 1.76$$

Using these numbers at, for example, 3% Nd_2O_3, χ_a = 0.021, we would get

$$(1 - \eta/\eta_0) = 425\chi_q{}^{Fe} + 135\chi_q{}^{Cu}$$

At 3%, $(1 - \eta/\eta_0)$ is observed to be 0.11, hence assuming $\chi_q{}^{Fe} = \chi_q{}^{Cu}$ one would obtain

$$\chi_q = 0.000197$$

which corresponds to about 30 ppm atomic impurity for each ion. Of course, this calculation is strictly an order of magnitude estimate and can be taken to mean only that the resonance transfer mechanism explanation of the concentration quenching effect is conceivable. If one replots Figure 3-9 in terms of $(1-\tau/\tau_0)$ and $(\%_{Nd} \times \mathrm{O.D./cm}$ at $1.1\,\mu)$, as in Figure 3-13, it is observed that the curve is approximately linear in the first portion. This indicates that at least for low impurity concentrations the above explanation may be valid.

3.4 Effects of Base Glass Composition on Neodymium Fluorescence

The first and most obvious conclusion to be seen from the data in Appendix A is that both the fluorescence and absorption of neodymium in glass vary over wide ranges from one glass to another. Fluorescence intensity and lifetime, for example, each vary over an order of magnitude at a given neodymium concentration level. Linewidths vary by a factor of two from about 220 Å to 440 Å, with most glasses falling at about 330 Å. These observations can be classified on a strictly empirical basis in which correlations are made between compositional changes in glass and the effect of these changes on the spectral properties of neodymium. A number of these correlations have been found and are outlined below. A complete knowledge of the empirical effect of compositional changes on the spectral properties of neodymium will require the study of many more glasses, especially the study of selected series of compositional changes designed to elucidate the effect of a particular constituent in the glass and any possible perturbations of this effect by the rest of the glass composition. While such a study would be possible, it would clearly be very time consuming. It would be much more desirable if, from the spectral data on a

FIG. 3-13

(1-T/To) VS. (CATION FRACTION Nd) x (Fe^{+2} CONC)

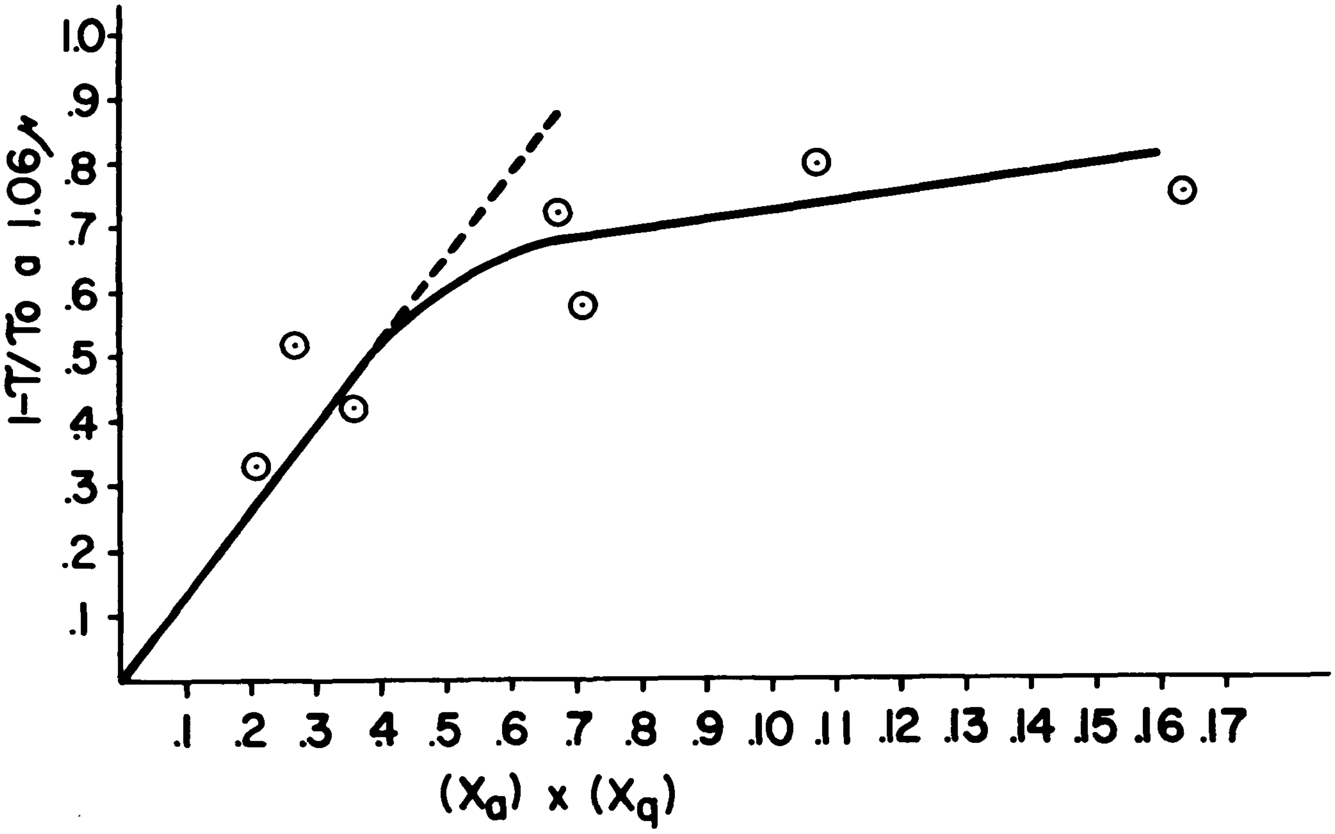

few characteristic series of glasses, some interpretation could be developed as to <u>why</u> a particular compositional change causes a particular spectral result. On the basis of such a semi-theoretical study, a limited number of new glasses would then be studied to test specific features of the interpretation.

3.4.1 Expected Effects

The spectral properties of a neodymium ion will be influenced by its host matrix in three principle ways:

(1) The immediate neighbors, and to some extent its next-nearest neighbors, will perturb the electronic structure of Nd^{+3} and thus modify its spectral properties.

(2) Other Nd^{+3} ions, if they are close enough, will interact with the Nd^{+3} ion in question, and modify its properties. This can lead to concentration quenching effects or slight level splitting.

(3) Impurity ions, especially those with spectral transitions overlapping one of the transitions of the Nd^{+3}, can also modify the properties of the Nd^{+3}. This is an impurity quenching effect.

The principle compositional effect of interest is the crystal field effect of the immediate neighbors of neodymium, — oxygen atoms in oxide glasses. If the number of oxygen atoms around each Nd^{+3} ion as well as the electronic state of these oxygen atoms and resultant crystal field at the Nd^{+3} are known, it should be possible to account for changes in the Nd^{+3} emission and absorption spectra. In the case of glass, a few problems must be faced before this can be done.

(1) <u>Coordination of Nd^{+3} in Glass</u>

The glass has a random structure although some degree of local order may exist around the Nd^{+3} ions. The disorder is certainly enough, however, to cause a distribution of crystal fields around various Nd^{+3} sites. There is, unfortunately, no clear cut way to determine the average number of oxygen atoms coordinated with each Nd^{+3}. According to the ratio of crystal radii of Nd^{+3} to O^{-2}, Nd^{+3} should have an oxide coordination number of 8. The ease with which Nd^{+3} can achieve such a state will depend on the composition and structure of the glass. For example, in some glasses the oxygen may be bound by other ions in the glass so as to leave very few interstices where Nd^{+3} can be near 8 oxygens. Or, on the other hand, there may be such places but they may be filled with other ions.

(2) <u>Electronic "State" of the Oxygen in Glass</u>

A distinctive feature of glass and one which has profound effects on all of its properties is that the oxygen ions are not all equivalent. Some of them are covalently bound to two network cations such as silicon, boron or phosphorus. These tightly bound oxygens are called "bridging" oxygens. On the other hand, some oxygens are only bound to one network former and have a net ionic charge (which is balanced by a positively charged modifier ion such as Na^{+} or Ca^{+2} in the immediate vicinity). As an illustration of the difference between these two types of oxygen, Stevels (3-4) has found that the molar refractivity for the "bridging" oxygen is 3.66, while for "non-bridging" oxygen it is 4.38 in a simple soda silicate glass. The effect of neighboring oxygen atoms on a Nd^{+3} ion, then, will depend not only on the number and symmetry of the oxygen neighbors but also on whether they are "bridging" or "non-bridging" ions.

Another way to express this is to say that the polarization of each oxygen ion will depend on its neighbors, and the polarization of oxygen ions will influence the degree to which they interact or "couple" with Nd^{+3}. In a quantitative sense, it is very difficult to determine the average polarization of oxygen in glass. The relative ability of cations to polarize oxygen ions is frequently indicated by their field strengths, z/a^2 where "z" is the ionic valence and "a" is the cation-to-oxygen distance.

If these problems can be overcome, it may be possible to determine how the ability of oxygen to couple with Nd^{+3} depends on the glass composition. If the coupling is strong, one would expect the absorption spectra to be strong, the fluorescence to be intense and the fluorescence lifetime to be short. On the other hand, if the coupling is weak, one would expect absorption to be weaker, fluorescence of lower intensity, and longer fluorescence lifetime. This superficial analysis is, of course, subject to many possible pitfalls. One important problem is that even though absorption may be strong, the fluorescence may be weakened by some quenching process, causing the absorbed energy to be converted to heat. There is, therefore, no necessary connection between fluorescence intensity and lifetime from one base glass to another.

3.4.2 Observed Effects

A simple and direct evaluation of the data in Appendix A reveals a number of empirical correlations between glass composition and fluorescence properties as enumerated below:

1. Of the alkali oxides, Li_2O gives the highest fluorescent intensity and the shortest lifetime, with decreasing intensity and increasing

lifetime for heavier alkali ions. For example, the addition of Cs and Rb to certain glasses tends to increase the lifetime, e.g., a Cs_2O-SiO_2 at 2% Nd_2O_3 has a lifetime of 1m sec.

2. Of the oxides of Mg, Ca, Sr, and Ba, intensity and lifetime increase with atomic weight, so that Ba is best, except when more than 5% Al_2O_3 is present.
3. The optimum Nd^{3+} level is about 5 x 10^{20} ions/cc. with a maximum in fluorescent intensity and a broad minimum in calculated pulse threshold from 3 to 7 x 10^{20} ions/ccm.
4. Heavy oxides, La_2O_3 in particular, added to a glass tend to increase the fluorescent intensity greatly and the lifetime slightly. This effect has been noticed particularly in borate and phosphate glasses. The evidence is not conclusive in silicates, partially because La_2O_3 is not as readily dissolved in silicate glasses.
5. Invert glasses generally have a greater fluorescence intensity than normal glasses.
6. In a soda-lime glass, a maximum in fluorescent intensity occurs with the addition of about 1% Sb_2O_3. This effect is believed unrelated to the original purpose of Sb_2O_3 of enhancing fining action.
7. UO_2 quenches both lifetime and intensity.
8. Some glass networks can apparently couple energy out of the excited state by some unidentified quenching mechanism. For example, the addition of B_2O_3 in almost any concentration to a glass shortens the fluorescence lifetime. B_2O_3 also decreases fluorescence intensity, although it may require as much as 10 mol % B_2O_3 or more to be noticeable. The addition of Al_2O_3 also tends to shorten lifetime and

decrease fluorescence intensity, although the effect is less pronounced than with B_2O_3.

9. Glasses which contain B_2O_3 or Al_2O_3 often show high absorption cross sections, particularly at 5800 Å and in the UV, although, as noted above, the stored energy is not emitted efficiently as 1.06 micron fluorescence. Phosphate, germanate and tellurate glasses also show high absorption cross sections throughout the spectrum, but in these cases, the absorbed energy is more efficiently emitted as 1.06 micron radiation.
10. Al_2O_3 in excess of 5 mol % in a glass upsets the relative effects of the glass modifiers on the lifetime and fluorescence intensity as described in No. 1 above.

In addition to these empirical correlations, more detailed analysis of the fluorescence data has been initiated with the objective of understanding the <u>causes</u> of the observed correlations. The factors involved in setting up a suitable model on which to base an interpretation have been outlined in Section 3.4.1. Working on the assumption that the availability of oxygen to Nd^{+3} will be the determining factor, a correlation between fluorescence lifetime and the average concentration of oxygen ions per cc. of glasses listed in Table 3-IX.*

* Concentration of oxygen ions per cc. of glass was calculated from the relation:

$$N_o = RA\rho/G$$

where R is the atomic fraction of oxygen per molecule of glass.
A is Avagadro's number, 6.023×10^{23} molecules/mole.
ρ is the glass density in grams/cc.
G is the glass molecular weight in grams/mole.
Densities are tabulated in Table 3-IX.

Table 3-IX

Code #	Mole Composition	Lifetime sec	Ref. Index	Density g/cm^3
95CDX	$75SiO_2+10CaO+15Na_2O$	622	1.5143	2.481
95CDZ	$75SiO_2+10CaO+15K_2O$	750	1.5262	2.508
95CEA	$75SiO_2+10CaO+15Rb_2O$	775	1.5215	2.866
95CEB	$75SiO_2+10CaO+15Cs_2O$	800	1.5419	3.187
95CEN	$75SiO_2+15Na_2O+10ZnO$	645	1.5132	2.597
95CIP	$75SiO_2+15Na_2O+10CdO$	465	1.5258	2.724
95CEH	$75SiO_2+15Na_2O+10MgO$	656	1.4995	2.431
95CEL	$75SiO_2+15Na_2O+10PbO$	630	1.5612	3.061
95CIN	$75SiO_2+15Na_2O+10SrO$	610	1.521	2.686
95CIT	$55SiO_2+15Na_2O+30PbO$	380	1.656	4.433
95CIS	$65SiO_2+15Na_2O+20PbO$	500	1.6407	3.752

Although a fairly good correlation was found for Series 1, Series 2 and 3 did not fit. The correlation was considerably improved, however, when the effect of refractive index on fluorescence lifetime was taken into consideration.

The relation between fluorescence lifetime and refractive index can be found in the relation between spontaneous and stimulated transitions first developed by Einstein(C-1) and outlined in Appendix C. The conclusion of this analysis, equation (5) in Appendix C, is that the fluorescence lifetime is inversely proportional to the cube of the refractive index. When this relation is considered in the analysis of the data in Table 3-IX, a much better correlation is found. Figure 3-15 shows the relation between $\tau\eta^3$ and N_O, the concentration of oxygen ions per cc. of glass. With the exception of one point, a good inverse linear relationship was found. It should be noted that the refractive indices used in this analysis and listed in Table 3-IX are the indices for the D-line of sodium, although the index of interest for Nd^{+3} is at 1.06 microns. Use of the 5890 Å index is not expected to significantly influence the conclusions of the analysis, since the dispersions of these glasses are all relatively low.

The reason for the relation shown in Figure 3-15 can be seen by referring to the raw data in Table 3-IX. In Series 1, changes of the alkali ion from Li to Na to K to Rb to Cs cause significant increases in the lifetime as the number of oxygen ions per cc. decrease (thus reducing the O-Nd interaction). At the same time, the refractive index does not change very much, being 1.514 for the Na glass and 1.542 for the Cs glass. On the other hand, in Series 2 and 3, substitution of heavier bivalent ions for Ca causes an increase in refractive index in addition to the decrease in No, the number of oxygen ions per cc. In other words, the O-Nd interaction is

FIG 3-15

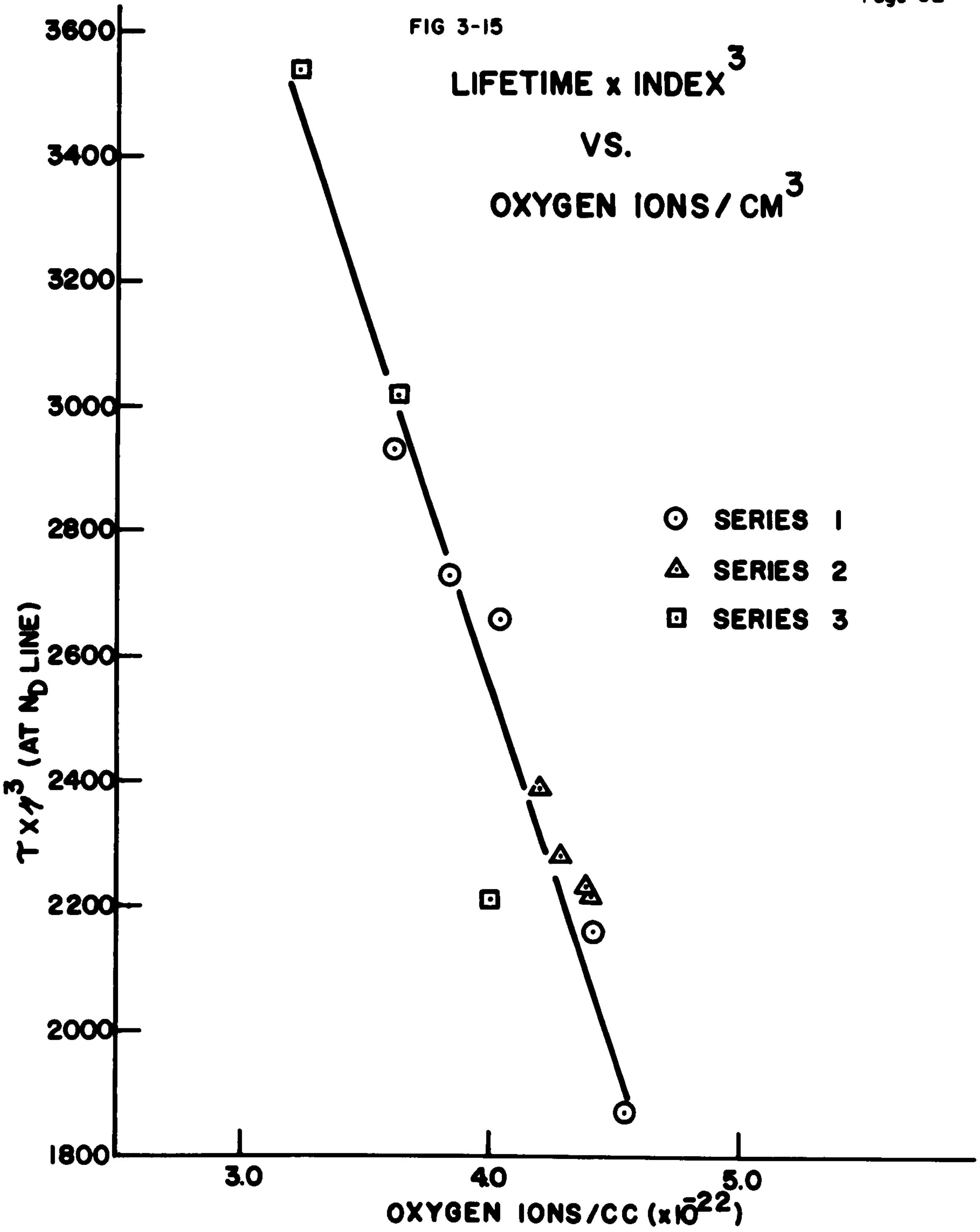

LIFETIME x INDEX^3 VS. OXYGEN IONS / CM^3

de-coupled by dilution of the oxygen content, but the refractive index increases. This increase in refractive index decreases the fluorescence lifetime, but the relation between $\tau\eta^3$ and No is the same as for Series I. The same analysis has also been applied to a number of glasses picked more or less at random from other glass systems. Some of the results fall on the line plotted in Figure 3-15, while others do not. The glasses which do not fit usually contain appreciable amounts of Al_2O_3 or B_2O_3. Further, all glasses containing more than a minor amount of alkali fall on the line. The correlation will be analyzed further to try to unravel the factors involved.

4. NEODYMIUM GLASS LASER PERFORMANCE

The measured thresholds presented in Appendix A were made on lasers prepared from small laboratory glass melts. An analysis of these measurements convinced us that it was impossible and probably meaningless to continue this type of measurement until it is known how the optical quality and other extrinsic properties of the laser rod affect the performance.

We have amassed a large body of neodymium fluorescence data on a wide variety of glass compositions. The problem is to try and predict laser performance using this data.

This is a less severe problem for crystals since the fluorescent properties can only be adjusted by changes in doping level, and impurities — not by gross changes in the composition of the host. (This is not universally true — Van Uitert of BTL did much with $CaWO_4$, but glass is infinitely more variable in any case.)

In predicting performance as a laser, it is necessary to decide what type of laser you have in mind — an application e.g., high power Q-spoiled, high energy pulsed, low energy pulsed, continuous, etc. In most of these applications, the relationship between spectral properties and laser performance is only known in a general fashion. For example, in a Q-spoiled high power system, it is obviously important to have a long lifetime for the excited state so as to store the maximum amount of energy in the excited state before the cavity is "un-spoiled".

We decided to use the threshold as our measure of glass performance. A low threshold signifies efficiency in converting pump light into laser light. Glasses with low threshold would be useful for high and low energy pulsed operation as well as a continuously operating laser. We did not extend the analysis to include factors which would be important for an energy storage laser (one of which was mentioned above). We believe we have sufficient data on the fluorescence properties but insufficient data as yet on other properties to characterize the glass for this mode of operation.

4.1 Theoretical Analysis of Pulsed Laser Threshold

The relative pulsed threshold of a laser can be calculated from primary spectral data such as that given in Appendix A using the following major assumptions.

(1) The rate loss of excited atoms due to stimulated emission is negligible.

(2) The spectral distribution of the fluorescence measuring lamp is the same as the laser flash lamp.

(3) The time dependence and the frequency dependence of the laser flash lamp are separable.

(4) Quantum efficiency is independent of wavelength.

The result of the calculation, assuming equal losses, shows that the pulse threshold should be proportional to

$$\frac{\eta^2}{F_{max}\ f(t)_{max}} \cdot \frac{a}{b(a+b)} \tag{1}$$

where η is the refractive index, F_{max} is the relative fluorescence intensity at 1.06μ, and $f(t)_{max}$ is directly proportional to the number of atoms excited to the metastable state which is read from a computer derived plot of fluorescence lifetime versus $f(t)_{max}$. This function is derived using the a, and b coefficients which describe the shape of the flash lamp pulse and the fluorescence lifetime. Figure 4-1 shows two curves derived for 1/2 and

FIG. 4-1

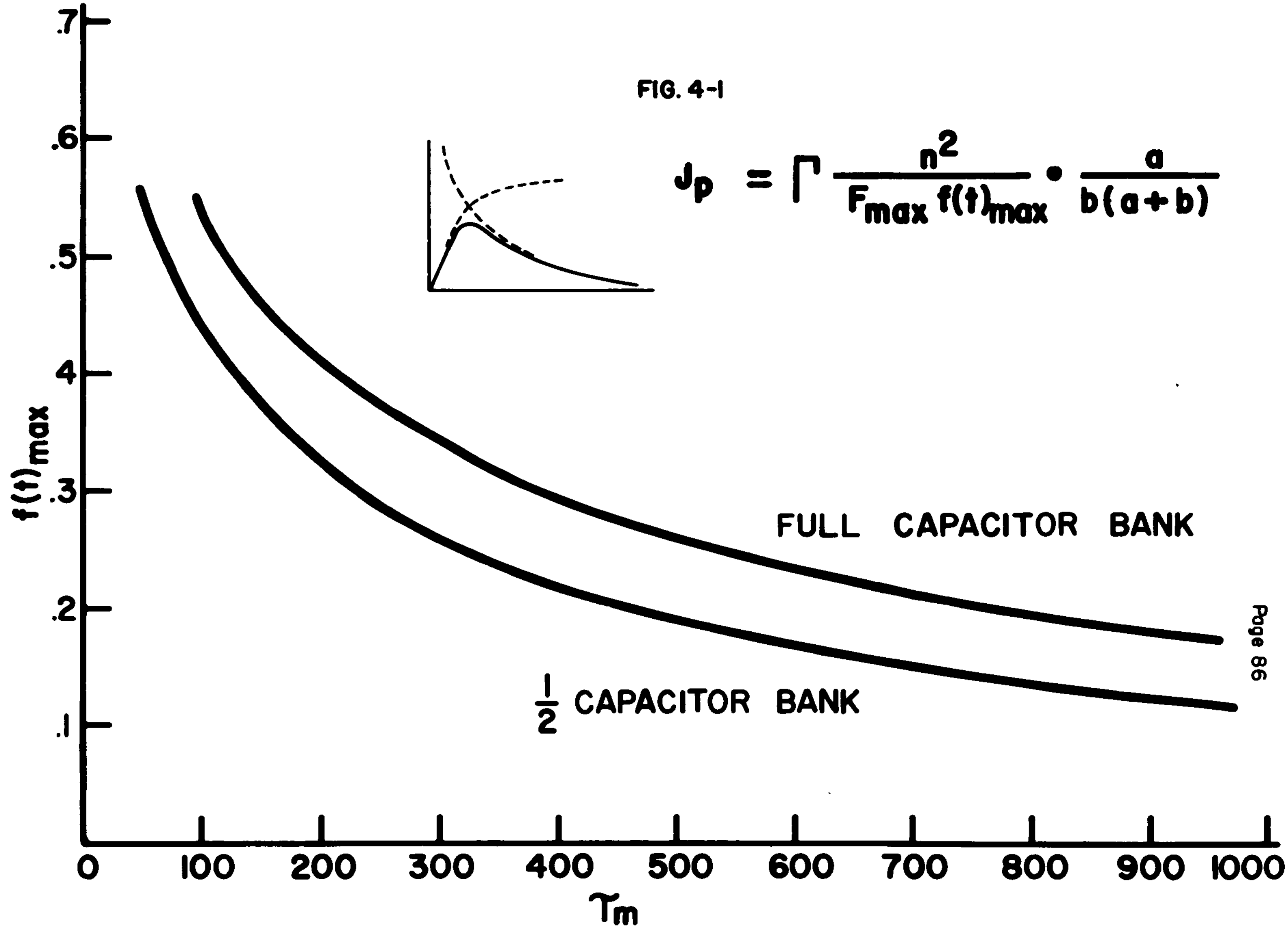

$$J_p = \Gamma \frac{n^2}{F_{max}\, f(t)_{max}} \bullet \frac{a}{b(a+b)}$$

full capacitor bank conditions in an E.G. and G. 10 tube laser simulator.

The complete derivation of equation I is given in Appendix B beginning on page 118.

The computed pulse thresholds for most glasses studied are given, as mentioned in Section 3.2, in Appendix A. A plot of the calculated relative pulse threshold versus the neodymium concentration for a large variety of different glass compositions is shown in Figure 4-2. Notice that there is qualitative agreement between the calculated values and the experimental threshold minimum in the vicinity of 5-6 wt. % neodymium as found by us and others.

When quantitative agreement between relative pulse thresholds and measured thresholds is sought, significant discrepencies are found. A reappraisal of our analysis and especially a reexamination of the major assumptions enumerated above have shown plausible reasons for these discrepencies.

Measurement of the flash lamp lifetime and intensity as a function of wavelength has shown that the time dependence and the frequency dependence of the laser flash lamp are not separable as assumed. Furthermore, these same measurements have shown that the spectral distribution of the flash lamp and the fluorescence measuring lamp are not the same. This latter effect alone is not sufficient to invalidate our analysis: if the spectral distributions of the continuous and flash lamps remained constant relative to each other, the calculated threshold would be in the correct relative order. A more disconcerting factor is that the spectral distribution and the lamp lifetime are significant functions of the lamp voltage (heretofore we have changed the voltage to arrive at a measured

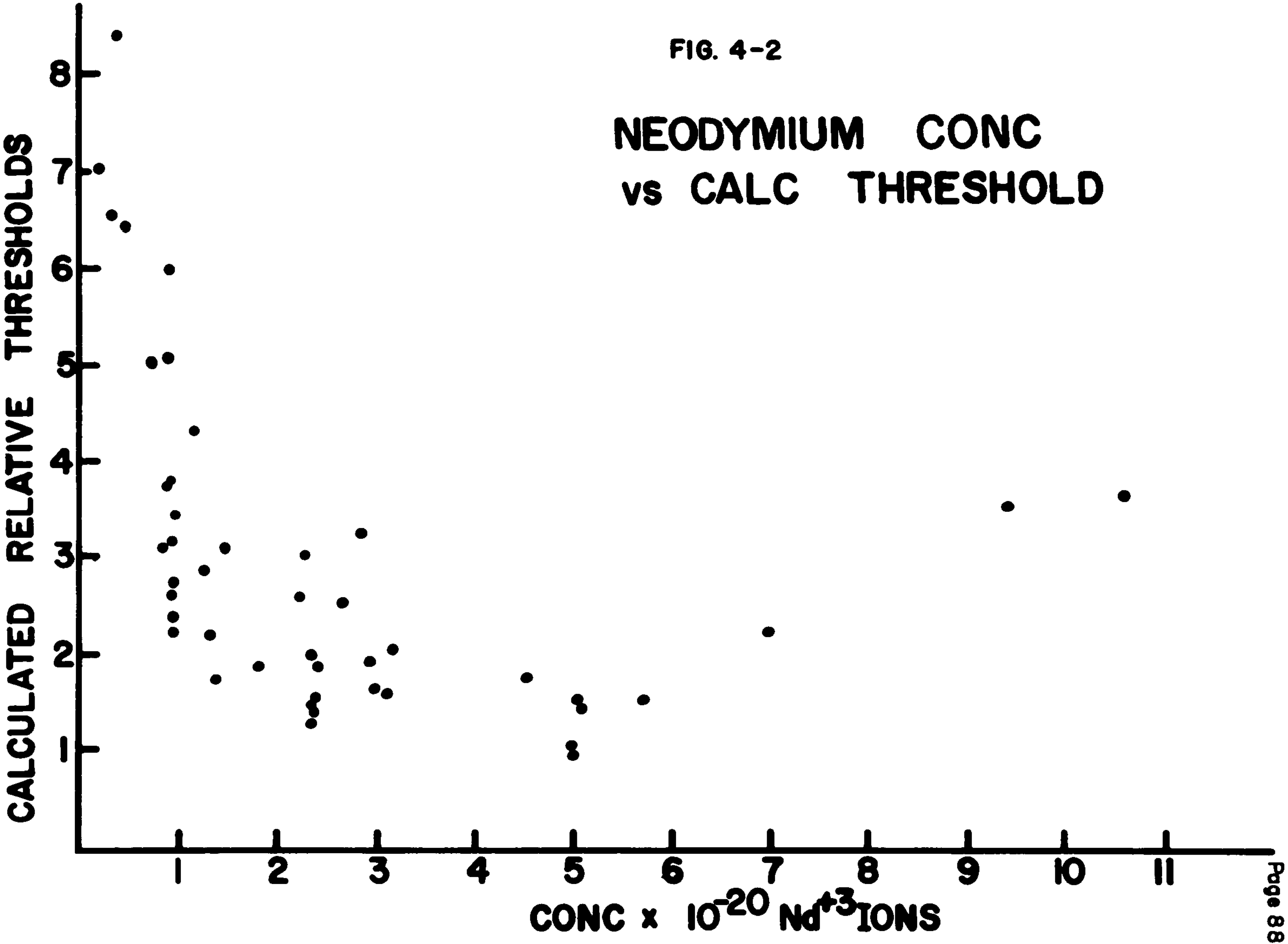

FIG. 4-2

NEODYMIUM CONC
vs CALC THRESHOLD

laser threshold). Thus, it is not surprising that quantitative agreement between calculated and measured thresholds has not been achieved.

4.2 Experimental Verification of Predicted Pulse Thresholds

We now understand why preliminary attempts to correlate experimental and calculated thresholds were not satisfactory. The problems are found to be associated with the measuring techniques rather than the theoretical analysis. The final analysis will take the aforementioned shortcomings into account.

We plan to remove the internal loss effects by using a series of laser rods having different end reflectivities. The thresholds on these rods will be measured without changing the lamp excitation conditions. Another method to check the theory will be to examine the effect of pulse shape on the threshold.

5. LARGE SCALE LASER GLASS MELT

A soda-lime silicate laser glass has been melted in a continuous melting process. The glass was formed with a 1-1/2 inch diameter mold and rods were cut to 24 and 40 inch lengths.

The optical quality obtained was excellent. A variation of 1/10 to 1/20 fringe (over a 2-1/2 inch length) corresponding to a change of less than 9 in the seventh decimal place of the refractive index was achieved (see Figure 4-3).

Other optical measurements on this glass are planned or underway. We are also evaluating the reproducibility of laser thresholds.

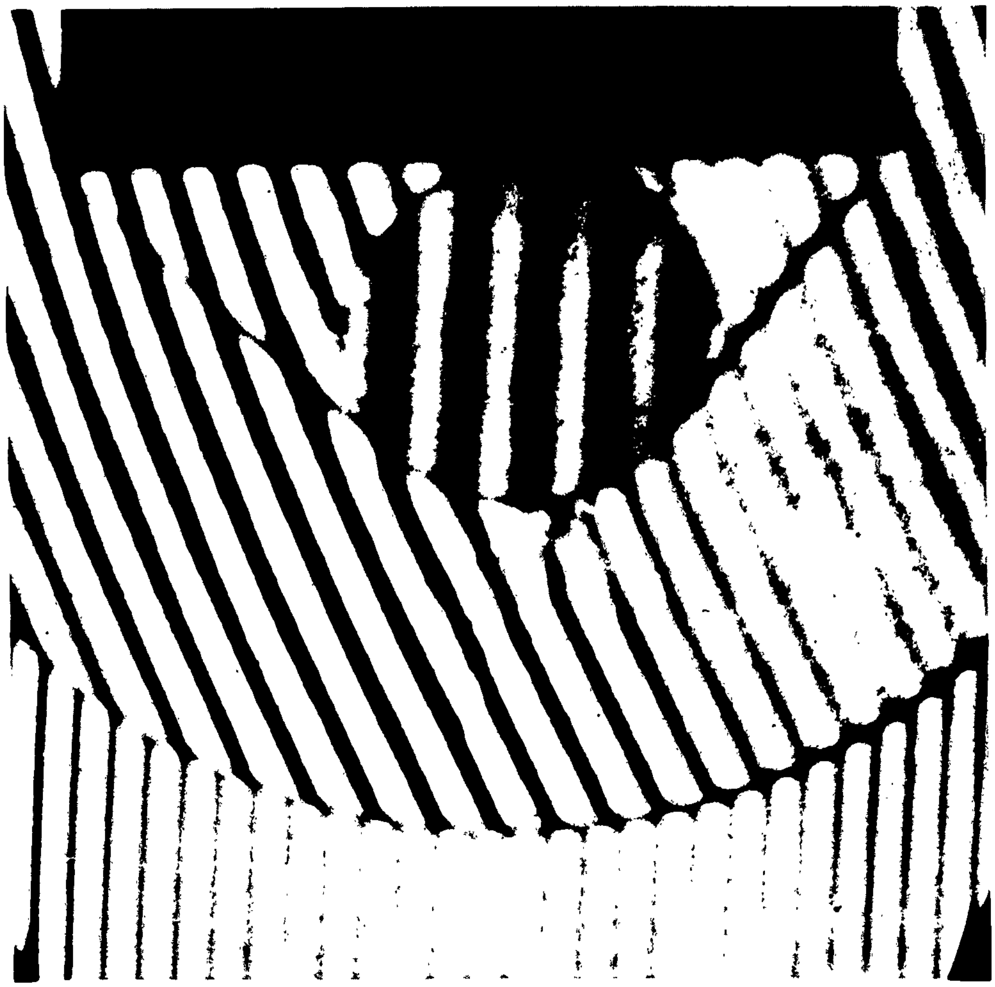

Fig. 4-3 Interferometer photograph of continuous tank melt laser glass (through 2-1/2"; 1-1/2" diameter).

6. SUMMARY

During the past year we have surveyed the fluorescence properties of a large number of neodymium doped glasses and made an intensive study of a particular composition. The work has been concentrated mainly on silicates and especially on those glasses where past experience would give a reasonable expectation of being able to manufacture the glass in good optical quality on a fairly large scale. Realizing that the performance of any particular glass laser device will depend on a large number of different properties, and that it would be impractical to measure all of these properties in all possible glasses, we have concentrated in the first instance on measuring the intrinsic spectral properties of a large number of different glasses. We already have extensive experience in relating properties other than rare earth fluorescence to the glass composition, and it was necessary to fill this gap in order to pick the best overall glass when the laser device requirements became more clearly defined. As a result of this program, we now have extensive knowledge of the absorption and fluorescence spectra, linewidths, lineshifts and lifetimes of neodymium ions in these glasses, and how these spectral properties are affected by changes in the glass composition, in the concentration of neodymium and in the concentration of various impurities. Detailed interpretation of these data, where possible, is underway and will continue for some time. It should be added here that although we have examined all of the other rare earth ions, and a number of them are known to exhibit laser action in glass, we have not found any systems that remotely approach neodymium in efficiency and ease of operation.

The performance of a glass laser will depend on a number of other properties in addition to the spectral properties noted above. Some of these are intrinsic properties of the material such as expansion coefficient, thermal conductivity and refractive index, while others are extrinsic properites such as optical quality, pumping geometry, etc. Since the intrinsic material properties of the glasses studied in this program can fairly readily be estimated from our glass experience, it has not been necessary to measure these properties for all the glasses studied.

During the course of this work we have developed a theoretical model to predict, on the basis of the measured spectral properties, the relative merit of all the experimental glasses in a simple pulsed laser device. The theoretical model was not developed to directly evaluate the glasses in high power devices (which are extremely complicated) but to make sure the fluorescent properties could be related to laser performance. Hence, this simple step was taken first. Experimental confirmation of the model remains to be concluded.

A large scale continuous unit melt has been made and preliminary studies of the optical quality and absorption at 1 micron are very favorable. Experiments have shown index variations of less than 1 part in 10^6.

REFERENCES

(1-1) Maiman, T.H., Nature 187, 493, (1960).

(1-2) Dieke, G.H., Advances in Quantum Electronics, edited by J.R. Singer (Columbia University Press, New York, 1961, p. 170.

(1-3) Yariv, A. and Gordon, J.P., Proc. I.E.E.E. 51, 4, (1963).

(2-1) Dieke, G.H., Advances in Quantum Electronics, Columbia University Press, New York, 1961.

(2-2) Runciman, W.A., Repts. Progr. in Phys. 21, 30, (1958).

(2-3) Fowler, W.B. and Dexter, D.L., Phys. Rev. 128, 2154, (1962).

(2-4) Miles, P.A. and Goldstein, I., to be published, I.E.E.E. Transactions.

(2-5) Miles, P.A., private communication.

(2-6) Miles, P.A., Progress Report 31, Laboratory for Insulation Research, M.I.T. (1962).

(3-1) Glass Industry 26, 417, (1945).

(3-2) Zachariasen, W.H., J. Am. Chem. Soc. 54, 3841-3851, (1932).

(3-3) Stanworth, J.E., Physical Properties of Glass, Clarendon Press, Oxford, 1950.

(3-4) Stevels, J.M., Progress in the Theory of the Physical Properties of Glass, Elsevier, New York, 1948.

(3-5) Jones, Gwyn O., Glass, Methuen, London, 1956.

(3-6) Morey, G.W., The Properties of Glass, Reinhold, New York, 1954.

(3-7) Volf, M.B., Technical Glasses, Pitman, London, 1961.

(3-8) Gooding, E.J. and Turner, W.E.S., J. Soc. Glass Tech. 18, 32, (1934).

(3-9) Green, R.L., J. Am. Ceram. Soc. 25, 83 (1942).

(3-10) Trap, H.J.L. and Stevels, J.M., Glastech. Ber. 32K VI, 31-52, (1959).

(3-11) Shand, E.B., Glass Engineering Handbook, McGraw-Hill, New York, 1958.

(3-12) Eastman Kodak Co., Semi-Annual Rept. to ONR, Contract 3834(00).

(3-13) Van Uitert, L.G. and Iida, S., J. Chem. Phys., 37, 986, (1962).

(3-14) Peterson, G.E., and Bridenbaugh, P.M., J.O.S.A., 53, 301, (1963).

(3-15) Woodcock, R.F., Opt. Soc. Meeting, Jacksonville, Fla., March 1963.

(3-16) Dexter, D.L., J. Chem. Phys. 21, 836, (1953).

(3-17) Dexter, D.L., and Schulman, J.H., J. Chem. Phys., 22, 1063, (1954).

(3-18) Maurer, R.D., Appl. Optics, 2, 87, (1963).

Appendix A

Experimental Data Taken on Neodymium Laser Glasses

The meaning of the column headings of this Appendix is described on page 36 of the text.

SERIES I BASE GLASS $75SiO_2+10CaO+15Na_2O$ (Mole %)

Glass Code	Base +	Nd^{3+} (10^{20} ions/cc)	Relative Intensity	τ Microseconds	$\Delta\lambda$(Å)	Calc. Rel. Pulse Thresh.	Meas. Thresh.	σ_{3500} ($10^{-20}cm^2$)	$\Delta\nu_{3500}$ (cm^{-1})	σ_{5800} ($10^{-20}cm^2$)	$\Delta\nu_{5800}$ (cm^{-1})	σ_{8000} ($10^{-20}cm^2$)	$\Delta\nu_{8000}$ (cm^{-1})	σ_{8800} ($10^{-20}cm^2$)	$\Delta\nu_{8800}$ (cm^{-1})
95CDX	0	0.9	90	622	324	4.9	118	0.73	1050	5850 2.36 5725 1.95	720	0.87	430	0.31	330
95CVA Opal	$-7.5Na_2O+7.5Li_2O$	0.2	52	460	312	5.1		CUT OFF		5825 2.36 5725 1.60	300 400	1.03	410	0.51	290
95CVB	$-15SiO_2+15Li_2O$	0.9	113	500		3.4		0.71	1100	5850 2.33 5750 1.47	610	1.11	350	0.32	350
95CVD	$-10CaO+10Na_2O$	0.9	103	580	298	4.1		0.95	1100	5825 2.63 5700 1.95	690	1.11	350	0.32	350
95CYS	$-10CaO+{5Na_2O \atop 5SiO_2}$	0.9	98	600		4.4		0.64	1100	5850 2.35 5725 2.13	370	0.85	410	0.31	350
87R	$-7.5Na_2O+7.5Li_2O$	5.1	184	190		1.3		0.79	1100	1.84	740	1.19	300	0.40	320
95DEL	$-15Na_2O+15Li_2O$	1.0	50	725		9.7		0.41	1100	5850 1.95 5725 2.27	360 290	0.51	410	0.18	350
95DEM	$-15Na_2O+15K_2O$	3.0	172	655		2.7		0.76	1100	5850 2.46 5725 2.62	400 260	0.94	350	0.32	410
95CJN$_2$	$-15SiO_2-10CaO$ $+15ZrO_2+10Na_2O$	2.6	150	460	335	2.5	165	0.68	1100	5850 2.38 5725 1.95	850	0.97	330	0.29	350

SERIES 2 BASE GLASS $75SiO_2+15Na_2O+10MO$ (Mole %)

Glass Code	10 MO	Nd^{3+} (10^{20} ions/cc)	Relative Intensity	τ Microseconds	$\Delta\lambda$(Å)	Calc. Rel. Pulse Thresh.	Meas. Thresh.	σ_{3500} ($10^{-20}cm^2$)	$\Delta\nu_{3500}$ (cm^{-1})	σ_{5800} ($10^{-20}cm^2$)	$\Delta\nu_{5800}$ (cm^{-1})	σ_{8000} ($10^{-20}cm^2$)	$\Delta\nu_{8000}$ (cm^{-1})	σ_{8800} ($10^{-20}cm^2$)	$\Delta\nu_{8800}$ (cm^{-1})
95CEN	ZnO	0.9	83	645	345	5.4	134	0.52	1100	5850 2.20 5725 2.39	400 270	0.65	470	0.23	350
95CIP	CdO	1.0	93	509		4.2	> 490	EVIDENT LOSS OF CADMIUM ALTERED BASE COMPOSITION							
95CEH	MgO	0.9	67	656	340	6.8	405	0.63	1100	5960 2.28 5725 2.06	730	0.90	410	0.32	330
95CEL	PbO	1.1	109.0	573	430	4.1	212								
95CDX	CaO	0.9	90	622	324	4.9	118	0.73	1050	5850 2.36 5725 1.95	720	0.87	430	0.31	330
95CIN	SrO	1.0	90	605	335	4.8	86	0.68	1100	5850 2.38 5725 1.95	850	0.97	330	0.29	350
95CEJ	BaO	1.0	100	627	420	4.5	124	0.68	1000	5850 2.28 5725 1.91	850	1.0	330	0.32	320
95CEI	BaO	0.2	21	560	330	19.7		0.69	1000	5860 2.59 5725 1.88	740	0.91	220	0.35	330

SERIES 3 BASE GLASS $SiO_2+PbO+15M_2O$ (Mole %)

Glass Code	PbO	$15M_2O$	Nd^{3+} (10^{20} ions/cc)	Relative Intensity	τ Microseconds	$\Delta\lambda$(Å)	Calc. Rel. Pulse Thresh.	Meas. Thresh.	σ_{3500} (10^{-20} cm^2)	$\Delta\nu_{3500}$ (cm^{-1})	σ_{5800} (10^{-20} cm^2)	$\Delta\nu_{5800}$ (cm^{-1})	σ_{8000} (10^{-20} cm^2)	$\Delta\nu_{8000}$ (cm^{-1})	σ_{8800} (10^{-20} cm^2)	$\Delta\nu_{8800}$ (cm^{-1})
95CEL	10	Na_2O	1.1	109	630	430	4.1									
95CIS	20	Na_2O	1.3	175	500	310	2.2		0.79	1100	5850 2.52 5725 2.00	690	1.14	340	0.38	340
95CIT	30	Na_2O	1.6	188	380	310	1.8		CUT OFF		5850 2.62 5725 1.89	720	1.41	450	0.43	330
87V	30	Na_2O	5.0	116	150		1.9		CUT OFF		OFF SCALE		1.38	400	0.49	310
95CGP	20	K_2O	1.3		740											
95CIU	20	K_2O	1.3		700											
95CIV	20	Cs_2O	1.5		750											
95CGR	20	Cs_2O	1.5		800											

(Pure Materials)

SERIES 4 BASE GLASS $SiO_2 + \Sigma MeO$ Me = Mg, Ca, Sr, Ba, Zn (Mole %)

Glass Code	SiO_2	MeO	Nd^{3+} (10^{20} ions/cc)	Relative Intensity	τ Microseconds	$\Delta\lambda$(Å)	Calc. Rel. Pulse Thresh.	Meas. Thresh.	σ_{3500} (10^{-20} cm^2)	$\Delta\nu_{3500}$ (cm^{-1})	σ_{5800} (10^{-20} cm^2)	$\Delta\nu_{5800}$ (cm^{-1})	σ_{8000} (10^{-20} cm^2)	$\Delta\nu_{8000}$ (cm^{-1})	σ_{8800} (10^{-20} cm^2)	$\Delta\nu_{8800}$ (cm^{-1})
95CES	60	8	1.2	102	360	371	3.2	> 490	0.89	1200	2.45	660	1.29	350	0.47	330
95CEQ	50	10	1.3	123	330	355	2.5	> 490	0.86	900	2.45	660	1.34	330	0.49	330
95CEW	40	12	1.4	175	340	328	1.8	136	CUT OFF		2.60	670	1.29	350	0.47	330
95CZI	40	12	3.0	210	280		1.4		CUT OFF		2.63	630	1.52	350	0.47	410
95CZJ	40	12	9.1	169	226		1.6		CUT OFF		OFF SCALE		1.78	294	0.64	350

SERIES 5 BASE GLASS $SiO_2 + B_2O_3 + 10MgO + 15Na_2O$ (Mole %)

Glass Code	SiO_2	B_2O_3	Nd^{3+} (10^{20} ions/cc)	Relative Intensity	τ Microseconds	$\Delta\lambda$(Å)	Calc. Rel. Pulse Thresh.	Meas. Thresh.	σ_{3500} (10^{-20} cm^2)	$\Delta\nu_{3500}$ (cm^{-1})	σ_{5800} (10^{-20} cm^2)	$\Delta\nu_{5800}$ (cm^{-1})	σ_{8000} (10^{-20} cm^2)	$\Delta\nu_{8000}$ (cm^{-1})	σ_{8800} (10^{-20} cm^2)	$\Delta\nu_{8800}$ (cm^{-1})
95CEH	75	0	0.9	67	656	340	6.8		0.63	1100	5860 2.28 5725 2.06	730	0.90	410	0.32	330
95CJY	65	10	0.9	68	360	365	4.8		0.78	1100	2.85	670	1.29	355	0.34	350
95CJZ	65	10	2.2	108	280	350	2.6		0.91	1100	5850 2.74 5725 1.96	700	1.36	410	0.39	390

SERIES 6 BORATE GLASSES (Mole %)

Glass Code	B_2O_3 +	Nd^{3+} (10^{20} ions/cc)	Relative Intensity	τ Microseconds	$\Delta\lambda$(A)	Calc. Rel. Pulse Thresh.	Meas. Thresh.	σ_{3500} ($10^{-20}cm^2$)	$\Delta\nu_{3500}$ (cm^{-1})	σ_{5800} ($10^{-20}cm^2$)	$\Delta\nu_{5800}$ (cm^{-1})	σ_{8000} ($10^{-20}cm^2$)	$\Delta\nu_{8000}$ (cm^{-1})	σ_{8800} ($10^{-20}cm^2$)	$\Delta\nu_{8800}$ (cm^{-1})
884J	85+15Na_2O	1.4	20	70	326	8.4		0.76	1000	2.84	410	1.20	300	0.31	300
884I	75+25BaO	1.3	28	65		5.9		1.30	1000	3.71	550	1.24	350	0.25	350
884K	72+28CaO	1.7	28	100		6.8		0.56	1100	1.73	580	0.85	350	0.21	350
884G	75+25Na_2O	1.5	19	70	370	8.8		0.67	1100	2.52	580	1.24	350	0.25	350
884F	75+25Li_2O	1.6	29	60	347	5.7									
95CKI	60+5Li_2O+35BaO	1.2	36	68		4.6	47								
884N	65+25Cs_2O+10PbO	1.4	26	100		7.2		CUT OFF		2.52	600	0.85	350	0.36	350
884S	100	94.2	4	< 50											
95CWS	29+22Al_2O_3+29CaO +19B_2O+1.4K_2O	1.1	27	200	284	9.0		1.05	1100	3.12	540	1.71	350	0.50	410
NONE	KODAK GLASS	4.4	71	53	356	2.2		2.13	1020	3.18	700	2.24	350	0.77	390
95CJC	KODAK TYPE (LANTHANUM BORATE)	2.2	63	100		3.0		CUT OFF		4.03	590	1.50	350	0.49	330
95CJB	KODAK TYPE (LANTHANUM BORATE)	2.2	55	95		2.9		CUT OFF		4.10	570	1.74	310	0.50	330
884R	KODAK TYPE (LEAD BORATE)	4.2	84	110		2.2		CUT OFF		OFF SCALE		1.48	295	0.43	350
884BB	67+33Na_2O	1.0	20	65		8.3									
884BC	67+33Na_2O	3.1	46	70	347	3.6									
884BD	67+33Na_2O	6.4	34	55	370	4.7									
884BE	67+33 Na_2O	14.2	20	42	347	7.7									

SERIES 7 BASE GLASS $68SiO_2+8AL_2O_3+5B_2O_3+20Na_2O$ (Mole %)

Glass Code	Nd^{3+} (10^{20} ions/cc)	Relative Intensity	τ Microseconds	$\Delta\lambda$(Å)	Calc. Rel. Pulse Thresh.	Meas. Thresh.	σ_{3500} (10^{-20} cm^2)	$\Delta\nu_{3500}$ (cm^{-1})	σ_{5800} (10^{-20} cm^2)	$\Delta\nu_{5800}$ (cm^{-1})	σ_{8000} (10^{-20} cm^2)	$\Delta\nu_{8000}$ (cm^{-1})	σ_{8800} (10^{-20} cm^2)	$\Delta\nu_{8800}$ (cm^{-1})
95CDM	0.2	17	560	339	24.3	> 490	0.69	1000	5725 2.19 5860 2.44	290 360	0.85	490	0.40	380
95CJI	0.7	53	555	325	7.7	> 490	0.65	1100	5850 2.36 5725 2.27	380 290	0.91	410	0.35	330
95CDP	0.9	70	580	325	6.0	121	0.62	1100	5850 2.29 5725 2.19	720	0.84	440	0.26	320
95CJH	2.7	150	500	295	2.8	134	0.65	1100	5720 2.26 5850 2.40	710	0.91	410	0.35	330
950AF	4.6	175	340		1.8		0.69	1100	5850 2.37 5725 2.20	740	0.91	410	0.32	350
95CJF	7.0	110	210	325	2.3	96	0.62	1000	OFF SCALE		0.81	410	0.32	330
95CJE	9.4	58	136	353	3.8	131	0.62	1000	OFF SCALE		0.72	470	0.36	290

SERIES 7a

Glass Code	Base +	Nd^{3+} (10^{20} ions/cc)	Relative Intensity	τ Microseconds	$\Delta\lambda$(Å)	Calc. Rel. Pulse Thresh.	Meas. Thresh.	σ_{3500} ($10^{-20}cm^2$)	$\Delta\nu_{3500}$ (cm^{-1})	σ_{5800} ($10^{-20}cm^2$)	$\Delta\nu_{5800}$ (cm^{-1})	σ_{8000} ($10^{-20}cm^2$)	$\Delta\nu_{8000}$ (cm^{-1})	σ_{8800} ($10^{-20}cm^2$)	$\Delta\nu_{8800}$ (cm^{-1})
95CJG	$+5SiO_2-5Na_2O$	4.8	53	200	582	4.7	> 490	0.85	1100	OFF SCALE		1.03	410	0.33	330
95DAF	0	4.6	175	340		1.8		0.69	1100	5850 2.37 5725 2.20	740	0.91	410	0.32	350
95DAG	$-5SiO+5Na_2O$	4.1	195	420		1.8		1.11	1000	5850 3.93 5725 3.49	840	1.52	350	0.48	350

SERIES 8 BASE GLASS $70SiO_2+15AL_2O_3+15MO$ (Mole %)

Glass Code	MO	Nd^{3+} (10^{20} ions/cc)	Relative Intensity	τ Microseconds	$\Delta\lambda$(Å)	Calc. Rel. Pulse Thresh.	Meas. Thresh.	σ_{3500} ($10^{-20}cm^2$)	$\Delta\nu_{3500}$ (cm^{-1})	σ_{5800} ($10^{-20}cm^2$)	$\Delta\nu_{5800}$ (cm^{-1})	σ_{8000} ($10^{-20}cm^2$)	$\Delta\nu_{8000}$ (cm^{-1})	σ_{8800} ($10^{-20}cm^2$)	$\Delta\nu_{8800}$ (cm^{-1})
95CYA	SrO	1.0	84	440		4.3		1.10	1200	3.52	660	1.19	410	0.37	350
95CXT	BaO	2.7	82	292		3.5		1.04	1100	3.12	700	1.11	410	0.35	350
95CXW	MgO	0.9	115	420		3.1		1.23	1100	3.49	450	1.54	350	0.31	410
95CXZ	CaO	2.4	138	340		2.8		0.95	1100	3.18	580	1.33	350	0.40	410

SERIES 9 $SiO_2+Al_2O_3+BaO$ (Mole %)

Glass Code	Al_2O_3	BaO	Nd^{3+} $(10^{20}\frac{ions}{cc})$	Relative Intensity	τ Microseconds	Δλ(Å)	Calc. Rel. Pulse Thresh.	Meas. Thresh.	σ_{3500} $(10^{-20}cm^2)$	$\Delta\nu_{3500}$ (cm^{-1})	σ_{5800} $(10^{-20}cm^2)$	$\Delta\nu_{5800}$ (cm^{-1})	σ_{8000} $(10^{-20}cm^2)$	$\Delta\nu_{8000}$ (cm^{-1})	σ_{8800} $(10^{-20}cm^2)$	$\Delta\nu_{8800}$ (cm^{-1})
95CYC	20	20	1.2	82	440		4.4		1.04	1100	3.04	700	1.17	410	0.32	350
95CYE	25	25	1.2	109	360		3.0		1.07	1100	3.36	680	1.14	410	0.31	350
95CYG	30	30	1.3	120	415		2.9		1.09	1100	3.02	780	1.24	410	0.38	410
95CXQ	25	5	1.2	103	440		3.5		1.00	1100	3.48	550	1.24	350	0.33	350
95CXT	15	15	2.7	82	292		3.5		1.04	1100	3.22	700	1.11	410	0.35	350
95CXU	5	25	1.2	130	480		2.9		1.38	1200	5875 1.79 5750 1.45	720	1.27	370	0.41	410
95CYD	20	20	2.9	91	310		3.3		0.97	1100	2.94	580	1.07	370	0.32	410
95CYF	25	25	3.0	117	290		2.5		0.89	1100	2.65	670	1.01	400	0.31	410
95CYH	30	30	3.2	140	300		2.1		1.12	1100	2.75	650	1.09	410	0.33	410
95CXR	25	5	2.4	160	320		1.9		1.02	1100	3.50	550	1.23	350	0.36	470

SERIES 10 ALUMINO-SILICATES BASE GLASS $SiO_2+AL_2O_3+B_2O_3$ + ... (Mole %)

Glass Code	SiO_2	AL_2O_3	B_2O_3	Li_2O	Na_2O	Cs_2O	MgO	CaO	BaO	La_2O_3	Nd^{3+} 10^{20} Ions/cc	Relative Intensity	τ Microseconds	$\Delta\lambda$(Å)	Calc. Rel. Pulse Thresh	Meas. Thresh	σ_{3500} ($10^{-20}cm^2$)	$\Delta\nu_{3500}$ (cm^{-1})	σ_{5800} ($10^{-20}cm^2$)	$\Delta\nu_{5800}$ (cm^{-1})	σ_{8000} ($10^{-20}cm^2$)	$\Delta\nu_{8000}$ (cm^{-1})	σ_{8800} ($10^{-20}cm^2$)	$\Delta\nu_{8800}$ (cm^{-1})
95CIW	70	5	0	0	25						0.9	79	640	330	5.7	> 490	0.68	1100	5850 2.39 5725 2.13	390 310	0.91	320	0.30	330
95CVG	70	5	0	25							1.1	78	480	326	4.8		0.70	1100	2.31	540	1.00	350	0.30	410
95CVH	70	5	0	0		25					1.2	51	320		5.9		OPAL				0.40	470	0.16	294
95CJW	65	10	0	0	15	0	10				0.9	69	440	380	5.2	> 490	0.93	1100	2.85	670	1.29	355	0.42	410
95CJS	65	10	0	15	0	0	10				0.9	65	380	370	5.1	> 490	0.94	1100	2.76	620	1.47	410	0.52	530
95CJT	65	10	0	15	0	0	10				2.3	95	300	397	3.1	> 490	0.91	1100	2.60	610	1.41	330	0.42	355
95CIL	65	17.5	0	0	0	0	0	0	0	17.5	1.4	100	330	410	3.1	> 490	CUT OFF		2.55	630	1.01	350	0.37	440
95CJX	65	10	0	0	15	0	10				2.3	94	320		3.2	> 490								
95CIK	71	1	0	0	15	0	0	13			1.4	135	540	320	2.9		0.67	1100	2.26	710	0.88	330	0.34	330
95CEF	58	25	0	0	2	0	0	15			1.0	93	440	441	3.8	95								
95CED	58	15	4	0	1	0	7	10	5		0.9	58	260	394	4.7	> 490	0.73	1100	5860 2.28 5725 2.06	730	0.90	410	0.32	330
95CIQ	38	5	17	0	0	0	0	0	39		1.2	73	420	335	4.8		0.72	1200	5850 2.20 5725 1.68	660	1.08	330	0.32	440

SERIES 11 BASE GLASS $71SiO_2+1Al_2O_3+12CaO+15Na_2O$ (Weight %)

Glass Code	Base +	Nd^{3+} (10^{20} ions/cc)	Relative Intensity	τ Microseconds	$\Delta\lambda$(Å)	Calc. Rel. Pulse Thresh.	Meas. Thresh.	σ_{3500} ($10^{-20}cm^2$)	$\Delta\nu_{3500}$ (cm^{-1})	σ_{5800} ($10^{-20}cm^2$)	$\Delta\nu_{5800}$ (cm^{-1})	σ_{8000} ($10^{-20}cm^2$)	$\Delta\nu_{8000}$ (cm^{-1})	σ_{8800} ($10^{-20}cm^2$)	$\Delta\nu_{8800}$ (cm^{-1})
869GI	0	0.4	50	580		8.4	290	0.74	1100	5875 2.31	700	0.89	350	0.39	350
869GH	0	0.7	83	580		5.1	161	0.69	1100	5850 2.40 5750 1.77	700	1.03	350	0.34	350
8698G	0	1.5	125	520	338	3.2	50	0.60	1100	5860 2.01 5730 1.48	690	0.94	375	0.30	330
8698GI	0	3.0	200	480	312	2.0	92	0.79	1130	5820 2.40 5749 1.78	720	1.06	360	0.35	340
869GC	0	5.7	167	235		1.6	71	0.67	1090	OFF SCALE		0.97	360	0.33	330

SERIES IIa BASE GLASS $71SiO_2+1Al_2O_3+12CaO+15Na_2O$ (Weight %)

Glass Code	Base + Sb_2O_3	Nd^{3+} (10^{20} ions/cc)	Relative Intensity	τ Microseconds	$\Delta\lambda$(Å)	Calc. Rel. Pulse Thresh.	Meas. Thresh.	σ_{3500} (10^{-20} cm^2)	$\Delta\nu_{3500}$ (cm^{-1})	σ_{5800} (10^{-20} cm^2)	$\Delta\nu_{5800}$ (cm^{-1})	σ_{8000} (10^{-20} cm^2)	$\Delta\nu_{8000}$ (cm^{-1})	σ_{8800} (10^{-20} cm^2)	$\Delta\nu_{8800}$ (cm^{-1})
8698G	0	1.5	125	520	338	3.2	50	0.60	1100	5860 2.01 5730 1.48	690	0.94	375	0.30	330
869GK	0.3	1.5	168	560		2.5		0.66	1100	5850 2.01 5730 1.48	690	1.03	350	0.34	350
869GD	0.7	1.5	178	540		2.3	35	0.72	1150	5870 2.51 5750 1.88	680	1.09	375	0.36	320
869GL	1.0	1.5	193	540	310	2.1		0.69	1100	5850 2.38 5725 1.82	680	0.96	350	0.35	350
869GM	1.4	1.5	188	560		2.2		0.69	1100	5875 2.40 5750 1.81	700	1.06	350	0.35	350
95CZH	1.0	2.0	230	520		1.7		0.79	1000	5850 2.49 5750 1.88	700	1.11	350	0.36	350
95CZG	1.0	3.0	268	460		1.4		0.75	1000	5875 2.46 5750 1.80	700	1.08	350	0.35	350
87S	1.0	5.0	235	260		1.2		0.74	1000	5875 OFF SCALE 5730 1.85		1.05	390	0.36	333

SERIES 12 BASE GLASS $67SiO_2+2Al_2O_3+9CaO+8Na_2O+9K_2O+3.5ZnO$+ADDITIVES OF VARIOUS OXIDES (Mole %)

Glass Code	Nd^{3+} (10^{20} ions/cc)	Relative Intensity	τ Microseconds	$\Delta\lambda$(Å)	Calc. Rel. Pulse Thresh.	Meas. Thresh.	σ_{3500} ($10^{-20}cm^2$)	$\Delta\nu_{3500}$ (cm^{-1})	σ_{5800} ($10^{-20}cm^2$)	$\Delta\nu_{5800}$ (cm^{-1})	σ_{8000} ($10^{-20}cm^2$)	$\Delta\nu_{8000}$ (cm^{-1})	σ_{8800} ($10^{-20}cm^2$)	$\Delta\nu_{8800}$ (cm^{-1})
843KJ	0.5	65	575		6.5		0.70	1100	5875 2.50 5750 2.08	700	1.00	410	0.30	410
843KK	0.9	113	600	340	3.8	246	0.69	1000	5875 2.48 5750 2.14	710	1.04	350	0.35	350
843KL	1.4	153	590		2.8		0.67	1100	5875 2.36 5750 1.99	700	0.96	350	0.33	350
87U	5.0	219	280		1.3		0.67	1000	OFF SCALE		0.98	440	0.34	330

Glass Code	Nd^{3+} (10^{20} ions/cc)	Relative Intensity	τ Microseconds	$\Delta\lambda$(Å)	Calc. Rel. Pulse Thresh.	Meas. Thresh.	σ_{3500} (10^{-20} cm^2)	$\Delta\nu_{3500}$ (cm^{-1})	σ_{5800} (10^{-20} cm^2)	$\Delta\nu_{5800}$ (cm^{-1})	σ_{8000} (10^{-20} cm^2)	$\Delta\nu_{8000}$ (cm^{-1})	σ_{8800} (10^{-20} cm^2)	$\Delta\nu_{8800}$ (cm^{-1})
SERIES 13		BASE GLASS	$79P_2O_5+21La_2O_3$ (Mole %)											
95ZP	0.9	79	310	296	3.8		0.74	1000	5790 3.25 5710 2.35	650	1.40	350	0.38	295
95ZQ	1.8	143	260	288	1.9		0.97	1000	5790 OFF SCALE 5720 2.39		1.54	295	0.47	295
95ACE	3.0	153	220	282	1.7		0.80	1000	OFF SCALE		1.23	350	0.43	295
87W	5.2	208	180		1.3		0.86	880	OFF SCALE		1.24	358	0.39	333
SERIES 13a		BASE GLASS	$50P_2O_5+50Li_2O$ (Mole %)											
884AZ	0.8	15	60				1.26	1000	2.63	450	2.68	240	0.77	350
884BA	4.2	21	107				0.24	970	0.71	430	0.49	260	0.14	290
SERIES 14		BASE GLASS	$42GeO_2+6ZrO_2+42BaO+3CaO+3.5\ Al_2O_3+4ZnO$ (Mole %)											
95CDY	0.3	43	280	349	6.6		CUT OFF		4.18	670	2.0	360	0.64	390
95CEO	1.6	120	300	356	2.4		CUT OFF		2.79	750	1.64	470	0.60	360
87X	5.0	162	160		1.4									

SERIES 15 BASE GLASS $48SiO_2+10.4Na_2O+10.4K_2O+10.4CaO+10.4Li_2O+10.4MgO$ (Mole %)

Glass Code	WT. % Fe_2O_3	WT. % As_2O_5	Nd^{3+} (10^{20} ions/cc)	Relative Intensity	τ Microseconds	Calc. Rel. Pulse Thresh.	σ_{3500} ($10^{-20}cm^2$)	$\Delta\nu_{3500}$ (cm^{-1})	σ_{5800} ($10^{-20}cm^2$)	$\Delta\nu_{5800}$ (cm^{-1})	σ_{8000} ($10^{-20}cm^2$)	$\Delta\nu_{8000}$ (cm^{-1})	σ_{8800} ($10^{-20}cm^2$)	$\Delta\nu_{8800}$ (cm^{-1})
95CML	0	0	0.9	159	450	2.3	0.85	1100	5850 2.71 5725 1.90	690	1.61	350	0.45	350
95CMM	0	0	2.4	221	380	1.4	0.89	1080	5850 2.59 5725 1.86	690	1.62	350	0.49	350
95DCV	0	0	4.8	183	210	1.4	0.78	1100	5875 2.00 5750 1.71	690	1.18	350	0.41	350
95CMN	0	3	0.9	137	440	2.6	0.76	1100	5850 2.53 5725 1.86	700	1.46	410	0.44	350
95CMO	0	3	2.4	223	360	1.5	0.79	1100	5850 2.42 5725 1.74	700	1.57	350	0.44	350
95DCW	0	3	4.8	195	223	1.3	0.75	1000	5825 1.96 5750 1.67	800	1.13	295	0.39	295
95CMR	0.01	0	0.9	116	450	3.1	0.86	1100	5875 2.70 5750 1.94	700	1.62	350	0.53	350
95CMS	0.01	0	2.4	215	370	1.5	0.70	1125	5875 2.34 5750 1.81	690	1.48	294	0.43	340
95DCX	0.01	0	4.8	195	214	1.3	0.74	1000	5825 2.10 5750 1.72	720	1.22	350	0.40	350

SERIES 15 (continued) BASE GLASS $48SiO_2+10.4Na_2O+10.4K_2O+10.4CaO+10.4Li_2O+10.4MgO$ (Mole %)

Glass Code	WT. % Fe₂O₃	WT. % As₂O₅	Nd^{3+} (10^{20} ions/cc)	Relative Intensity	τ Microseconds	Calc. Rel. Pulse Thresh.	σ_{3500} ($10^{-20}cm^2$)	$\Delta\nu_{3500}$ (cm^{-1})	σ_{5800} ($10^{-20}cm^2$)	$\Delta\nu_{5800}$ (cm^{-1})	σ_{8000} ($10^{-20}cm^2$)	$\Delta\nu_{8000}$ (cm^{-1})	σ_{8800} ($10^{-20}cm^2$)	$\Delta\nu_{8800}$ (cm^{-1})
95CMP	0.01	3	0.9	153	470	2.4	0.72	1100	5850 2.54 5725 1.85	680	1.45	294	0.47	350
95CMQ	0.01	3	2.4	233	360	1.4	0.87	1100	5850 2.56 5725 1.82	690	1.59	340	0.47	340
95DCY	0.01	3	4.8	162	204	1.5	0.71	1000	5875 OFF SCALE 5750 1.67	700	1.14	350	0.39	295
95CMT	0.1	0	0.9	110	420	3.2	CUT OFF		5875 2.53 5750 1.80	660	1.51	350	0.48	350
95CMU	0.1	0	2.4	155	340	2.0	CUT OFF		5875 2.40 5750 1.80	660	1.50	294	0.50	350
95DCZ	0.1	0	4.8	178	196	1.3	CUT OFF		5825 1.99 5750 1.73	700	1.20	350	0.40	295
95CMV	0.1	3	0.9	123	400	2.8	CUT OFF		5875 2.49 5725 1.78	670	1.54	410	0.53	340
95CMW	0.1	3	2.4	21	200	11.5	0.63	1100	5850 2.59 5725 1.85	660	1.43	294	0.54	294
95DDA	0.1	3	4.8	34	146	6.3	0.55	950	5875 OFF SCALE 5750 1.63	700	1.22	350	0.39	350

SERIES 16 BASE GLASS $65SiO_2+15Na_2O+20PbO$ (Mole %)

Glass Code	Nd^{3+} (10^{20} ions/cc)	Relative Intensity	τ Microseconds	$\Delta\lambda$(Å)	Calc. Rel. Pulse Thresh.	σ_{3500} ($10^{-20}cm^2$)	$\Delta\nu_{3500}$ (cm^{-1})	σ_{5800} ($10^{-20}cm^2$)	$\Delta\nu_{5800}$ (cm^{-1})	σ_{8000} ($10^{-20}cm^2$)	$\Delta\nu_{8000}$ (cm^{-1})	σ_{8800} ($10^{-20}cm^2$)	$\Delta\nu_{8800}$ (cm^{-1})
95CIS	1.3	175	500	310	2.2	0.79	1100	5850 2.52 5725 2.00	690	1.14	340	0.38	340
95CZD	2.0	203	500		1.9	0.66	1050	5850 2.48 5725 1.70	700	0.99	350	0.32	350
95CZC	3.1	215	420		1.6	0.81	1100	5850 2.65 5725 1.99	830	1.20	350	0.41	350
95CZF	5.1	185	260		1.5	0.76	1000	OFF SCALE		1.07	350	0.38	350
95CZE	10.6	54	120		3.7	OFF SCALE		OFF SCALE		OFF SCALE		0.41	410

SERIES 17a COMMERCIAL BASE GLASSES

Glass Code	Nd^{3+} (10^{20} ions/cc)	Relative Intensity	τ Microseconds	$\Delta\lambda$(Å)	Calc. Rel. Pulse Thresh.	Meas. Thresh.	σ_{3500} ($10^{-20}cm^2$)	$\Delta\nu_{3500}$ (cm^{-1})	σ_{5800} ($10^{-20}cm^2$)	$\Delta\nu_{5800}$ (cm^{-1})	σ_{8000} ($10^{-20}cm^2$)	$\Delta\nu_{8000}$ (cm^{-1})	σ_{8800} ($10^{-20}cm^2$)	$\Delta\nu_{8800}$ (cm^{-1})
95CXC	4.0	100	160	340	2.2		0.91	1100	2.62	670	1.42	410	0.42	350
95CXD	2.7	213	560		1.9		0.63	1100	5850 2.30 5725 2.01	860	0.88	410	0.30	350
95CXE	3.1	185	240	312	1.4		0.57	NEAR CUT OFF	5850 2.66 5750 1.87	780	1.33	350	0.39	350
95CXF	3.0	181	280	312	1.6		0.55	NEAR CUT OFF	5825 2.58 5700 1.91	735	1.35	350	0.41	350
95CXG	3.1	265	460	312	1.4	102	0.82	1000	5825 2.47 5700 2.04	730	1.05	350	0.34	350
87Q (OPHTHALMIC)	5.0	200	180		1.2		0.83	1100	2.03	700	1.37	390	0.44	333
KODAK	4.4	69	53	356	2.3		2.13	1020	3.18	700	2.24	350	0.77	390
95DGP (Ba Crown)	5.1	280	545	312	1.5		0.67	1040	5830 2.04 5700 2.07	370 290	0.64	418	0.24	335
95DET	5.1	223	286		1.3									

SERIES 17b VARIATIONS OF 95CXG

Glass Code	Base +	Nd^{3+} (10^{20} ions/cc)	Relative Intensity	τ Microseconds	$\Delta\lambda$(Å)	Calc. Rel. Pulse Thresh.	Meas. Thresh.	σ_{3500} ($10^{-20}cm^2$)	$\Delta\nu_{3500}$ (cm^{-1})	σ_{5800} ($cm^{-20}cm^2$)	$\Delta\nu_{5800}$ (cm^{-1})	σ_{8000} ($10^{-20}cm^2$)	$\Delta\nu_{8000}$ (cm^{-1})	σ_{6800} ($10^{-20}cm^2$)	$\Delta\nu_{8800}$ (cm^{-1})
95CXG	0	3.1	250	460	312	1.4	102	0.82	1000	5825 2.47 5700 2.04	730	1.05	350	0.34	350
87T	Nd_2O_3	5.1	268	300		1.1				1.85	810	0.99	330	0.34	333
$87T_2$	Pure Materials	5.1	268	330		1.2									
$87T-H_2O$	Water Free	5.1	276	373		1.2									
87Y	Sb_2O_3	5.1	299	327		1.0									
87Z	$+Li_2O-Na_2O$	5.1	OPAQUE												
87AA	$+Li_2O-Na_2O$ $+BaO-CaO$	5.1	195	159		1.1									
87AB	+BaO–CaO	5.1	400	400		0.8	96								

SERIES 17c VARIATIONS OF 95DET

Glass Code	Nd^{3+} (10^{20} ions/cc)	Relative Intensity	τ Microseconds	$\Delta\lambda$(Å)	Calc. Rel. Pulse Thresh.	Meas. Thresh.	σ_{3500} ($10^{-20}cm^2$)	$\Delta\nu_{3500}$ (cm^{-1})	σ_{5800} ($10^{-20}cm^2$)	$\Delta\nu_{5800}$ (cm^{-1})	σ_{8000} ($10^{-20}cm^2$)	$\Delta\nu_{8000}$ (cm^{-1})	σ_{8800} ($10^{-20}cm^2$)	$\Delta\nu_{8800}$ (cm^{-1})
95DGO	0.9	106	519		3.7	180								
95DGN	1.8	198	519		2.0	108								
95DGM	2.8	250	464		1.5	108								
95DGL	3.7	267	395		1.3	126								
95DET (Harrodsburg)	4.0	260	319	324	1.2		0.79	1070	5860 2.42 5730 1.89	700	0.98	403	0.35	357

SERIES 18a BASE GLASS $72SiO_2+23Na_2O+5CaO$ (Weight %)

Glass Code	Nd^{3+} (10^{20} ions/cc)	Relative Intensity	τ Microseconds	Calc. Rel. Pulse Thresh.	σ_{8000} ($10^{-20}cm^2$)	$\Delta\nu_{8000}$ (cm^{-1})	σ_{8800} ($10^{-20}cm^2$)	$\Delta\nu_{8800}$ (cm^{-1})
Typical or average values taken for different raw materials	0.9	95	560	4.4				
	2.6	220	530	1.8				
	3.5	237	436	1.5				
	4.4	260	422	1.4				
	6.1	228	290	1.3				
	6.9	230	255	1.2				
	8.7	160	190	1.5				
	11.6	150	155	1.5				
	20.0	53	< 50					

SERIES 18b BASE GLASS 81% $SiO_2+15Na_2O+4CaO$ (Weight %)

884EO	0.8	88	570	4.7				
884EP	2.6	194	570	2.2	0.83	350	0.28	350
884EQ	6.3	223	365	1.5				
884ER	9.3	204	225	1.3	0.74	350	0.27	350

SERIES 18c BASE GLASS $75SiO_2+25Na_2O$ (Weight %)

Glass Code	Nd^{3+} (10^{20} ions/cc)	Relative Intensity	τ Microseconds	Calc. Rel. Pulse Thresh.	σ_{8000} ($10^{-20}cm^2$)	$\Delta\nu_{8000}$ (cm^{-1})	σ_{8800} ($10^{-20}cm^2$)	$\Delta\nu_{8800}$ (cm^{-1})
884DC	0.9	126	600	3.4				
884EG	0.9	103	618	4.3				
884DD	2.5		572					
884EH	2.5	219	617	2.0				
884AO	3.4	262	540	1.5				
884AR	3.4	262	540	1.5				
884EW	4.3	290	486	1.3				
884DE	5.0		400					
884EI	6.0	310	472	1.2				
884EN	6.0	324	400	1.1	0.84	410	0.32	350
884AN	6.8	283	318	1.1				
884AS	6.8	285	346	1.1				
884EX	6.8	315	373	1.0				
884EJ	8.6	316	273	0.9				
884DF	8.6		282					
SERIES 18d	BASE GLASS	$82SiO_2+18Na_2O$	(Weight %)					
884ES	0.8	91	610	4.8				
884EU	2.5	207	590	2.1				
884ET	5.8	252	430	1.4				
884EV	8.3	115 (?)	300	2.5 (?)				

SERIES 19 FLUORIDE GLASS BASE GLASS $20BeF_2+30BaF_2+25AlF_3+15MgF_2+10CaF_2+NdF_3$ (Weight %)

Glass Code	Nd^{3+} (10^{20} ions/cc)	Relative Intensity	τ Microseconds	$\Delta\lambda$(Å)	Calc. Rel. Pulse Thresh.	σ_{3500} ($10^{-20}cm^2$)	$\Delta\nu_{3500}$ (cm^{-1})	σ_{5800} ($10^{-20}cm^2$)	$\Delta\nu_{5800}$ (cm^{-1})	σ_{8000} ($10^{-20}cm^2$)	$\Delta\nu_{8000}$ (cm^{-1})	σ_{8800} ($10^{-20}cm^2$)	$\Delta\nu_{8800}$ (cm^{-1})
8161H	0.8	99	600	288	4.4	OPAQUE		1.42	460	1.39	295	0.33	295
8161G	2.6	153	420	253	2.3	OPAQUE		1.34	440	1.22	295	0.33	295

SERIES 20 SILICA-FREE ALUMINO-BORATES BASE GLASS $22Al_2O_3+29B_2O_3+29CaO+19BaO+1.4K_2O$ (Mole %)

Glass Code	Base +	Nd^{3+} (10^{20} ions/cc)	Relative Intensity	τ Microseconds	Calc. Rel. Pulse Thresh.	σ_{3500} ($10^{-20}cm^2$)	$\Delta\nu_{3500}$ (cm^{-1})	σ_{5800} ($10^{-20}cm^2$)	$\Delta\nu_{5800}$ (cm^{-1})	σ_{8000} ($10^{-20}cm^2$)	$\Delta\nu_{8000}$ (cm^{-1})	σ_{8800} ($10^{-20}cm^2$)	$\Delta\nu_{8800}$ (cm^{-1})
95DBA	0	1.0	49	186	4.8	0.84	1100	2.76	710	1.85	325	0.49	350
95DBF	0	3.0	69	88	2.6	0.75	1100	2.38	600	1.44	350	0.42	350
95DBB	$+5Al_2O_3$	1.0	38	109	5.1	0.87	1100	2.74	630	1.73	350	0.50	410
95DBG	$-5B_2O_3$	3.0	62	88	2.9	0.86	1100	2.68	600	1.55	350	0.46	380
95DBC	+5CaO	1.0	47	103	4.0	0.80	1100	2.57	590	1.57	350	0.37	410
95DBH	-5BaO	3.0	74	89	2.5	0.82	1050	2.51	740	1.53	325	0.44	360
95DBD	+5BaO	1.0		101									
95DBI	-5CaO	3.0	61	79	2.9	0.84	1000	2.61	620	1.59	300	0.46	350
95DBE	+5CaO	1.0	42	97	4.4	0.81	1100	2.59	600	1.66	350	0.45	400
95DBJ	$-5B_2O_3$	3.0	74	89	2.5	0.79	1100	2.41	640	1.49	325	0.45	400

SERIES 21a KCl for K_2O BASE GLASS $75SiO_2+15K_2O+10CaO$ (Mole %)

Glass Code	Base +	Nd^{3+} (10^{20} ions/cc)	Relative Intensity	τ Microseconds	$\Delta\lambda$(Å)	Calc. Rel. Pulse Thresh.	Meas. Thresh.	σ_{3500} (10^{-20} cm^2)	$\Delta\nu_{3500}$ (cm^{-1})	σ_{5800} (10^{-20} cm^2)	$\Delta\nu_{5800}$ (cm^{-1})	σ_{8000} (10^{-20} cm^2)	$\Delta\nu_{8000}$ (cm^{-1})	σ_{8800} (10^{-20} cm^2)	$\Delta\nu_{8800}$ (cm^{-1})
95DEL	0	1.0	50	725		9.7		0.41	1100	5850 1.95 5725 2.27	360 290	0.51	410	0.18	350
95DEM	0	3.0	172	655		2.7		0.76	1100	5850 2.46 5725 2.62	400 260	0.94	350	0.32	410
95DEN	$+5K_2Cl_2$ $-5K_2O$	1.0	63	686		7.4		0.52	1150	5850 2.20 5725 2.39	400 270	0.65	470	0.23	350
95DEO	$+5K_2Cl_2$ $-5K_2O$	3.0	161	582		2.6		0.78	1100	5850 2.52 5725 2.56	740	0.81	410	0.29	350
95DEP	$+10K_2Cl_2$ $-10K_2O$	1.0	108	632		4.1									
95DEQ	$+10K_2Cl_2$ $-10K_2O$	3.0	182	391		1.9									
95CDU	0	0.2		720											
95CDZ	0	0.9		750											

SERIES 21b NaF for Na_2O BASE GLASS $75SiO_2+15Na_2O+10CaO$ (Mole %)

Glass Code	Base +	Nd^{3+} (10^{20} ions/cc)	Relative Intensity	τ Microseconds	$\Delta\lambda$(Å)	Calc. Rel. Pulse Thresh.	Meas. Thresh.	σ_{3500} (10^{-20} cm^2)	$\Delta\nu_{3500}$ (cm^{-1})	σ_{5800} (10^{-20} cm^2)	$\Delta\nu_{5800}$ (cm^{-1})	σ_{8000} (10^{-20} cm^2)	$\Delta\nu_{8000}$ (cm^{-1})	σ_{8800} (10^{-20} cm^2)	$\Delta\nu_{8800}$ (cm^{-1})
95CDX	0	0.9	90	622	324	4.9	118	0.73	1050	5850 2.36 5725 1.95	720	0.87	430	0.31	330
95DFO	$+5Na_2F_2$ $-5Na_2O$	1.0	169	535		2.4									

SERIES 22a HIGH TEMPERATURE INVERTS BASE GLASS $50SiO_2+12.5ThO_2+12.5LaO_{1.5}+12.5BaO+12.5TaO_{2.5}$ (Mole %)

Glass Code	Nd^{3+} (10^{20} ions/cc)	Relative Intensity	τ Microseconds	$\Delta\lambda$(Å)	Calc. Rel. Pulse Thresh.	σ_{3500} ($10^{-20}cm^2$)	$\Delta\nu_{3500}$ (cm^{-1})	σ_{5800} ($10^{-20}cm^2$)	$\Delta\nu_{5800}$ (cm^{-1})	σ_{8000} ($10^{-20}cm^2$)	$\Delta\nu_{8000}$ (cm^{-1})	σ_{8800} ($10^{-20}cm^2$)	$\Delta\nu_{8800}$ (cm^{-1})
95DEU	1.0	380	270	360	0.7					2.03	350	1.57	420
95DEV	3.0	123	263		2.0	0.23	1100	1.52	650	0.68	410	0.20	350
SERIES 22b	BASE GLASS	$50SiO_2+20ThO_2+10LaO_{1.5}+10BaO+10TaO_{2.5}$	(Mole %)										
95DEW	1.0	143	184		1.6	3.05	1200	OFF SCALE		5.28	350	1.55	410
95DEX	3.0	177	215		1.4	0.84	1200	3.13	650	1.39	350	0.42	410

APPENDIX B

Here we describe how fluorescence data may be related to the pulse threshold.

Energy Threshold for Pulsed Lasers

I. Theoretical Considerations

Consider first the population in the excited metastable state as a function of time. The rate of production of excited atoms by the pumping pulse is given by

1) $$\epsilon \int \frac{I_p(\nu,t)}{h\nu} \alpha(\nu) d\nu$$

where

$I_p(\nu,t)$	is the intensity of the pumping light per unit frequency interval.
$\alpha(\nu)$	is the absorption coefficient.
ϵ	is the efficiency of conversion of absorbed photons into excited atoms in the meta stable state.

The rate of loss out of the metastable state by spontaneous emission is

2) $$\frac{N_e}{\tau_m}$$

where

N_e	is the ions/cc in the metastable state at time "t".
τ_m	is the measured lifetime.

If we ignore the rate of loss due to stimulated emission, the differential equation governing the population of the metastable state as a function of time is,

$$3) \qquad \dot{N}_e = \epsilon \int \frac{I_p(\nu,t)\,\alpha(\nu)}{h\nu}\, d\nu \quad - \frac{N_e}{\tau_m}$$

The intensity of the pumping pulse can be assumed to be of the form

$$4) \qquad I_p(\nu,t) = I_o(\nu)\, g_1(t)$$

where $I_o(\nu)$ is the spectral distribution of the lamp and $g_1(t)$ is the shape of the pulse. A good approximation for $g_1(t)$ is given by

$$5) \qquad g_1(t) = (1-e^{-at})\, e^{-bt}$$

where a and b are constants that can be determined experimentally. Eqn. 4 then becomes

$$6) \qquad I_p(\nu,t) = I_o(\nu)(1-e^{-at})\, e^{-bt}$$

substituting Eqn. 6 into Eqn. 3 gives the following

$$7) \qquad \dot{N}_e + \frac{N_e}{\tau_m} = \left\{ \epsilon \int \frac{I_o(\nu)\,\alpha(\nu)}{h\nu}\, d\nu \right\} (1-e^{-at})\, e^{-bt}$$

The solution of the equation, with the boundary condition that at t = 0, $N_e = 0$, yields

$$8) \quad N_e = \epsilon \int \frac{I_o(\nu)\,\alpha(\nu)}{h\nu}\, d\nu \left\{ \frac{a\,\tau_m^{\,2} \quad e^{-t/\tau_m}}{\left[1-\tau_m(a+b)\right]\left[1-b\tau_m\right]} + \frac{\tau_m e^{-bt}}{1-b\tau_m} - \frac{\tau_m e^{-(a+b)t}}{1-\tau_m(a+b)} \right.$$

or rewriting in a more compact form

$$9) \qquad N_e = Kf(t)$$

where

10) $$K = \tau_m \epsilon \int \frac{I_o(\gamma)\,\alpha(\gamma)}{h\gamma}\, d\gamma ,$$

$$f(t) = \frac{a\tau_m\, e^{-t/\tau_m}}{\left[1-\tau_m(a+b)\right]\left[1-b\tau_m\right]} \quad \frac{e^{-bt}}{1-b\tau_m} - \frac{e^{-(a+b)t}}{1-\tau_m(a+b)}$$

Now at threshold the population N_c must fulfill the following condition

11) $$N_c^{(thr.)} = \frac{\alpha loss}{\sigma_m}$$

where αloss is the absorption coefficient corresponding to the losses and σ_m is the amplification cross section. We are concerned with the value of E that will make

$$N_e = N_c^{(thr)}$$

at some time t_c, $N_e = N_c^{(thr)}$ where N_c is a maximum. Therefore, the necessary condition at threshold is

12) $$\tau_m \epsilon \int \frac{I_o(\gamma)\,\alpha(\gamma)}{h\gamma}\, d\gamma = \frac{\alpha\ loss}{\sigma_m f(t)_{max}}$$

where $I_o(\gamma)$ is now the intensity needed to make this equality. The question is how is this to be related to the threshold energy E? The energy output of the lamp corresponding to this $I_o(\gamma)$ is

13) $$E^c = G \int_0^\infty I_p(\gamma,t)\, dt$$

where G is a geometric constant in units of area. Or, using Eqn. 4, Eqn. 13 becomes

14) $$E^c = \frac{Ga}{b(a+b)} \int I_o(\gamma)\, d\gamma$$

The problem now is to eliminate the $I_o(\nu)$ between Eqns. 12 and 13 this can be accomplished by the following method. Dividing Eqn. 13 by Eqn. 12 one obtains

15) $$E^c = \frac{\alpha_{loss}}{\tau_m \sigma_m f(t)_{max}} \; \frac{Ga}{b(a+b)} \; \frac{\int I_o(\nu)\, d\nu}{\epsilon \int \frac{I_o(\nu)\,\alpha(\nu)}{h\nu}\, d\nu}$$

In the fluorescence spectrum measurement, there exists a steady-state process given by

16) $$N_e = \tau_m \epsilon \frac{I'(\nu)\alpha(\nu)}{h\nu}\, d\nu$$

where $I'(\nu)$ is now the spectral intensity relating to fluorescence spectrum measurement. The intensity of an emission line is given by, in this case the Nd $^4F_{3/2} - {}^4I_{11/2}$ transition,

17) $$\int I_f \, d\nu = \tau_m h\nu P_{3/2-11/2} \; G'\epsilon \int \frac{I'(\nu)\alpha(\nu)}{h\nu}\, d\nu$$

where $P_{3/2-11/2}$ is the transition probability and G is a geometric factor having the dimension of length. Assuming a given line shape for the emission line it can also be seen that

18) $$\int I_f \, d\nu = I_{f\,max}\, \Delta\nu_s$$

Now we must digress to develop the basis for the next step.

Quantum mechanical theory gives the following two expressions

a) $$\tau_m = \frac{\hbar c^3}{64\pi^4 e^2 \nu^3 |x_{n,m}|^2}$$

and

b) $$\int \sigma\, d\nu = \frac{8\pi^3 e^2}{\hbar c} |x_{n\,m}|^2$$

where $|X_{n,m}|$ is the matrix element of the transition and σ is the absorption cross section. Solving for $|X_{n,m}{}^2|$ and eliminating it between the two equations the following expression results

$$\text{c)}\qquad \frac{1}{\tau} = P_{3/2-11/2} = \frac{8\pi n^2\nu^2}{c_0{}^2}\int \sigma_{3/2-11/2}\, d\nu$$

This is written for the desired transition ${}^4F_{3/2} - {}^4I_{11/2}$ and $\sigma_{3/2-11/2}$ is now an amplification coefficient since we are dealing with stimulated emission rather than absorption. The integral over the cross section σ can be expressed in terms of its maximum value σ_m and the half width multiplied by some shape factor depending on the line shape assumed.

$$\text{d)}\qquad \int \sigma_{3/2-11/2}\, d\nu = S\sigma_m\,\Delta\nu$$

$$\text{d)}\qquad \begin{cases} S = 1/2\sqrt{\pi/\ln 2}, & \text{Gaussian line shape} \\ S = \pi/2, & \text{Lorentzian line shape} \end{cases}$$

Therefore combining Eqn. e, c and d one obtains the equation for σ_m

$$\text{f)}\qquad \sigma_m = \frac{c_0{}^2}{8\pi n^2\nu^2 S\Delta\nu}\cdot P_{3/2-11/2}$$

Equating equations 17 and 18 and making use of Eqn. (f) for $P_{3/2-11/2}$ one obtains for σ_m

$$\text{19)}\qquad \sigma_m = \frac{I_{f\ \max}\, c_0{}^2}{\tau_m G' h\nu\varepsilon\left\{\int \frac{I'(\nu)\alpha(\nu)}{h\nu}\, d\nu\right\} 8\pi n^2\nu^2}$$

The equation for E^c, Eqn. 15, after substituting in for σ_m Eqn. 19, yields the following expression

$$\text{20)}\qquad E^c = \frac{8\pi\nu^3 G' h}{c_0{}^2}\cdot\frac{\alpha_{loss}}{f(t)_{max}}\cdot\frac{a\eta^2}{b(a'b)}\cdot\frac{\int I_0(\nu)\, d\nu}{\int \frac{I_0(\nu)\alpha(\nu)}{h\nu}\, d\nu}\cdot\frac{\int \frac{I'(\nu)\alpha(\nu)}{h\nu}\, d\nu}{I_{f\ \max}}$$

Assuming one can write the intensity distributions in the form,

$I'(\nu) = I'_o \, g_2(\nu)$ $g_2(\nu)$ is the shape function of the spectral distribution

$I_o(\nu) = I_{oo} \, g_2(\nu)$

21) and

$I_{f\ max} = \xi \, I'_o \, F_{max}$ (the actual measured value of the relative fluorescence intensity)

One obtains the final desired result

22) $$E_c = \frac{G' h \nu}{\xi F_{max}} \cdot \frac{8\pi n^2 \nu^2}{c_o^2} \cdot \frac{\alpha \mathrm{loss}}{f(t)_{max}} \cdot \frac{Ga}{b(a+b)} \int g_2(\nu)\, d\nu$$

Grouping the terms that are constants one gets

23) $$E_c = \Gamma \frac{N^2}{F_{max} f(t)_{max}} \cdot \frac{a}{b(a+b)}$$

where $$\Gamma = \frac{G' h \nu^3}{\xi c_o^2} \, 8\pi G \int g_2(\nu)\, d\nu \ \alpha_{loss}$$

II. Evaluation of Calculated Relative Threshold

Eqn. 23 shows that E_c can be evaluated on a relative basis since all the quantities on the right side are either constant or measurable directly or can be evaluated from the measured data. The constants a and b can be computed from the lamp pulse shape. The index of refraction, fluorescence lifetime and maximum relative fluorescence intensity are all measured quantities. This leaves only $f(t)_{max}$ to be computed. This can be accomplished by the following method: for each set of a, b values, corresponding to the shape of the lamp pulse, f(t) is plotted vs. t for a number of τ_m values. The maximum f(t) is then plotted against the corresponding τ_m value.

Once these curves are obtained, one need only know τ_m to obtain the appropriate $f(t)_{max}$. This calculation has been programmed on the IBM 1620 computer. Curves of τ_m vs. $f(t)_{max}$ are given in Figure 4-1 for several lamp geometries and flash tube arrangements.

APPENDIX C

RELATION BETWEEN LIFETIME AND REFRACTIVE INDEX

Two coefficients, A and B, are commonly used to describe spontaneous and stimulated transitions. The first is the probability of spontaneous transition per unit time and the second is the probability of induced transition per unit time per unit intensity per unit frequency interval. Einstein (C-1) demonstrated the necessity for a relation between A and B using the principle of detailed balancing in equilibrium. Consider an atom with upper state n and lower state m in equilibrium with a black body radiation cavity. Then the following relation must hold.

1) $$N_n \left(A_{nm} + B_{nm} 4\pi I \right) = B_{mn} 4\pi I N_m$$

where I is the undirectional intensity per unit solid angle per unit frequency interval, N_i is the number of atoms in state i, and A and B are the quantities mentioned above referred to the specific transition from n to m or m to n. The quantity I is related to the energy density by $e = 4\pi I/c$. From this, Einstein showed

2) $$B_{nm} = B_{mn} \equiv B$$

$$\frac{A}{B} = \frac{8\pi h\nu^3}{c^2}$$

Often the B coefficient is expressed in terms of the energy density and an extra factor of c appears in the denominator of (2). The right-hand side arises from the intensity of radiation inside a black cavity--that is, a cavity with black walls. Hence the c is the velocity of light appropriate to the medium which fills the cavity. This first appearance of the refractive index in transition probabilities may be traced back to the higher density of states in a black cavity filled with a medium, but it is not possible from Equation (2) to say to what extent this influence is in A or B separately. The importance of Equation (2) is that spontaneous and induced transitions are not independent but are related by a simple expression. Thus, there is only one quantity necessary to characterize all aspects of such a simple two state transition.

The heuristic argument used to obtain Equation (2) was replaced by a unified theory with the advent of quantum electrodynamics. This theory treats the radiation field within the cavity and the atomic states as a single system with weak interaction between the two parts. Matrix elements result having the form(C-2):

$$-\frac{e}{m}\left[\frac{h(N+1)}{\nu}\right]^{1/2}\int \psi_n^* \, e^{i(Kr)} \, P_e \, \psi_o \, d\tau$$

where N is the number of quanta of energy h . This yields induced transitions from the N and spontaneous transitions from the "one". Even though spontaneous and induced transitions are coupled with the same factor in this matrix element, the spontaneous transition probability shifts relative to the induced transition probability because the density of states enters into the computation for the former and not the latter.(C-3) Thus, when B is expressed in terms of an energy density, $A/B = \rho(\nu)h = 8\pi h\nu^3/c^3$ (Equation 2) where $\rho(\nu)$ is the density of states.

Returning to the quantities A and B as defined at the start, equations relating these to measurable parameters are

3) $$A = \frac{1}{\tau}$$

where γ is the spontaneous emission lifetime, and

4) $$B = \frac{1}{n\nu}\int \sigma \, d\nu$$

where σ is the optical absorption cross section associated with the transition. These formulas hold strictly only for transitions between two fairly well defined states. In any solid, degenerate states will be split into many levels and this adds further complications. However, for rare earths in glasses this problem is not very serious and (3) and (4) adequately describe many situations.

An approximation will be chosen to estimate the influence of refractive index on these properties. It will be assumed that the wave functions of the atom are unchanged on varying the glass. Then, since(C-2)

$$B = \frac{2\pi e^2}{c\hbar^2} \, / \, \bar{X}_{on} / ^{2}$$

where

$$/X_{on}/ \equiv \int \psi_n^{*} X \psi_o \, dv$$

we have

5) $$\gamma = \frac{\hbar c^3}{32\pi^3 e^2 \nu^3 / X_{on}/^2}$$

6) $$\int \sigma \, d\nu = \frac{4\pi^2 e^2 \nu}{\hbar c} \, / X_{on} / ^{2}$$

From (5), it is seen that the lifetime will decrease with the cube of the refractive index, while the absorption increases with the first power. Although the assumption underlying (5) and (6) will never be exactly correct, various glass composition can be compared on this basis.

REFERENCES

(C-1) Einstein, A., Phys. Zeits. 18, 121 (1917).

This derivation can be found in almost any book on quantum mechanics, such as: Mott and Sneddon, Wave Mechanics and Its Applications, Oxford University Press, 1948.

(C-2) Mott and Sneddon, op. cit.

(C-3) Schiff, L.I., Quantum Mechanics, McGraw-Hill Book Co., 1949. pages 386-87.

Distribution

Department of the Army

Dr. Robert A. Watson
Dr. Hans K. Ziegler
Dr. E. M. Reilley
Dr. Harrison J. Merrill
Dr. Edwin Minor
Mr. William D. McKnight

Department of the Navy

Mr. Ben Rosenberg
Mr. C. H. Harry
Dr. G. C. Sponsler
Dr. Sidney Reed
Mr. Frank Isakson
Dr. Van O. Nicolai
Dr. Irving Rowe
Dr. Fred W. Quelle
Dr. Elliot Weinberg
Mr. Lloyd A. White
Dr. Jack A. Soules
Dr. Francis T. Byrne
Mr. J. W. Smith
Dr. C. C. Klick
Dr. L. F. Drummeter

Department of the Air Force

Major E. N. Myers
Mr. Robert Feik
Lt. Col. Ivan Atkinson
Major H. I. Jones, Jr.
Mr. Don Lewis
Mr. Don Neuman
Capt. Marvin Atkins
Mr. Phillip Sandler
Mr. Thomas Henion

Advanced Research Projects Agency

Lt. Col. William B. Lindsay

Joint Chiefs of Staff

Col. C. A. Barninger

Materials Contractors

Mr. R. W. Young
Mr. R. D. Maurer
Mr. Wayne L. McKusick
Dr. J. W. Nielson
Dr. James F. Miller
Dr. C. B. Sclar